Design and Performance Evaluation of Refrigeration Systems using Thermodynamic Models

by

Jameel ur Rehman Khan

A Thesis Presented to the

FACULTY OF THE COLLEGE OF GRADUATE STUDIES

KING FAHD UNIVERSITY OF PETROLEUM & MINERALS

DHAHRAN, SAUDI ARABIA

In Partial Fulfillment of the
Requirements for the Degree of

MASTER OF SCIENCE

In

MECHANICAL ENGINEERING

November, 1997

INFORMATION TO USERS

This manuscript has been reproduced from the microfilm master. UMI films the text directly from the original or copy submitted. Thus, some thesis and dissertation copies are in typewriter face, while others may be from any type of computer printer.

The quality of this reproduction is dependent upon the quality of the copy submitted. Broken or indistinct print, colored or poor quality illustrations and photographs, print bleedthrough, substandard margins, and improper alignment can adversely affect reproduction.

In the unlikely event that the author did not send UMI a complete manuscript and there are missing pages, these will be noted. Also, if unauthorized copyright material had to be removed, a note will indicate the deletion.

Oversize materials (e.g., maps, drawings, charts) are reproduced by sectioning the original, beginning at the upper left-hand corner and continuing from left to right in equal sections with small overlaps.

Photographs included in the original manuscript have been reproduced xerographically in this copy. Higher quality 6" x 9" black and white photographic prints are available for any photographs or illustrations appearing in this copy for an additional charge. Contact UMI directly to order.

Bell & Howell Information and Learning
300 North Zeeb Road, Ann Arbor, MI 48106-1346 USA
800-521-0600

UMI®

Design and Performance Evaluation of Refrigeration Systems Using Thermodynamic Models

BY

Jameel Ur Rehman Khan

A Thesis Presented to the

FACULTY OF THE COLLEGE OF GRADUATE STUDIES

KING FAHD UNIVERSITY OF PETROLEUM & MINERALS

DHAHRAN, SAUDI ARABIA

In Partial Fulfillment of the
Requirements for the Degree of

MASTER OF SCIENCE

In

MECHANICAL ENGINEERING

NOVEMBER 1997

UMI Number: 1398759

UMI Microform 1398759

Bell & Howell Information and Learning Company
300 North Zeeb Road
P.O. Box 1346
Ann Arbor, MI 48106-1346

KING FAHD UNIVERSITY OF PETROLEUM AND MINERALS
DHAHRAN, SAUDI ARABIA

COLLEGE OF GRADUATE STUDIES

This thesis, written by

Jameel Ur Rehman Khan

under the direction of his Thesis Advisor, and approved by his Thesis committee, has been presented to and accepted by the Dean, College of Graduate Studies, in partial fulfillment of the requirements for the degree of

MASTER OF SCIENCE IN MECHANICAL ENGINEERING

Thesis Committee:

Dr. Syed M. Zubair (Chairman)

Dr. Ahmet Z. Sahin (member)

Dr. Esmail M.A. Mokheimer (member)

Mr. M. Yaqub (member)

Dr. Mohammad O. Budair
Department Chairman

Dean, College of Graduate Studies

Date: 16 - 2 - 98

كلية الدراسات العليا
COLLEGE OF GRADUATE STUDIES

Dedicated to

my Parents,

Brothers & Sisters

Acknowledgment

> In the name of Allah, Most Gracious, Most Merciful. Read in the name of thy Lord and Cherisher, Who created. Created man from a {*leech-like* } clot. Read and thy Lord is Most Bountiful. He Who taught {the use of} the pen. Taught man that which he knew not. Nay, but man doth transgress all bounds. In that he looketh upon himself as self-sufficient. Verily, to thy Lord is the return {of all}.
>
> (The Holy Quran, Surah 96)

All praise to Almighty Allah, who bestowed me strength and patience to accomplish my goals.

Acknowledgement is due to King Fahd University of Petroleum & Minerals for providing support to this research work.

I would like to offer my indebtedness and sincere appreciation to my thesis committee chairman and advisor Dr. Syed M. Zubair, who has been a constant source of help and encouragement during this work. I also appreciate the cooperation and support extended by Dr. A.Z. Sahin, Dr. E. Mokheimer and Mr. Mohammad

Yaqub who served as committee members.

I am thankful to all my friends and colleagues, whose amicable and understanding attitude made my stay, as a graduate student, a pleasant experience.

Last but not the least, thanks are due to my parents, brothers and sisters for their prayers, guidance and moral support throughout my academic career. This work is dedicated to my parents and sisters for their hard work and taking pains to fulfill my academic pursuits. My parents advice, to strive for excellence, has made all this work possible.

Contents

List of Tables

List of Figures

Nomenclature

ΔMTS	Difference between T_{cond}^{main} and T^{out_sub}
$\dot{C}$	Capacitance rate for the external fluids ($\dot{C} = \dot{m}c_p$) (kW K^{-1})
COP	Coefficient of performance
f_h	Ratio of condenser effectiveness-capacitance product to the sum of the effectiveness-capacitance rate products for the condenser and evaporator of the cycle
h_j	Specific enthalpy of refrigerant at state point j (kJ kg^{-1})
κ	Constant thermal inventory (kW K^{-1})
$\dot{m}$	mass flow rate (kg s^{-1})
$\dot{Q}_{cond}$	Rate of heat rejection at the condenser (kW)
$\dot{Q}_{cond}^{loss}$	Rate of heat leak from the hot refrigerant (kW)
$\dot{Q}_{evap}$	Rate of heat absorbed at the evaporator (kW)
$\dot{Q}_{evap}^{loss}$	Rate of heat leak from the ambient to the cold refrigerant (kW)
$\dot{Q}_s^{loss}$	Net heat leak from ambient to the refrigerant ($\dot{Q}_{evap}^{loss} - (\dot{Q}_{cond}^{loss} + \dot{Q}_w^{loss})$) (kW)
$\dot{Q}_w^{loss}$	Rate of heat leak from the compressor shell to ambient (kW)
$\dot{S}_{igen}$	Internal entropy generation, due primarily to fluid friction losses in non-isentropic compression and expansion (kW/K)
T_{cond}	Refrigerant temperature in the condenser (K)

T_{cond}^{in}	Condenser coolant inlet temperature (K)
T_{evap}	Refrigerant temperature in the evaporator (K)
T_{evap}^{in}	Evaporator coolant inlet temperature (K)
T^{out_sub}	Temperature of the main cycle refrigerant after leaving the subcooler.
T^{sub}	Subcooler saturation temperature (K)
$\dot{W}$	Electrical power input to the compressor, (kW)
$\dot{W}_s$	Power required for isentropic compression (kW)

Greek Symbols

η	Efficiency
ε	Heat exchanger effectiveness

Subscripts

1, 2, 3,...	state points
Carnot	carnot cycle
comp	compressor
cond	condenser
evap	evaporator
igen	generation

ref	refrigerant
refg	refrigerating
simple	simple cycle
total	complete cycle
W	heat loss from compressor shell

Superscripts

HP	high pressure cycle
in	inlet
inst	interstage
loss	heat loss
LP	low pressure cycle
main	main cycle
out	outlet
sub	subcooler cycle

Abstract

Name: **Jameel Ur Rehman Khan**

Title: **Design and Performance Evaluation of Refrigeration Systems using Thermodynamic Models.**

Major Field: **Mechanical Engineering**

Date of Degree: **November, 1997**

Finite time thermodynamic models which simulate the working of actual vapor compression refrigeration systems are developed. The characteristic performance curves of the refrigeration systems that include simple vapor compression system, mechanical subcooling and two-stage systems are presented in terms of the coefficient of performance (COP) and cooling capacity of the system ($\dot{Q}_{evap}$). Using the data obtained from the thermodynamic models, performance curves of the systems are obtained. The resulting relationship between the COP and $\dot{Q}_{evap}$ is explained in light of various irreversible losses of the system. These losses are due to finite rate of heat transfer in the heat exchangers and the non-isentropic compression and expansion in the compressor(s) and expansion valve(s) of the systems, respectively. The thermodynaic models are also used for predicting an optimum distribution of the total heat exchanger area between the individual heat exchangers of the systems. The results obtained from the thermodynamic models are also compared with an actual performance of a simple vapor-compression system. It is found that the performance characteristics predicted by the thermodynamic model is very close (within $\pm 2\%$) than that shown by actual experimental results.

Master of Science Degree
Department of Mechanical Engineering
King Fahd University of Petroleum and Minerals
Dhahran, Saudi Arabia
November, 1997

ملخص الرسالة

الإسم : جميل الرحمن خان

عنوان الرسال، : تصميم وتقييم أداء أنظمة تبريد باستخدام نماذج ديناميكا الحرارية

التخصص الرئيسي : الهندسة الميكانيكية

تاريخ : الدرجة : نوفمبر ١٩٩٧

لقد تم تطوير نماذج ديناميكا حرارية ذات وقت محدد لكي تحاكي عمل أنظمة تبريد حقيقية تعمل طبقا لدورات الضغط البخاري • كما تم عرض منحنيات وصف أداء أنظمة تبريد مختلفة تشتمل على أنظمة تبريد بسيطة ذات تبريد ميكانيكي زائد وثنائية المراحل وذلك بدلالة معامل الأداء (COP) وسعة تبريد المنظومة ($\dot{Q}_{evap}$) • كما تم استخدام نتائج نماذج الديناميكا الحرارية في الحصول على معاملات الأداء كما تم شرح العلاقة بين معاملات الأداء ( )وسعة التبريد ($\dot{Q}_{evap}$) في ضوء مختلف الفواقد اللا انعكسابة للمنظومة • وترجع هذه الفواقد الى المعدل المحدود لانتقال الحرارة في المبادلات الحرارية بالإضافة الى عمليات الضغط والتمدد اللانعكاسي في الضاغط ومحبس التمدد على التوالي •

ولقد تم استخدام نماذج الديناميكا الحرارية أيضا في التنبؤ بأفضل توزيع لمساحات الأسطح بين المبادلات الحرارية لكل منظومة • كما تم مقارنة نتائج هذا النماذج مع نتائج معملية لدورة تبريد حقيقية تعمل طبقا لدورة ضغط بخاري بسيطة ووجد أن نتائج نماذج الديناميكا الحرارية تقترب في حدود + ٢ ٪ من النتائج المعملية •

درجة الماجستير في العلوم

قسم الهندسة الميكانيكية

جامعة الملك فهد للبترول والمعادن

الظهران – المملكة العربية السعودية

نوفمبر ١٩٩٧

Chapter 1

Introduction

Reciprocating chillers are commonly used in a wide range of commercial and industrial cooling applications. They represent a substantial fraction of the installed cooling systems. The chiller consists of an evaporator, reciprocating compressor, condenser and an expansion valve. For a simple cycle, all the components are connected in a closed loop, whereas for a two stage cycle, there are two compressors which are connected in series separated by a flash intercooler. The vapor generated by throttling the refrigerant from the condenser pressure to the interstage pressure is separated in the flash intercooler. This is known as flash vapor. The vapor from the low pressure compressor is de-superheated by evaporating the cold liquid in the flash intercooler. The above vapor along with the flash vapor is compressed in the high pressure compressor. On leaving the high pressure compressor, the vapor is condensed in the condenser, producing liquid refrigerant which enters the expansion

valve and then finally the evaporator. Thus, resulting in the increase of system Coefficient of Performance (COP) over a simple cycle.

The performance of a simple vapor compression refrigeration system can be significantly improved by further cooling the liquid refrigerant leaving the condenser coil which allows the refrigerant to enter the evaporator at a low quality, and thus allowing the refrigerant to absorb more heat in the evaporator. This subcooling of the liquid refrigerant can be accomplished by adding a mechanical subcooling loop in a conventional vapor compression cycle. The subcooling system can either be a dedicated mechanical subcooling system or an integrated mechanical subcooling system. In a dedicated mechanical subcooling system there are two condensers, one each for the main cycle and the subcooler cycle, whereas for an integrated mechanical subcooling system there is only one condenser serving both the main cycle and the subcooler cycle. In each of these systems, hot liquid refrigerant from the condenser of the main cycle is subcooled in the subcooler, resulting in the evaporation of the subcooler cycle refrigerant. On leaving the subcooler, the main cycle refrigerant is then passed through the expansion valve to the evaporator. The refrigerant vapor generated in the subcooler is compressed by the auxiliary compressor, which then rejects heat in the subcooling cycle condenser. Finally the liquid refrigerant on leaving the condenser is passed through an expansion valve to the subcooler.

The development of refrigeration system models, which simulate the actual working of a reciprocating chiller has been the goal of many researchers [1-8]. The most simple model is an ideal temperature dependent model without any irreversible losses. In case of simple cycles it is also known as the Carnot model. However for the mechanical subcooling refrigeration systems, the temperature-dependent model includes the irreversible losses due to the rate of heat transfer in the subcooler. An improved temperature dependent model has the capability to consider irreversible losses in all the heat exchangers of the system. However, the temperature dependent models do not take into account the actual properties of the refrigerants that are used in the systems. The property dependent thermodynamic models takes into account the refrigerant properties and are developed by considering the mass and energy balance across each component of the system. It should be noted that the finite-time thermodynamic model, accounts for the irreversibilities existing due to the finite temperature difference in the heat exchangers as well as the losses due to the non-isentropic compression and expansion in the compressors and the expansion valves of the system, respectively. The thermodynamic models can be modified by including the heat leaks to and from the system as shown in the schematic diagrams of the various systems investigated in this thesis.

The overall objective of this thesis is to develop temperature-dependent and property dependent thermodynamic models for the reciprocating refrigeration sys-

tems, which can simulate the performance of actual systems as close as possible. In this regard performance analysis of a simple vapor-compression refrigeration system, two-stage and mechanical subcooling system, are discussed with respect to various irreversible losses of the systems.

An extensive literature review on vapor-compression refrigeration systems is given in chapter 2. It also includes discussion on previous work related to thermodynamic modelling of refrigeration systems. Chapter 3 covers the analysis of an actual simple vapor compression refrigeration system to highlight various irreversible losses in the system, in addition to performance evaluation of the refrigeration systems using the thermodynamic model. The model is also used to study the performance of the variable-speed refrigeration system in which the evaporator capacity is varied by changing the mass flow rate of the refrigerant, while keeping the inlet chilled water temperature as constant.

Chapter 4 and 5 describes the performance evaluation of the dedicated and integrated mechanical subcooling systems. The temperature- and property-dependent models are developed to study the systems, particularly with respect to the subcooler saturation temperature in addition to the heat exchanger areas. The thermodynamic models are also used for diagonastic purpose, that is; for predicting system performance over a wide range of operating conditions and for predicting the optimum

distribution of total heat exchanger areas between the condenser and evaporator of the systems.

Similarly in chapter 6, the temperature- and property-dependent models for the two-stage vapor compression refrigeration system are developed to simulate the system performance with respect to interstage temperature and heat exchanger parameters. The models are also used for predicting the optimum distribution of the total heat exchanger area between the evaporator and condenser. Finally, chapter 7 summarizes the important conclusions of the study and some recommendations for future research in this field.

Chapter 2

Literature Reivew

Threlkeld [1] described thermodynamic analysis of vapor-compression heat pump cycles. In his work, a thermodynamic study is carried out for both heat pump operating with a constant temperature heat source and heat sink as well as for constant temperature heat source and a variable temperature heat sink. The ratio of COP of the cycle to the COP of the reversible (Carnot) heat pump is used to define the cycle efficiency. He showed that CFC-11 yields the highest theoretical efficiency as compared to CFC-12, CFC-21, CFC-113, CFC-114 and Ammonia cycles.

Wilson [2] demonstrated second law analysis of vapor compression refrigeration systems with the help of numerical examples. In his example problems, he has shown that:

1. The reversed Carnot cycle, having heat transfer through negligible differences,

is an ideal standard and is the criterion for minimum requirements of work input to the refrigeration cycle.

2. Departures from this ideal standard, such as fluid friction and heat transfer through finite temperature difference, will create entropy, degrade available energy and cause an increase in entropy of the universe.

3. Such departures require that the work input to the refrigeration cycle be greater than the ideal minimum.

4. This increased work input is equal to the product of the absolute temperature of the atmosphere and increase in entropy of the universe, $T_o \Delta S_{surr}$, and is equal to the sum of all available energies that are degraded by irreversibilities produced by the refrigerant in its cyclical operation and heat transfer through finite temperature differences.

Alefeld [3] derived an analytical equation for the coefficient of performance using the Second Law of Thermodynamics. He demonstrated that by using the Second law from the beginning of the study, the necessary knowledge about fluid properties is reduced to a few non-dimensional parameters. Also, he found that for Freons the most relevant parameter is the ratio cT/r, where c is the specific heat capacity of the liquid, r is the heat of vaporization and T is the evaporator temperature. Adrian

Bejan [4] investigated the dependence of the Second Law efficiency η_{II}, defined as

$$\eta_{II} = \frac{COP}{COP_C},$$

where COP_C is the coefficient of performance of a Carnot refrigerator operating between the same temperature levels (T_H, T_L) as that of an actual machine whose coefficient of performance is COP. He demonstrated that when plotted correctly, the empirical η_{II} values decreases as T_L decreases. Two theoretical arguments were offered as explanations for this trend. The first argument is based on a refrigeration plant model, the irreversibility of which is due solely to the 'internal' heat transfer that passes directly through the machine all the way to T_L. The second argument is based on a more refined model in which the refrigeration plant irreversibility is due to three heat transfer phenomena : the internal heat transfer, the external temperature difference between the plant and ambient, and the external temperature difference between the refrigeration load and the cold end of the refrigeration plant. He also showed that there exist optimum ways of allocating heat transfer equipment to the distinct parts of the plant, if the objective is to maximize the refrigeration capacity of the plant.

Thermodynamic analysis of vapor-compression refrigeration systems have been presented by Swers et al. [5], which is also discussed in ASHRAE Handbook of Fundamentals [6]. The analysis illustrates the effect of departure of a real cycle from the reversed Carnot cycle in terms of irreversible losses. In these references,

the effects of irreversibilities in a vapor compression refrigeration cycle are compiled for a range of operating conditions, and the irreversible losses of each component are optimized. Analysis are given for both vapor-compression refrigeration cycle and for a two-stage vapor-compression refrigeration cycles. But for two-stage vapor compression, the interstage pressure is considered as the geometric mean pressure, which is true for the perfect gas with complete intercooling.

Auracher [7-8] illustrated the application of exergy (or available energy) to refrigeration process optimization. According to him, it is exergy rather than energy which is of concern in all thermodynamic processes. The exergy losses are described for various components of a refrigeration cycle and the need for introducing the second law efficiency of refrigeration systems is highlited, which is similar to that proposed earlier by Threlkeld [1]. He discussed that the optimization of a plant design can be best guided by determination of the sources and magnitude of its exergy losses, with an example problem. Huang et al. [9] investigated the applicability of the Second Law of Thermodynamics using an entropy balance method to a single stage vapor compression refrigeration system. He concluded that expressions derived by the entropy balance method yield similar results to those given by the commonly used methods based on energy and exergy balance. Nevertheless, the advantage of the entropy balance method is that it shows the influence of irreversibilities of individual components on the coefficient of performance based on the properties of

the process, which are clearly defined without ambiguity. Also, in contrast to the exergy method, the entropy balance method yields design indexes by which the effectiveness of a process can be determined from system temperatures rather than from an undefined environmental temperature.

A thermodynamic model for a simple vapor compression refrigeration system was developed by Klein [10]. Using the model he has investigated the optimum distribution of the total heat exchanger area between the evaporator and the condenser, and found that at maximum coefficient of performance (COP), the condenser area should be larger as compared to the evaporator area. Radcenco et al. [11] showed that the intermittent operation of a defrosting vapor-compression refrigerator can be optimized with respect to: (1)the frequency of on/off operation, and (2) the way in which the heat exchanger surface is divided between evaporator and condenser. In this work the total heat exchanger surface was fixed. However, as an additional objective, they also showed that under certain conditions the fixed-surface constraint leads to results similar to those that would be obtained using the fixed total thermal conductance constraint, discussed in [10], [12], [13] and [14]. Gordon et al. [15] have investigated the loss mechanisms that dominate the chiller performance, and their influence at different cooling rates. They have found that chiller performance is dominated by competing effects of heat transfer and internal fluid friction losses. The former prevails at relatively high cooling rates and the latter at relatively low

cooling rates. Experimental data, that includes all the relevant parameters of both the water cooled and air-cooled reciprocating chillers have been used in their study. Gordon and Choon [16] have developed a thermodynamic model that pertains to all chillers, and is simple enough to yield analytic formulae for chiller performance characteristics. They have considered reciprocating, centrifugal, absorption, thermoelectric and thermoacoustic chillers for their modelling. A model for reciprocating chillers that could be valuable for diagonastic purposes, for predicting chiller performance characteristics over a wide range of operating conditions, is investigated by Gordon and Choon [17].

It should be noted that in the work of Gordon et al. [16-17], analytical expressions have been developed for calculating the losses and heat leaks in the components of the refrigeration system, whereas a thermodynamic model that uses the properties of the refrigerants has not been considered by Gordon et al. [15-17]. Also Gordon et al. [18] demonstrated that the simple thermodynamic model, originally developed for reciprocating chillers, can be succesfully used for predicting the fundamental relation between COP and cooling rate for the centrifugal chiller as well as for the diagonastic analysis of heat exchanger fouling on chiller performance. Leverenz and Bergan [19] described the development of a reciprocating chiller model for use in hourly building energy analysis computer simulation programs. The model and its development are described, along with a procedure for getting the model parameters

from the manufacturer's catalog data. The model accurately calculated the performance of an actual chiller in an HVAC system configuration using model parameters obtained from catalog data. The model agreed with the catalog data (within 3%) over a wide range of chiller sizes.

Again Gordon et al. [20] investigated a generalized finite-time thermodynamic model for reciprocating chillers and derived an analytic formulae for evaluating how the fixed finite resources of cycle time and heat exchanger inventory should be allocated so as to optimize chiller performance. They also compared their optimal operating schemes with detailed experimental data from different commercial chillers reported by Gordon et al. [15] and Bong et al. [21], and found excellent agreement between the theory and actual performance data. Besides quantitatively documenting the individual sources of irreversibility, they also showed how the limitations of currently-available chiller components affect optimal chiller design as well as the potential steps to improve chiller efficiency within a universal thermodynamic framework.

Chua et al. [22] investigated an absorption refrigeration system and developed a simple irreversible thermodynamic model and using the model have studied the following

1. The characteristic device performance curves over the full range of realistic

operating conditions. This refers, for example, to determining COP as a function of useful effect (cooling capacity) and the division of total heat rejection to total heat input between the two available heat reservoirs.

2. Predicting maximum system COP and under what operating conditions it can be attained. This also establishes the maximum possible improvement in device efficiency for a given technology, that is, for a fixed quality of individual components.

3. Determining to what extent commercial absorption systems have evolved to optimal or near-optimal designs.

Many researchers have investigated the dedicated as well as the integrated mechanical subcooling system. Bahel and Zubair [23], Zubair [24], and Zubair et al. [25] have investigated an integrated mechanical subcooling system from the thermodynamic stand point. They found that the subcooling system showed improvement in performance over the corresponding simple system, when the difference between the condensing and the evaporating temperatures is large. They also investigated the performance of the system with respect to the irreversible losses due to the expansion process and found that the best performance occurs when these losses are minimum. Also Khan [26] and Zubair and Khan [27] studied the integrated mechanical subcooling system and reported that the maximum COP of the system occured at a subcooling evaporator temperature, which is arithematic mean of the

condensing and the evaporating temperatures of the cycle. However they did not consider the irreversible losses due to rate of heat transfer in their study, which will be studied in this work.

Thornton et al. [28] in their paper have developed a temperature dependent thermodynamic model for predicting the performance of the mechanical subcooling system with irreversibility only in the subcooler. Using the above model they have found an optimum value of the subcooling evaporator temperature, at which COP of the system is maximum. They have also prepared a refrigerant property based thermodynamic model for the mechanical subcooling system, with irrversibilities in all the heat exchangers except the main cycle evaporator, and using the above model have investigated the performance of the mechanical subcooling system for various values of the subcooling evaporator temperature.

Couvillion et al. [29], have developed a detail mathematical model of the mechanical subcooling system, from the individual component models of the equipment involved in the system. The component subroutines are contained in a computer program that simulates the design and operation of the complete system. They have found an improvement of 6 to 80 percent in COP and 20 to 170 percent in capacity over the conventional simple cycle.

According to Soumerai [30], the selection of the compressors and other components of a two stage refrigeration system can be simplified when several refrigerant properties are grouped together and expressed in terms of the intermediate pressure, which can be selected arbitrarily. It is then possible to design a system that will balance at this assumed intermediate pressure by properly selecting the compressor displacement ratio. He also demonstrated the effect of compressor displacement ratios and volumetric efficiencies on the intermediate pressure of the cycle.

For multistage refrigeration systems, many research workers have investigated the optimum interstage pressure, for which the work required is minimum. According to Prasad [31], the optimum interstage pressure corresponding to minimum work is given by

$$P_{int} = (1 + a)^{n/2(n-1)}(P_{evap} * P_{cond})^{1/2} \tag{2.1}$$

It is assumed that the mass of flashed vapor is invariant with intermediate pressure, however, for real applications the mass of flashed vapor is directly related to the intermediate pressure.

This investigation was extended by Lal [32] after allowing for variations in mass of the flashed vapor with intermediate pressure. His analysis is complicated and it requires generation of whole superheated refrigerant properties. To simplify Lal's work, Charan and Verma [33] assumed linear variation in the mass flow of flashed

vapor with interstage pressure and finally found that the optimum interstage pressure corresponding to the minimum work, however, their expression is in terms of a set of differential equations, for which a closed form solution is not possible.

The discrete maximum principle discussed by Katz [34] has been used by Arora and Dhar [35] to solve the problem of optimum intermediate pressure allocation in multistage compression systems. They first derived the expression for the interstage pressure with intercooling between the stages. Their result shows that the optimum interstage pressure lies very close to the geometric mean pressure value, however, when the intercooler is incorporated, they found a considerable difference between the geometric mean pressure and optimal pressure. It should be emphasized that their equations are complicated and can not be solved, explicitly.

Ait-Ali [36] and Ait-Ali and Wilde [37], discussed that the irreversible work of heat transfer due to the finite-temperature approach represents a major fraction of the actual compressor work in low-temperature refrigeration cycles. They showed that this work is monotonic decreasing with the number of stages in constant boiling temperature cascades. For a finite number of stages, the minimum compressor work is obtained when every refrigerant inter-stage temperature is the geometric mean of the adjacent ones. This optimality rule when applied to a classical cascade natural gas liquefaction cycle (which comprises of a three-stage methane subcooling cycle,

a three stage ethylene liquefaction cycle and a two stage pre-cooling cycle) leads to a 7% saving in refrigeration work as compared to the non-optimum design.

Czaplinski [38] and Prasad [39] found that the inter-stage temperature of a two-stage refrigeration cycle is given by the geometric mean of the condensation and evaporation temperatures, which can be expressed as

$$T_{int} = (T_{cond} * T_{evap})^{1/2} \tag{2.2}$$

In the above equation all the temperatures are expressed in absolute units. It should be noted that his method uses approximate technique by ignoring superheat horn in comparison to the total work of compression. Prasad, also indicated that the above assumption is only true for R-12 system because the superheat horn for R-12 is negligible as compared to the total work of compression.

Behringer [40], found that, for two stage Ammonia cycle with liquid subcooling and desuperheating between the stages to saturation temperature, the optimum intermediate temperature is given by

$$T_{opt} = T_m + 5 \tag{2.3}$$

where T_m is the saturation temperature in Kelvin corresponding for equal pressure ratios in the first and second stage.

Zubair and Khan [27], demonstrated that the optimum interstage pressure for a two-stage refrigeration system can be approximated by the saturation pressure corresponding to the arithmetic mean of the condensing and evaporating temperatures. They also showed that the optimum performance of a refrigeration system with mechanical subcooling occured when the subcooler compressor (saturation suction) temperature corresponds to the arithmetic mean of the condensing and evaporating temperatures.

Chapter 3

Thermodynamic Analysis of a Simple Vapor Compression Refrigeration System

A simple vapor compression refrigeration system is shown in Fig. 3.1, while log (p)-h diagram is shown in Fig. 3.2 respectively. The major components of this cycle include compressor, condenser, expansion valve and evaporator. The components are connected in closed loop through piping that has heat transfer with the surroundings. The refrigerant leaves the evaporator at state point 3 as a low pressure, low temperature, saturated vapor and enters the compressor at state point 4. The refrigerant from state point 3 to point 4 undergoes heat transfer with the surroundings in the suction line. At point 5, it leaves the compressor as a high tem-

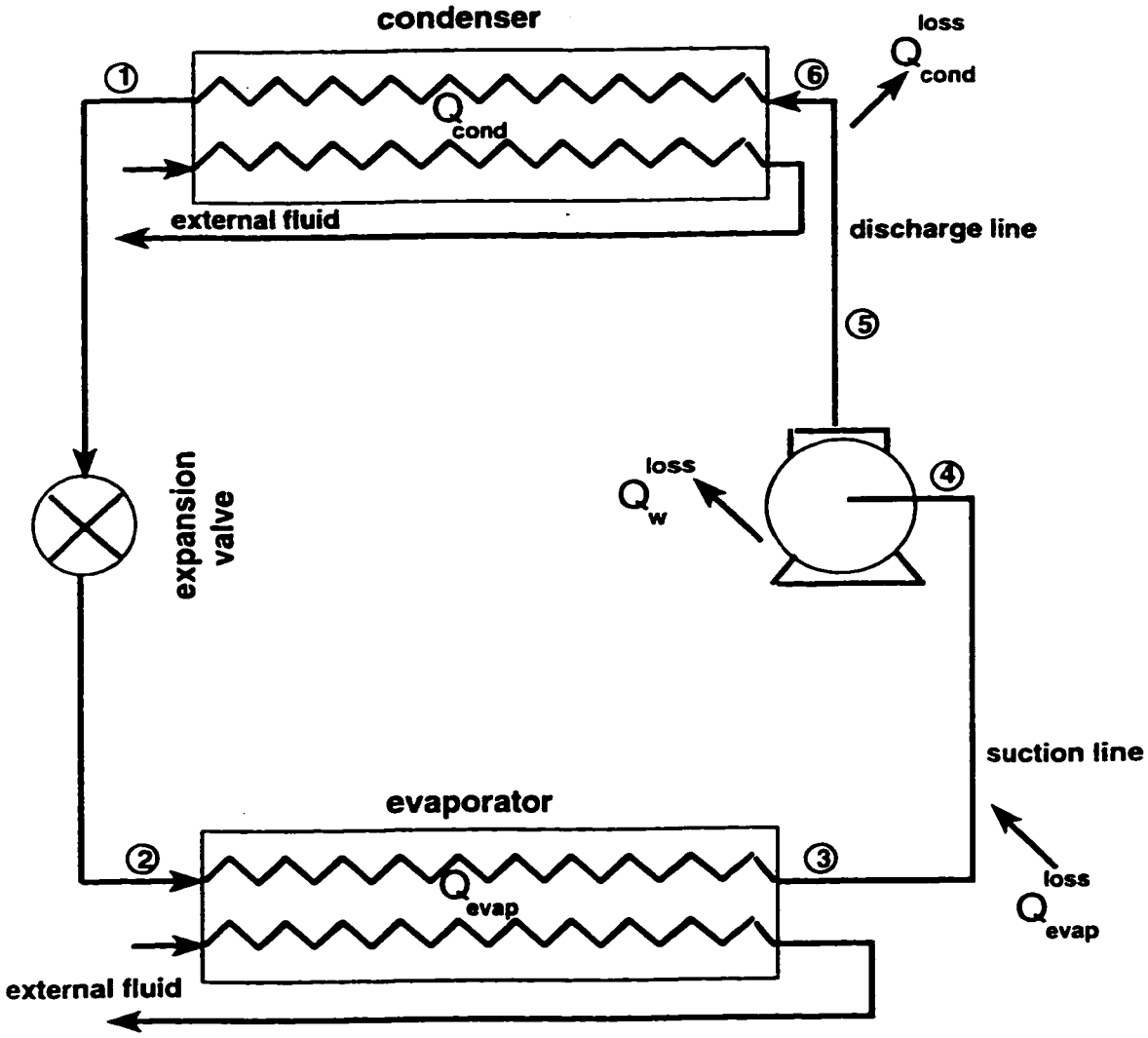

Figure 3.1: Schematic diagram of a simple refrigeration cycle

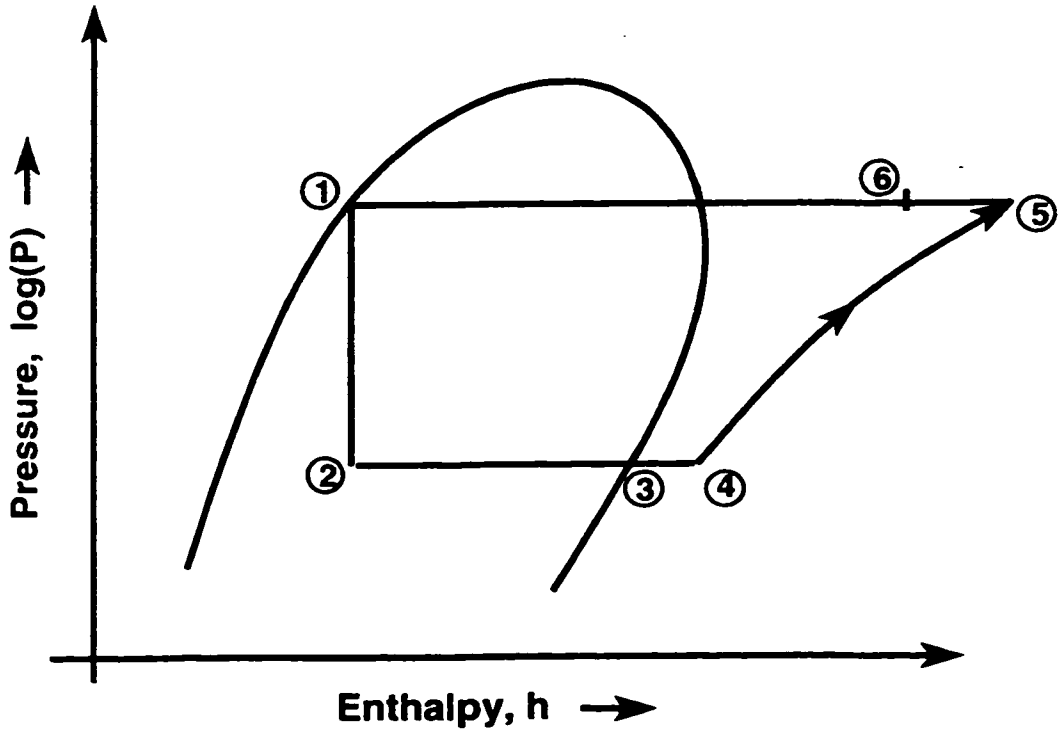

Figure 3.2: Pressure-enthalpy diagram of a simple refrigeration cycle

perature, high pressure, superheated vapor and enters the condenser at state point 6 after undergoing heat transfer in the discharge line. At point 1, the refrigerant leaves the condenser as a high pressure, medium temperature, saturated liquid and enters the expansion valve, where it expands irreversibly and adiabatically (constant enthalpy). At point 2, it leaves the expansion valve as a low-quality vapor and enters the evaporator, where it is evaporated irreversibly at constant pressure to the saturated state at point 3.

3.1 Analysis of an Actual System

Stoecker and Jones [41] have presented the performance data of each of the components of a vapor-compression refrigeration system. In this regard, the data for the refrigeration capacity and power requirement of a York (Division of Borg-Warner) hermetic reciprocating compressor (H62SP-22E, refrigerant 22, 1750 *rpm*) were represented by [41]

$$\begin{aligned}\dot{Q}_{evap} &= c_1 + c_2 T_{evap} + c_3 T_{evap}^2 + c_4 T_{cond} + c_5 T_{cond}^2 + c_6 T_{cond} T_{evap} \\ &\quad + c_7 T_{evap}^2 T_{cond} + c_8 T_{evap} T_{cond}^2 + c_9 T_{evap}^2 T_{cond}^2 \end{aligned} \tag{3.1}$$

and

$$\begin{aligned}\dot{W} &= d_1 + d_2 T_{evap} + d_3 T_{evap}^2 + d_4 T_{cond} + d_5 T_{cond}^2 + d_6 T_{cond} T_{evap} \\ &\quad + d_7 T_{evap}^2 T_{cond} + d_8 T_{evap} T_{cond}^2 + d_9 T_{evap}^2 T_{cond}^2 \end{aligned} \tag{3.2}$$

Table 3.1: Constants in Eqs (3.1) and (3.2)

c_1=137.402	d_1=1.00618
c_2=4.60437	d_2=-0.893222
c_3=0.061652	d_3=-0.01426
c_4=-1.118157	d_4=0.870024
c_5=-0.001525	d_5=-0.0063397
c_6=-0.0109119	d_6=0.03389
c_7=-0.00040148	d_7=-0.00023875
c_8=-0.00026682	d_8=-0.00014746
c_9=0.000003873	d_9=0.0000067962

The constants applicable to Eq. (3.1) and Eq. (3.2) for the above mentioned compressor is shown in Table 3.1. The rate of heat rejection required at the condenser is given by the sum of the refrigeration capacity and compressor power, for a given combination of evaporating and condensing temperatures

$$\dot{Q}_{cond} = \dot{Q}_{evap} + \dot{W} \tag{3.3}$$

The condenser performance, assuming a constant heat exchanger effectiveness for Bohn Heat Transfer Division air-cooled condenser, refrigerant 22, model number 36 was represented by [41]

$$\dot{Q}_{cond} = 9.39(T_{cond} - T^{in}_{cond}) \tag{3.4}$$

The evaporator refrigeration capacity for a Dunham-Bush, refrigerant 22, direct-expansion, inner-fin liquid chiller (CH660B) was represented by [41]

$$\dot{Q}_{evap} = 6.0[1 + 0.046(T^{in}_{evap} - T_{evap})](T^{in}_{evap} - T_{evap}). \tag{3.5}$$

The above set of equations can be been solved simultaneously for a given T^{in}_{evap} and T^{in}_{cond} by utilizing the Information-flow diagram shown in Fig. 3.3.

3.1.1 Performance Evaluation of the Actual System

The plot between $1.0/COP$ and $1.0/\dot{Q}_{evap}$ can be defined as characteristic chiller performance curves. The characteristic curves of the actual reciprocating chiller described in the previous section are shown in Fig. 3.4(a) for various values of the condenser inlet temperatures. The corresponding variation of the various temperatures of the system for $T^{in}_{cond} = 313\ K$ is shown in Fig. 3.4(b). The curve for an ideal CFC-22 model and the Carnot model is also shown in the same figure. The difference between the COP values of the ideal cycle model and the Carnot model is mainly due to non-isentropic losses in the expansion valve. The figure shows that there is an approximately a linear relation between the evaporator capacity and the COP of the system, for a range of evaporator capacities shown in the figure. The temperature difference between T^{in}_{cond} and T_{cond}, and T^{in}_{evap} and T_{evap} decreases as the evaporator capacity decreases, hence the irreversibilities due to finite temperature difference in the heat exchangers decrease as the evaporator capacity decreases. Therefore, the degradation in COP due to the finite temperature difference in the heat exchangers at the reduced evaporator capacity, is not significant, however the decrease in the COP is mainly due to the non-isentropic losses in the compressor and expansion valve. This fact can also be seen if the ideal CFC-22 model curve is

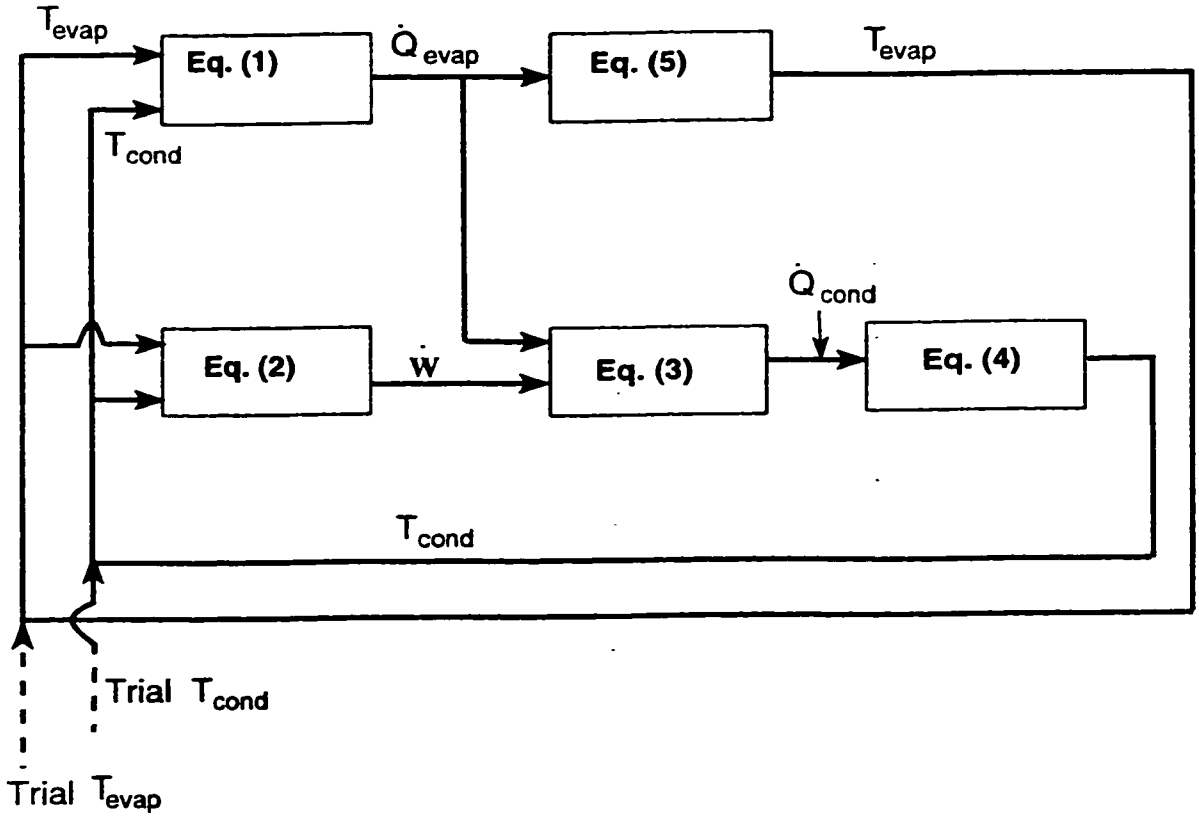

Figure 3.3: Information flow diagram

compared with its corresponding actual curve, the two curves for $T^{in}_{cond} = 313\ K$ are approximately parallel to each other which shows that the reduced COP is mainly due to the temperature difference $(T_{cond} - T_{evap})$ at low cooling capacities (refer to Fig. 3.4(b)).

The deviations of an actual refrigeration system with respect to an ideal reversible refrigeration system can also be explained by the refrigerating efficiency η_{refg} defined as

$$\eta_{refg} = \frac{COP}{COP_{Carnot}} \tag{3.6}$$

Fig. 3.5 shows the variations in refrigerating efficiency of the system described earlier in Fig. 3.4 as a function of $1.0/\dot{Q}_{evap}$ and T^{in}_{cond}. As expected, the efficiency decreases with the increase in capacity due to the increased irreversible losses in the heat exchangers at high refrigerating capacities (refer to Fig. 3.4(b)). However, at a fixed evaporator capacity, the efficiency increases with the increase in T^{in}_{cond}, since the irreversible losses increase with the reduced T^{in}_{cond}.

3.2 Analysis of the Cycle

Referring to Fig. 3.1, from the first law of thermodynamics and the fact that the change in internal energy is zero for a cyclic process, we can write

$$\dot{Q}_{cond} + \dot{Q}^{loss}_{cond} - (\dot{Q}_{evap} + \dot{Q}^{loss}_{evap}) - (\dot{W} - \dot{Q}^{loss}_{W}) = 0 \tag{3.7}$$

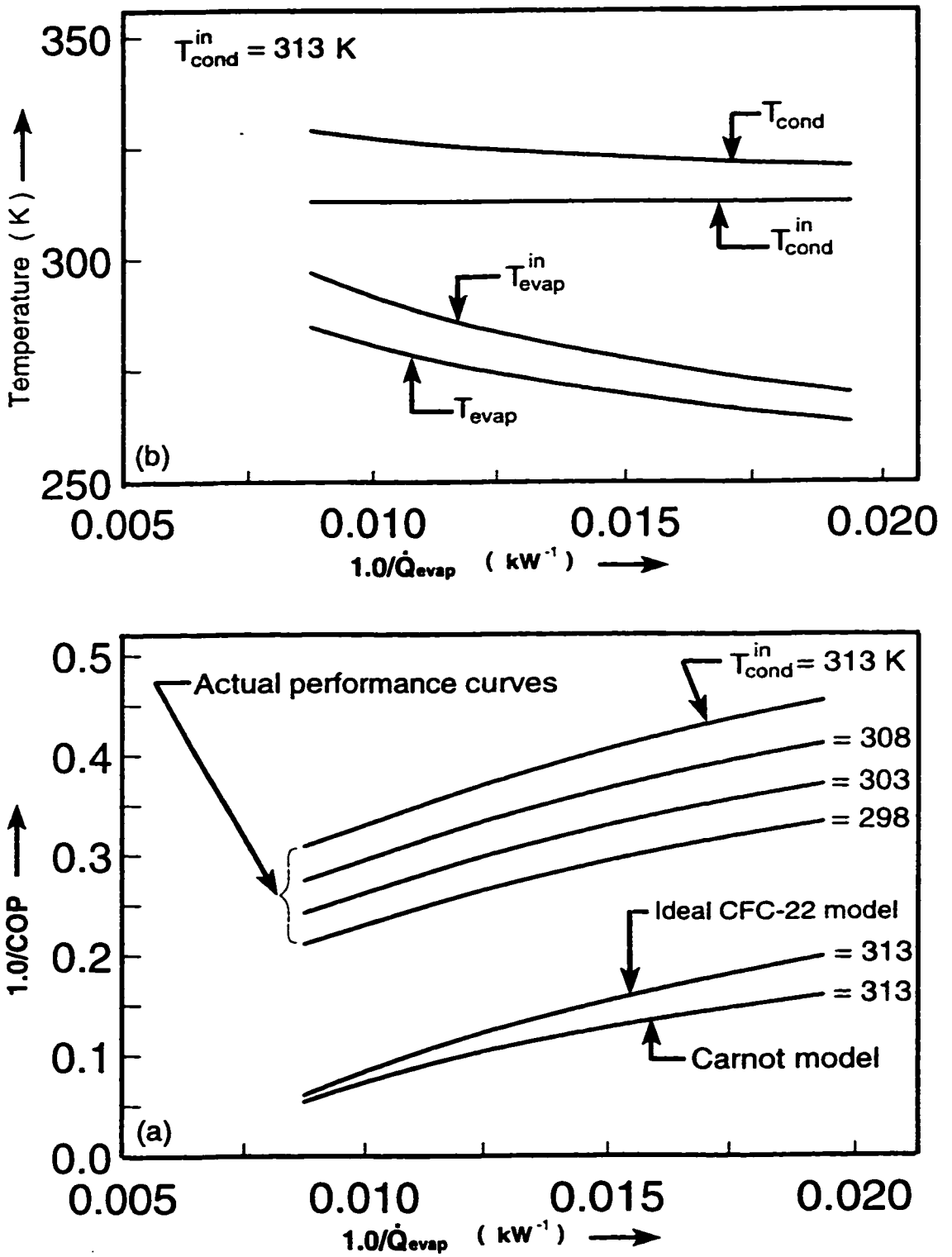

Figure 3.4: Performance curves (a), and variation of temperature for an actual vapor compression system (b).

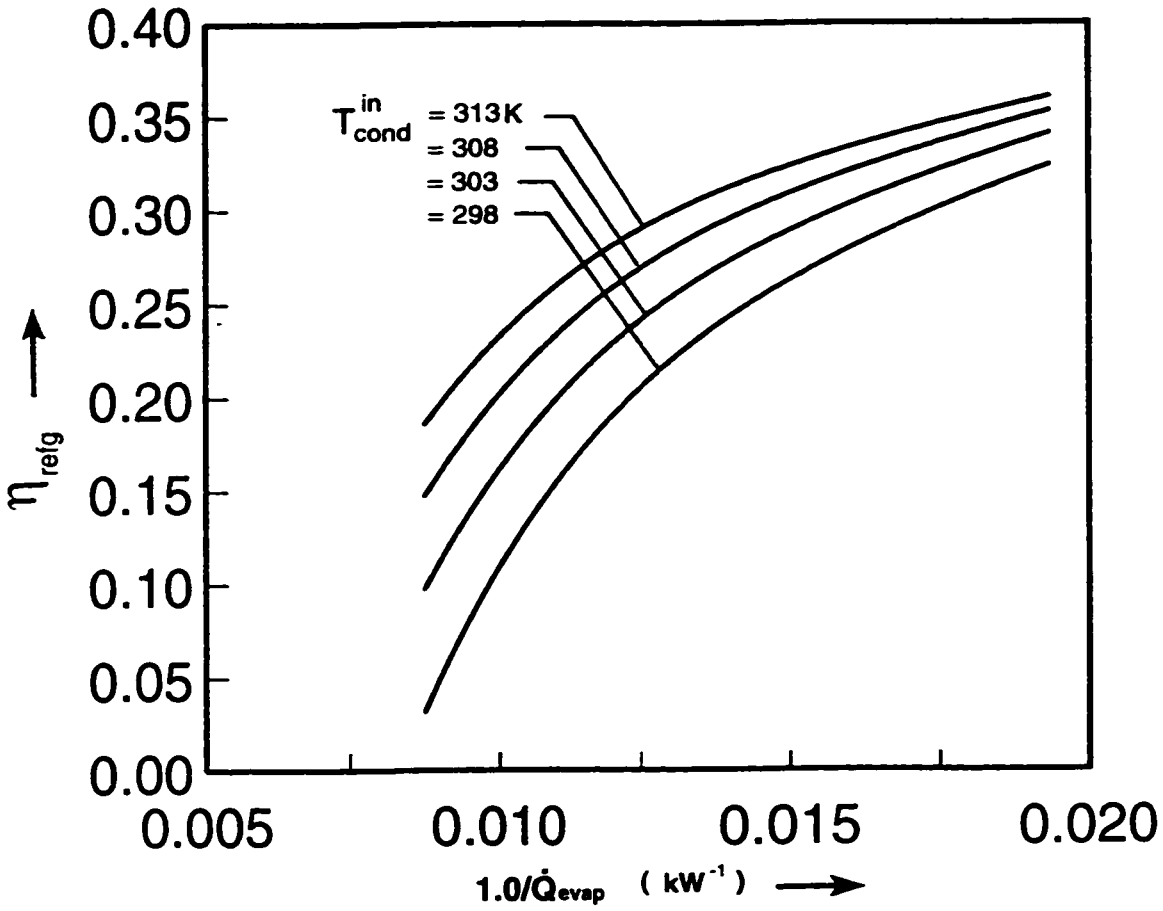

Figure 3.5: Variation of refrigerating efficiency with cooling capacity for an actual vapor compression system

Since entropy is a state function, it's net change over the cycle is zero. Therefore the contributions to the entropy generation are from heat transfer (at the condenser and evaporator) and the entropy generation due to non-isentropic compression and expansion in the compressor and the expansion valve, respectively. It can be expressed as

$$\frac{\dot{Q}_{cond} + \dot{Q}_{cond}^{loss}}{T_{cond}} - \frac{\dot{Q}_{evap} + \dot{Q}_{evap}^{loss}}{T_{evap}} - \dot{S}_{igen} = 0 \qquad (3.8)$$

The heat transfer to and from the cycle occur by convection to flowing fluid streams having finite mass flow rates and specific heats. Therefore, the rate of heat transfer to the cycle at the low temperature in the evaporator can be written as

$$\dot{Q}_{evap} = (\varepsilon \dot{C})_{evap}(T^{in}_{evap} - T_{evap}) \tag{3.9}$$

Where ε is the heat exchanger effectiveness defined by Kays and London [42].

Similarly the rate of heat transfer between the refrigeration cycle and the sink in the condenser is

$$\dot{Q}_{cond} = (\varepsilon \dot{C})_{cond}(T_{cond} - T^{in}_{cond}) \tag{3.10}$$

From Eq. (3.7) we have

$$\dot{W} = \dot{Q}_{cond} + \dot{Q}^{loss}_{cond} - (\dot{Q}_{evap} + \dot{Q}^{loss}_{evap}) + \dot{Q}^{loss}_{W}$$

Defining the COP as refrigerating effect over the net work input

$$COP = \frac{\dot{Q}_{evap}}{\dot{W}}$$

and expressing refrigeration temperatures in terms of the more readily available coolant temperatures one obtains an analytic formula for COP, as a function of cooling capacity, coolant temperatures, heat exchanger characteristics, heat leak terms and internal cycle losses as [15]

$$\frac{1}{COP} = \{-1 + \frac{T^{in}_{cond}\dot{S}_{igen} + \dot{Q}^{loss}_{w} - \dot{Q}^{loss}_{evap}}{\dot{Q}_{evap}}$$

$$
+\left[1+\frac{\dot{Q}^{loss}_{evap}}{\dot{Q}_{evap}}\right]\left[\frac{\frac{T^{in}_{cond}}{\dot{Q}_{evap}}}{\frac{T^{in}_{evap}}{\dot{Q}_{evap}}-\frac{1}{(\varepsilon\dot{C})_{evap}}}\right]
$$

$$
+\frac{1+\frac{\dot{Q}^{loss}_{evap}+\dot{Q}^{loss}_{s}}{\dot{Q}_{evap}}+\frac{\dot{Q}^{loss}_{s}\dot{Q}^{loss}_{evap}}{\dot{Q}^{2}_{evap}}}{(\varepsilon\dot{C})_{cond}\left[\frac{T^{in}_{evap}}{\dot{Q}_{evap}}-\frac{1}{(\varepsilon\dot{C})_{evap}}\right]}
$$

$$
+\frac{\dot{S}_{igen}}{(\varepsilon\dot{C})_{cond}}\left[1+\frac{\dot{Q}^{loss}_{s}}{\dot{Q}_{evap}}\right]\}
$$

$$
\cdot\{1-\frac{\dot{S}_{igen}}{(\varepsilon\dot{C})_{cond}}
$$

$$
-\frac{\left[1+\frac{\dot{Q}^{loss}_{evap}}{\dot{Q}_{evap}}\right]}{(\varepsilon\dot{C})_{cond}\left[\frac{T^{in}_{evap}}{\dot{Q}_{evap}}-\frac{1}{(\varepsilon\dot{C})_{evap}}\right]}\}^{-1} \qquad (3.11)
$$

In the above expression, if $\dot{S}_{igen}$ and heat leaks are equated to zero, the expression obtained will represent a thermodynamic model derived earlier by Klein [10].

Gordon et al. [15] have drawn characteristic performance curves using Eq. (3.11) for the input data shown in Table 3.2. The data given is from the experimental measurements of their water-cooled chiller. These plots are shown in Fig. 3.6.

The upper-most curve is calculated using Eq. (3.11) based on the above data. The next two lower curves are calculated from the pure thermodynamic chiller model (that is, the finite-rate heat transfer being the sole irreversibility), and from a thermodynamic chiller model with heat leaks. The lowest curve in the plot is for a carnot cycle for which COP is constant for all the values of the evaporator capacity.

Figure 3.6 is a hypothetical performance curve obtained by assuming a constant

Table 3.2: Input data for drawing chiller performance curve, shown in Fig. 3.6, obtained from [15]

Condenser inlet temperature	T_{cond}^{in}	$29.43°C$
Evaporator inlet temperature	T_{evap}^{in}	$12.39°C$
Work input to the compressor	$\dot{W}$	$3.98[KW]$
Rate of heat leak from hot refrigerant to ambient at the condenser	$\dot{Q}_{cond}^{loss}$	$0.006[KW]$
Rate of heat leak from ambient to the cold refrigerant at the evaporator	$\dot{Q}_{evap}^{loss}$	$0.219[KW]$
Rate of heat leak from compressor shell to ambient	$\dot{Q}_{W}^{loss}$	$0.195[KW]$
Internal entropy generation due to non isentropic compression and expansion	$\dot{S}_{igen}$	$0.00511[KWK^{-1}]$
Effectiveness-capacitance rate product for the condenser	$(\varepsilon\dot{C})_{cond}$	$0.838[KWK^{-1}]$
Effectiveness-capacitance rate product for the evaporator	$(\varepsilon\dot{C})_{evap}$	$0.594[KWK^{-1}]$

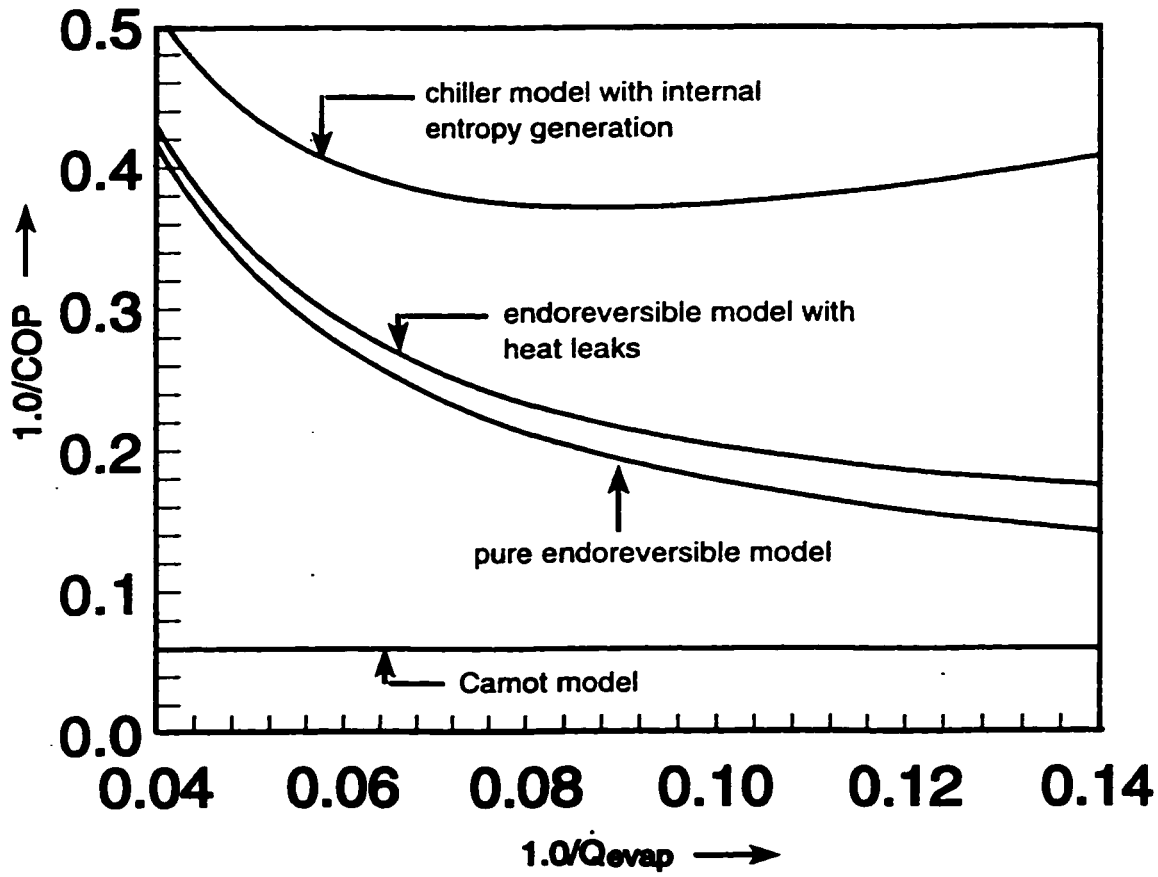

Figure 3.6: Performance curves for the water-cooled reciprocating chiller reported in [15], for CFC-22

value of T^{in}_{evap} (see Table 3.2) for the range of evaporator capacity $\dot{Q}_{evap}$ shown in the figure. However, the figure shows that at very high evaporator capacities the COP of the system is decreasing due to the increased irreversible losses resulting from the finite rate of heat transfer in the heat exchangers, as explained in section (3.1.1) of this chapter. Also at very low evaporator capacity COP is decreasing but at a lesser rate due to the non-isentropic compression and expansion in the compressor and the expansion valve of the system respectively. There is an intermediate range of cooling capacities in which COP passes through a maximum value.

Figs. 3.4 and 3.6 shows that the qualitative features for real chillers are such that COP should increase with cooling rates at low cooling rates due to irreversibilities such as fluid friction (some times referred to as isentropic losses since adiabatic compression and expansion processes that would ideally occur isentropically actually generate entropy). Losses that stem from finite-rate heat transfer will dominate at high cooling rates, so that COP should decrease as cooling rate increases.

3.3 A Finite Time Thermodynamic Model of the System

As mentioned earlier the heat transfer to and from the cycle occur by convection to flowing fluid streams having finite fluid capacitance rate ($\dot{C} = \dot{m}C_p$). Therefore,

the rate of heat transfer to the cycle in the evaporator can be expressed in terms of temperatures, and mass flow rate and change in enthalpy as

$$\dot{Q}_{evap} = (\varepsilon \dot{C})_{evap}(T^{in}_{evap} - T_{evap}) = \dot{m}_{ref}(h_2 - h_3) \tag{3.12}$$

Similarly the rate of heat transfer between the refrigeration cycle and the sink in the condenser is

$$\dot{Q}_{cond} = (\varepsilon \dot{C})_{cond}(T_{cond} - T^{in}_{cond}) = \dot{m}_{ref}(h_6 - h_1) \tag{3.13}$$

The compressor operation is described in terms of an isentropic efficiency, η_{comp}, so that its power requirement is given by

$$\dot{W} = \dot{m}_{ref}(h_5 - h_4) = \frac{\dot{W}_s}{\eta_{comp}} \tag{3.14}$$

From Eq. (3.7) work input to the compressor can also be expressed as

$$\dot{W} = \dot{Q}_{cond} + \dot{Q}^{loss}_{cond} - (\dot{Q}_{evap} + \dot{Q}^{loss}_{evap} + \dot{Q}^{loss}_{W}) \tag{3.15}$$

Assuming that an amount of $\dot{Q}^{loss}_{evap}$ of heat, leaks into the suction line, which can be expressed as

$$\dot{Q}^{evap}_{loss} = \dot{m}_{ref}(h_4 - h_3) \tag{3.16}$$

Similarly assuming that an amount of $(\dot{Q}^{loss}_{cond} + \dot{Q}^{loss}_{W})$ of heat leaks from the discharge line, given by

$$\dot{Q}^{loss}_{cond} + \dot{Q}^{loss}_{W} = \dot{m}_{ref}(h_6 - h_5) \tag{3.17}$$

The Coefficient of Performance (COP) is defined as the refrigerating effect over the net work input, i.e.,

$$COP = \frac{\dot{Q}_{evap}}{\dot{W}} \tag{3.18}$$

To solve the above set of Equations numerically, a complete set of thermodynamic properties is required. A computer program written by Kartsounes and Erth [43] and modified by Fisher and Rice [44] is available for calculating the thermodynamic properties of CFC-12, CFC-502 and CFC-22. Wilson and Basu [45] determined the thermodynamic properties of CFC-134a by performing experimental measurements. They have developed equations to describe the thermodynamic properties of CFC-134a, which can be tabulated by using these equations. In this regard, Khan [26] and Khan and Zubair [46] have carried out modifications in the existing computer programs to calculate the thermodynamic properties of HFC-134a. The calculated values of the thermodynamic properties are in excellent agreement with the data presented by McLinden et al. [47]. The flow chart representing the method of solving the equations is shown in Fig. 3.7, wherein the terms SATPRP and TRIAL represents the subroutines for calculating the refrigerant saturated and vapor properties, respectively, given any two independent intensive properties of the refrigerant. The program gives the COP and all other parameters of the system for the following set of input data: $\dot{Q}_{evap}$, $(\varepsilon\dot{C})_{cond}$, $(\varepsilon\dot{C})_{evap}$ and η_{comp}.

Figure 3.8 shows the characteristic chiller performance curve obtained by using

the model for $T_{cond}^{in} = 313.0\ K$ and $\eta_{comp} = 0.65$, while the curve obtained by using the actual performance of the system described in section (3.1) is also shown in the same figure. It can be seen from the figure that the two curves nearly overlap, indicating the validity of an endoreverisble model. We emphasize that the discrepancy with the actual values is mainly due to the fact that the compressor efficiency of an actual system is a function of the evaporator and condenser pressures, whereas in the present analysis it is taken as a constant representative value [25].

As an additional check for the model the data from the water to water heat pump, reported by Kuehn and Liang [48] was fed to the model, the values of the parameters obtained from the model was checked with the actual values given in their paper. The results of the comparison are summarized in Table 3.3. It can be seen from the table that the predicted and the experimental values agree very closely. Thus further confirming that model can be used for design and evaluation purpose.

3.4 Performance of a Variable Speed System

The performance characteristics of a refrigeration system in which the evaporator capacity is varied by varying the speed of the compressor is shown in Fig. 3.9. The curves shown in the figure were plotted for the following set of input data:

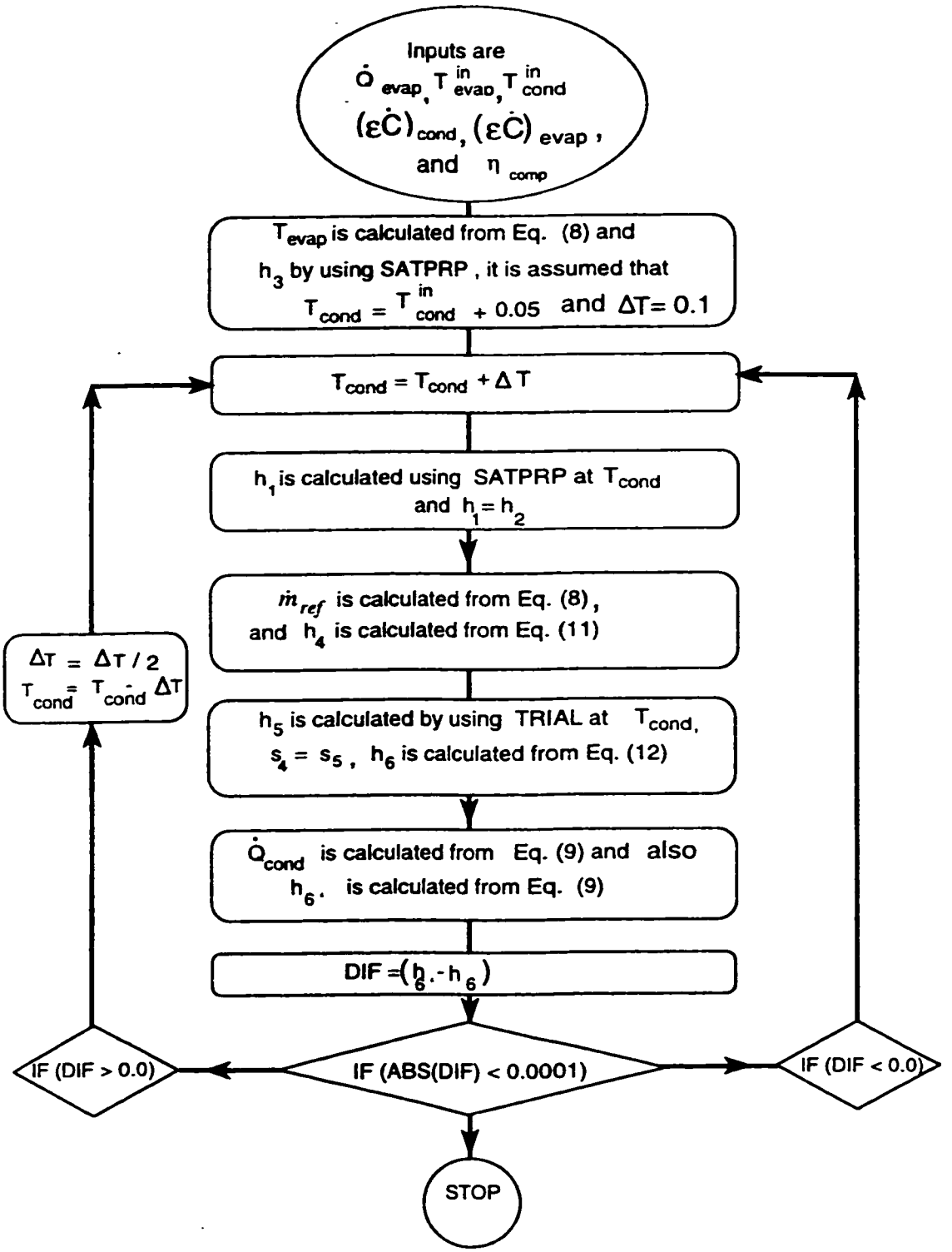

Figure 3.7: Flow chart for the thermodynamic model

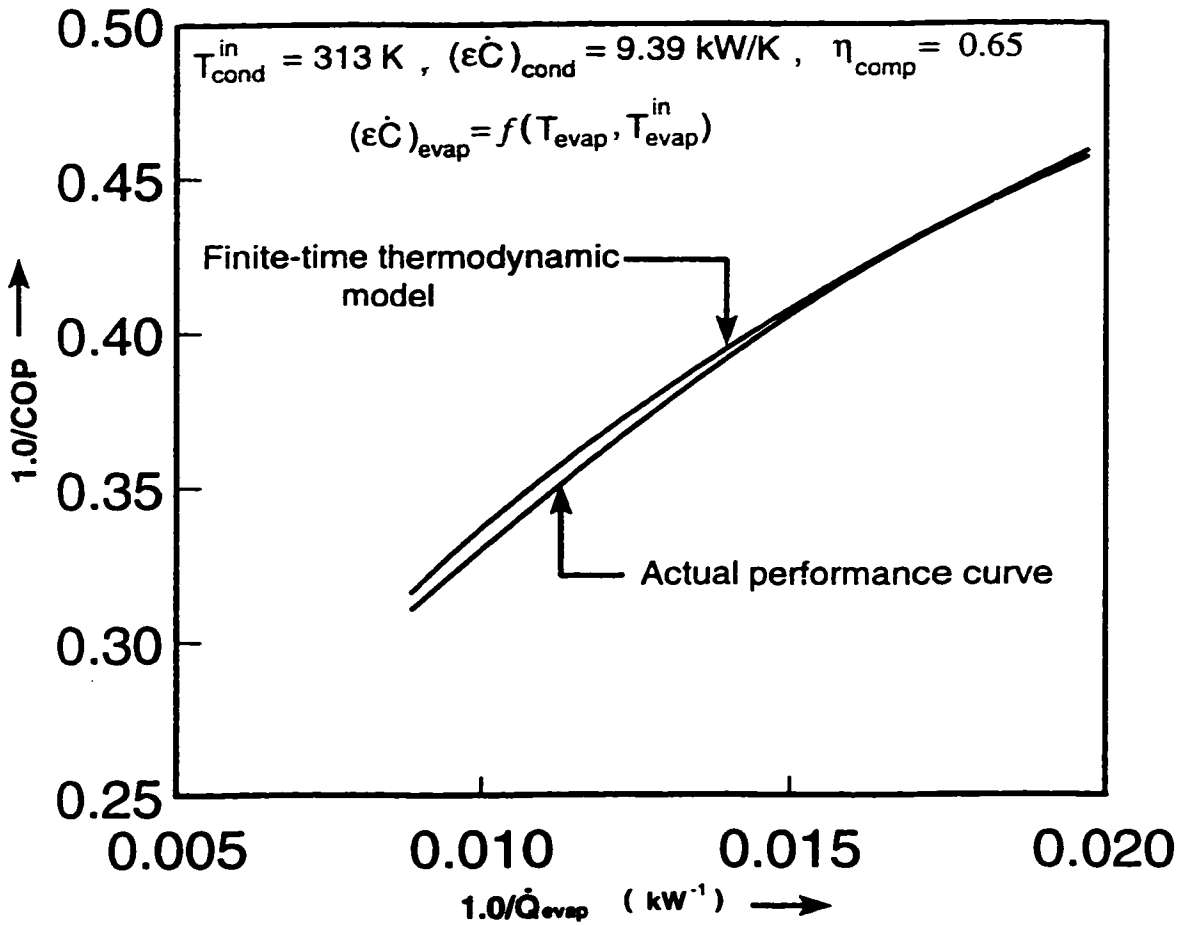

Figure 3.8: Performance curves of the actual system and the thermodynamic model

Table 3.3: Experimental and calculated values for water-to-water heat pump, as reported in [48]

System parameters	Experimental value	Calculated value
Inverse coefficient of performance, $(1.0/COP)$	0.263	0.263
Mass flow rate, $(\dot{m})$	0.041 kg/s	0.042 kg/s
Evaporator temperature, (T_{evap})	269.2 K	270.2 K
Condenser temperature, (T_{cond})	293.8 K	294.2 K
Pressure ratio across the compressor	2.45	2.14
Heat lost in the condenser, (Q_{cond})	9.47 kW	9.25 kW

$T^{in}_{evap} = 277\ K$, $T^{in}_{cond} = 313\ K$, $(\varepsilon\dot{C})_{cond} = 9.39\ kW/K$, $(\varepsilon\dot{C})_{evap} = 8.1975\ kW/K$ and $\eta_{comp} = 0.65$. The variation of system temperatures and the mass flow rate of the system are also shown in the figure. It should be noted that for an actual system as the capacity of the system varies the performance of the compressor and heatexchangers, represented by η_{comp} and ε, respectively, will not be constant. However for the present investigation, we have considered these parameters to be constant.

It can be seen from Fig. 3.9 that at high evaporator capacity the refrigerant mass flow rate through the system is increased and thus the temperature difference in the heat exchangers is also high. Therefore, the losses due to the finite temperature difference in the heat exchangers are also high and hence the COP is reduced. But as the capacity is decreased, the temperature difference in the heat exchangers also decreases, therefore the losses due to the finite rate of heat transfer also decreases and the COP of the system increases.

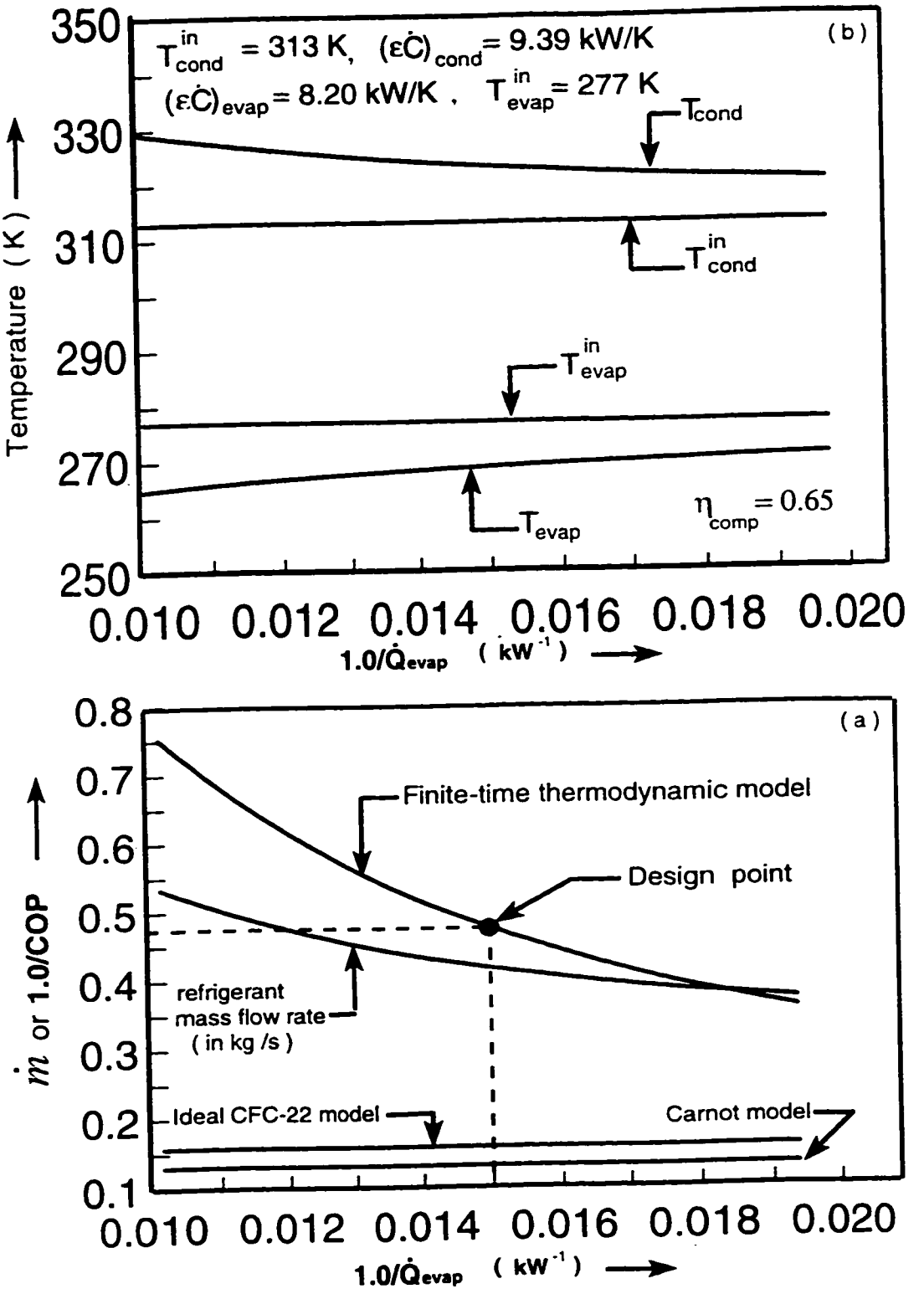

Figure 3.9: Performance curves (a) and variation of temperatures for a variable frequency model (b).

Figure 3.10 shows the variations in refrigerating efficiency for the actual system, and the variable speed system. As expected, the efficiency decreases with the increase in capacity due to the increased irreversible losses in the heat exchangers at high evaporator capacity (refer to Fig. 3.9(b)). However, the figure shows that for refrigerating capacity greater than the design point value, the efficiency of a variable speed system is greater than that of the actual system, whereas for lower capacities the actual system is predicting greater efficiency than the variable speed system.

3.5 Effect of Subcooling and Superheating

The superheating of the refrigerant (after exiting the evaporator and before entering the compressor), may occur due to the heat gain in the line joining the evaporator and compressor. This heat gain process is shown from state (3) to (4) in Fig. 3.2. We note that the specific volume of the vapor is increased due to superheating and it reduces the mass flow rate through the fixed displacement compressor. On the other hand, subcooling is cooling of the refrigerant beyond the saturated state after exiting the condenser and before entering the expansion valve. Again, this normally occurs due to heat losses in the line joining the condenser and expansion valve. We expect that subcooling increases the performance of the system because the specific refrigeration capacity increases with subcooling. Fig. 3.11 shows the

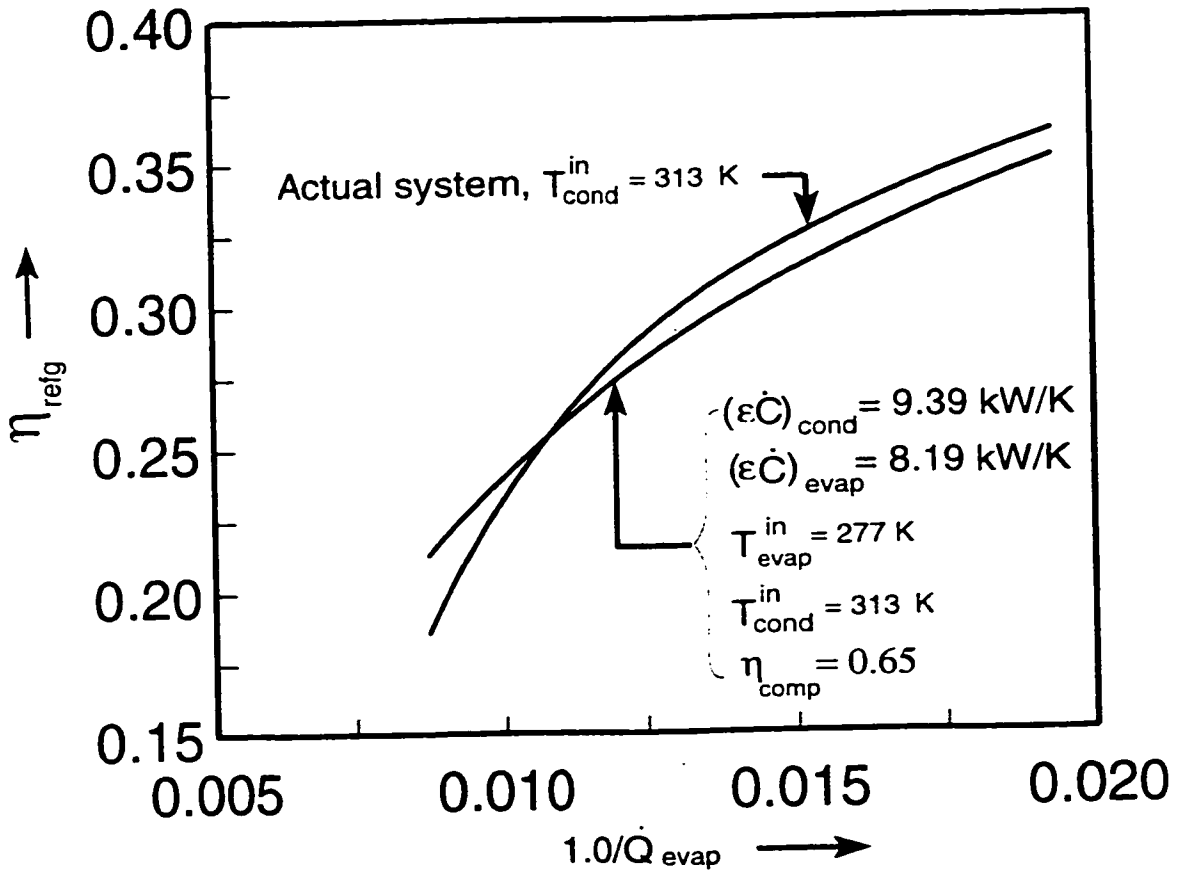

Figure 3.10: Variation of refrigerating efficiency with cooling capacity for a variable speed refrigeration system

individual effect of superheating, subcooling and both superheating and subcooling together. As expected, the superheating degrades the performance of the system, while the subcooling improves the COP of the system. When we take equal amount of superheating and subcooling, the performance degrades. Therefore, it indicates that for the given operating condition, the effect of superheating have more influence on the system overall performance.

3.6 Optimum Distribution of Heat Exchanger Area

The design of a refrigeration system involves proper selection of the external stream capacitance rates and the heat exchanger size. The heat exchanger effectiveness given by ε represents the heat exchanger surface area. The product $(\varepsilon\dot{C})$ of both the heat exchangers of the system is an expensive commodity and it determines the overall cost of the system. Increasing the size of the heat exchanger increases the overall performance of the system but it also increase the cost of the system, hence a compromise is sought between the first cost and the operating cost of the system. Generally chiller's total heat exchanger area defined in terms of

$$\kappa = (\varepsilon\dot{C})_{cond} + (\varepsilon\dot{C})_{evap} \tag{3.19}$$

is considered as the design constraint and the problem involved in the optimization is how to allocate the total heat exchanger area between the two heat exchangers so that maximum performance of the system is obtained. The above problem can

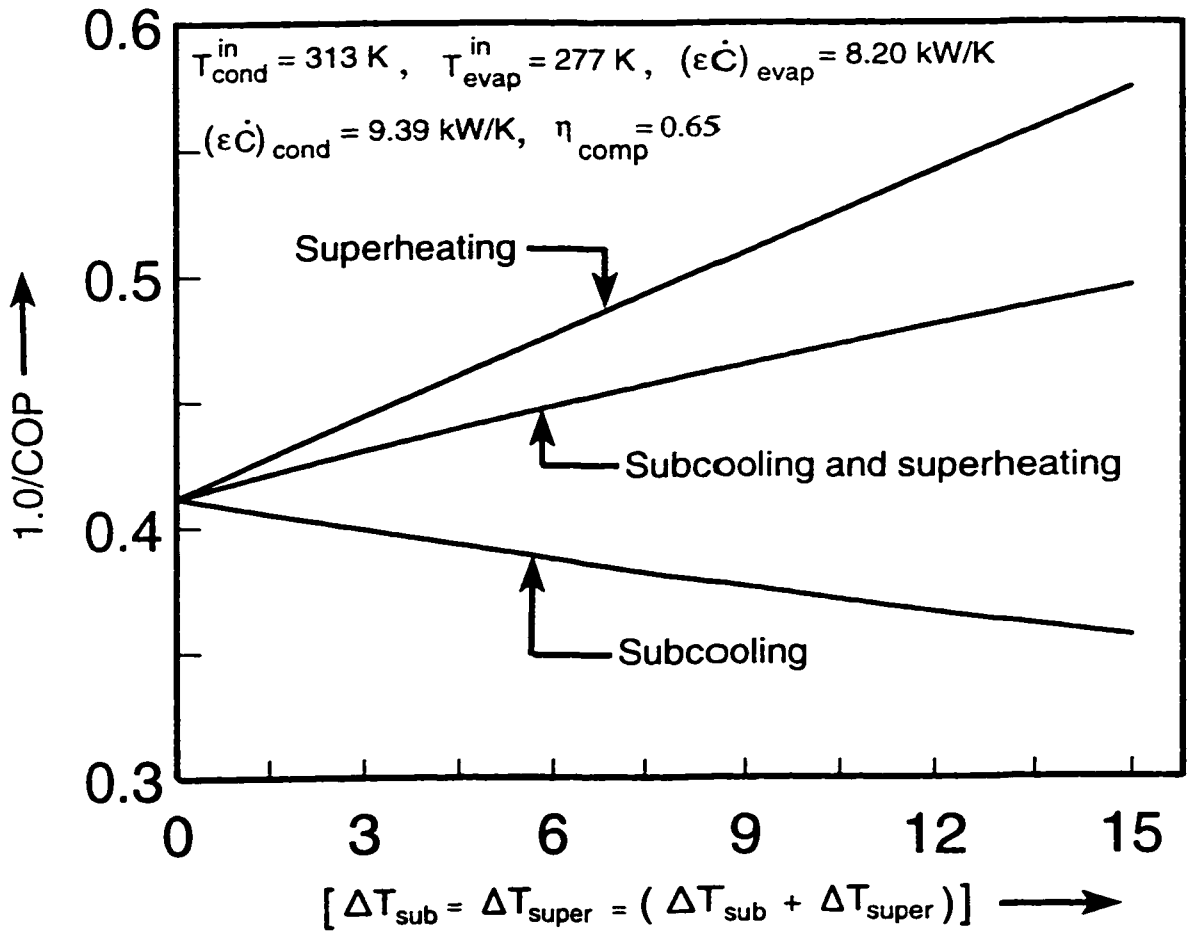

Figure 3.11: Effect of superheating and subcooling on the performance of simple vapor compression system

be solved by using the thermodynamic model presented earlier. the model simulates the working of an actual reciprocating systems very closely.

To investigate the effect of relative size of heat exchangers a factor f_h as defined by Klein [10]. is used to study the variation of (COP). It is given by

$$f_h = \frac{(\varepsilon \dot{C})_{cond}}{(\varepsilon \dot{C})_{cond} + (\varepsilon \dot{C})_{evap}} \tag{3.20}$$

A sample plot. shown in Fig. 3.12. is drawn between $1.0/COP$ and f_h using the output from the model. for the following set of input data and using CFC-22 as the refrigerant. $\dot{Q}_{evap} = 10.0\ KW$, $T^{in}_{evap} = 273.0\ K$ and $T^{in}_{cond} = 313.0\ K$. It is seen from the plot that as the value of heat exchangers inventory (κ) is increased beyond 200.0. the COP of the system reaches a constant value and is equal to the COP of an ideal refrigerant cycle for the same input conditions. Notice that the Carnot model and the ideal cycle model will have a constant COP values for all the values of f_h since the irreversibilities due to finite rate of heat transfer are not present in these models.

Figure 3.13 shows a plot between f_h and $1.0/\dot{Q}_{evap}$ for the actual simple vapor compression system, discussed earlier in section (3.1) of the chapter. The value of f_h is higher for lower evaporator capacity indicating that greater portion of the total heat exchanger area is allocated to the condenser and *vice-versa* for higher evaporator capacity. It should be noted that the curves for $T^{in}_{cond} = 298, 303, 308, 313\ K$. are very close to each other. indicating that the actual system is operating very close to

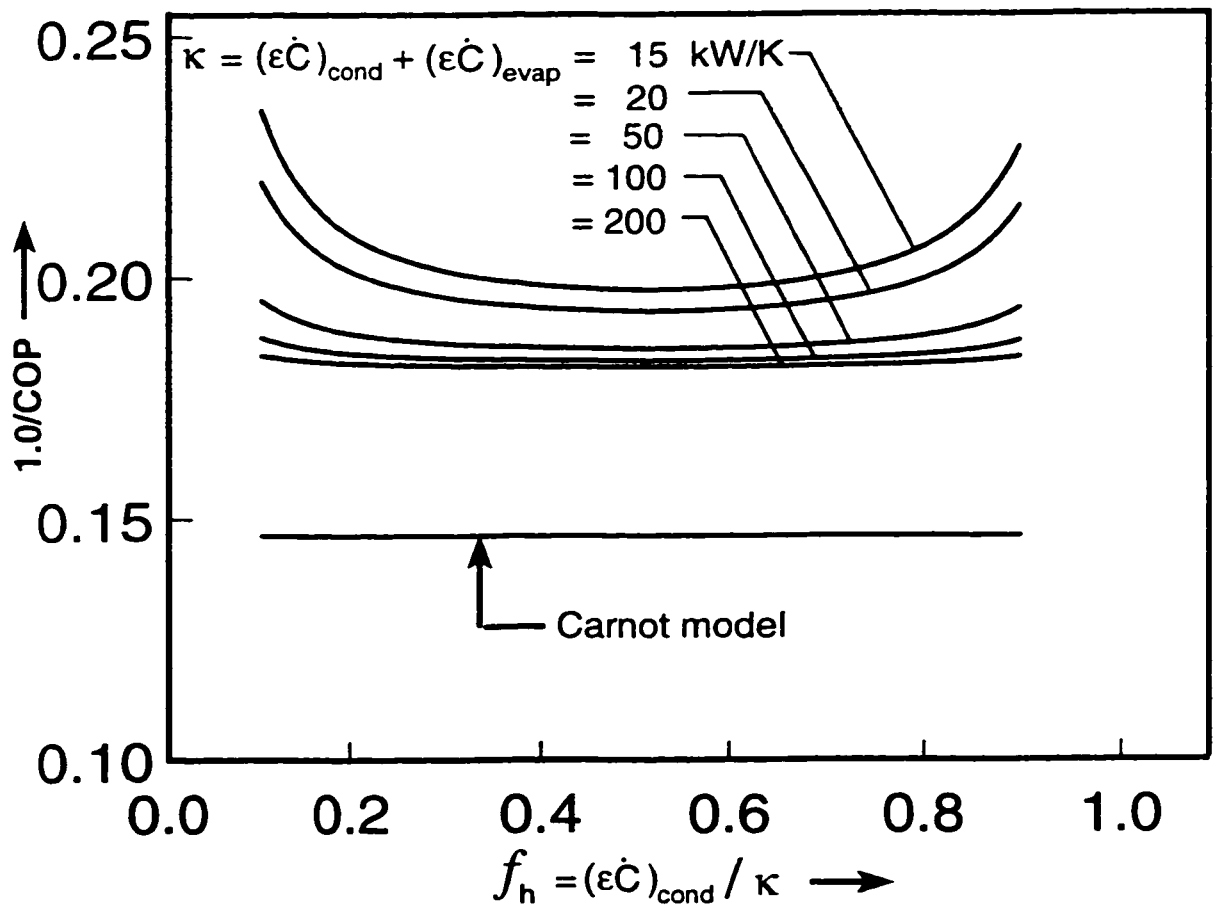

Figure 3.12: Plot between 1.0/COP and f_h obtained using the thermodynamic model

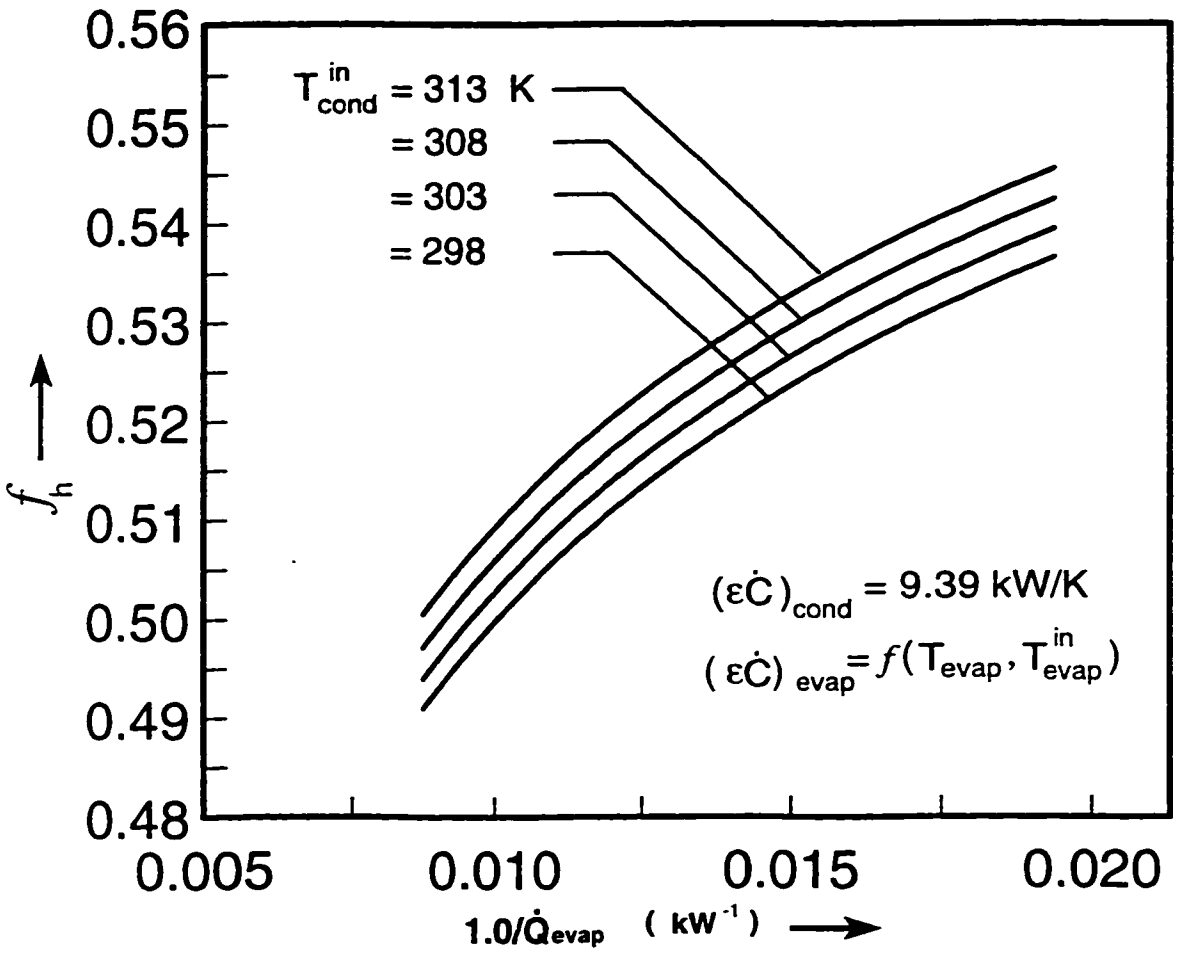

Figure 3.13: Plot between f_h and $1.0/\dot{Q}_{evap}$ for the actual system

optimum value of f_h for all the values of T^{in}_{cond}.

Chapter 4

Thermodynamic Analysis of a Dedicated Mechanical Subcooling Vapor Compression Refrigeration System

The major components of a dedicated mechanical subcooling system include two reciprocating compressors, two expansion valves, two condensers, an evaportor and a subcooler. The system consists of two simple cycles coupled to each other via a subcooler as shown in Fig. 4.1, while the pressure-enthalpy diagram is shown in Fig. 4.2. 4.2. The upper cycle is known as the subcooler cycle and the lower cycle is known as the main cycle. In practice, the components of the subcooler cycle are

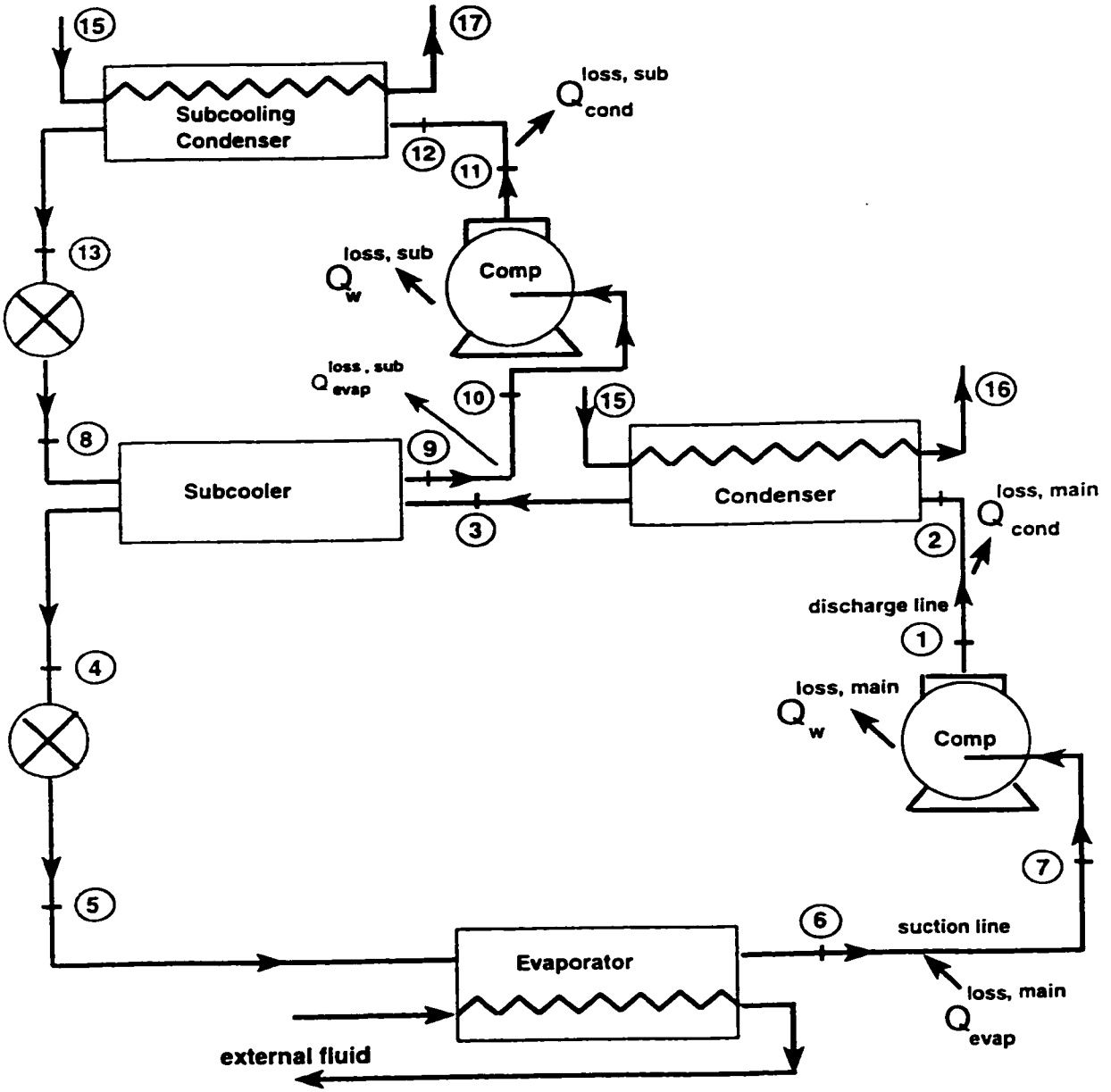

Figure 4.1: Schematic diagram of a dedicated mechanical subcooling refrigeration cycle

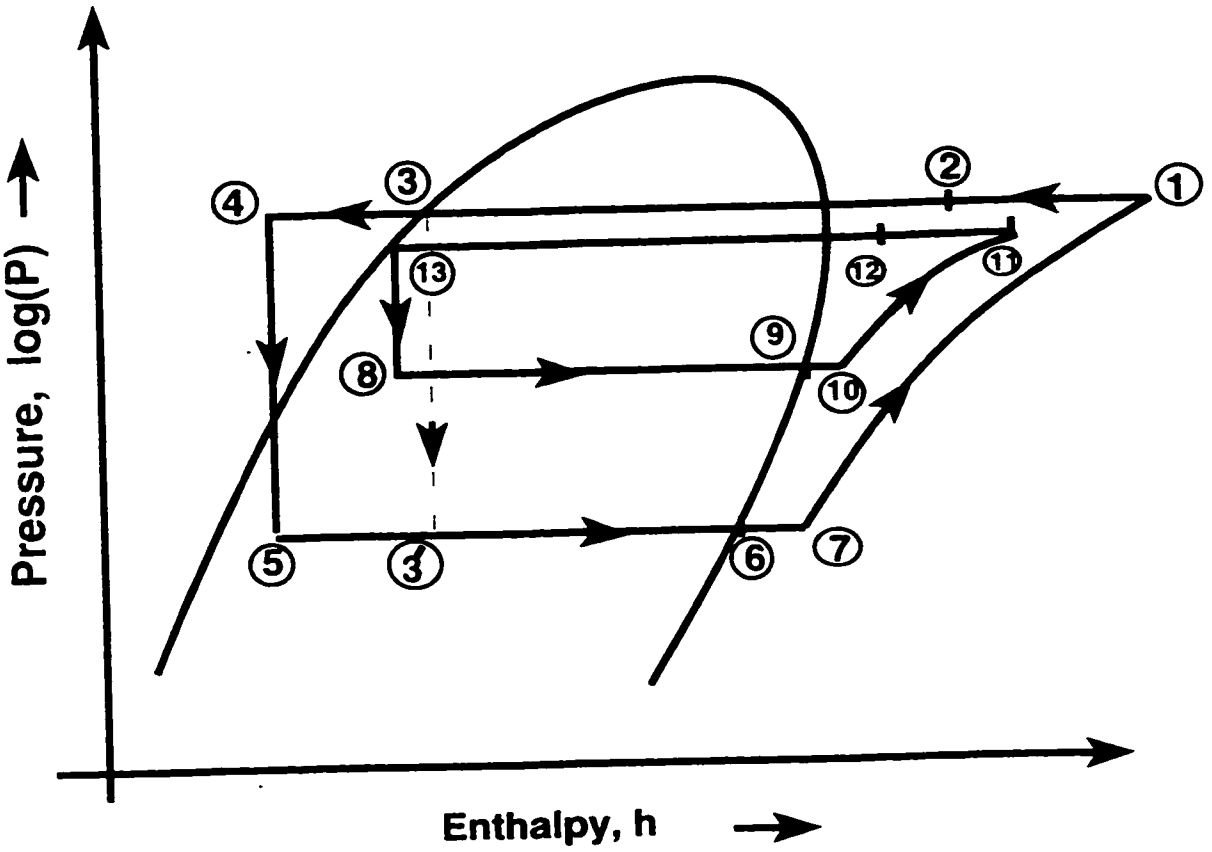

Figure 4.2: Pressure-enthalpy diagram of a dedicated mechanical subcooling refrigeration system

smaller than those of the main cycle. The system can have either the same refrigerant or different refrigerants flowing through the two cycles. The components of the two cycles are connected in a closed loop through a piping system that has heat transfer with the surroundings. The figure shows that the main cycle refrigerant leaves the main cycle evaporator at state point 6 as a low pressure, low temperature, saturated vapor and enters the main cycle compressor at state point 7. The refrigerant, from state point 6 to point 7 takes heat from the surroundings in the suction line. At state point 1, it leaves the compressor as a high temperature, high pressure, superheated vapor and enters the main cycle condenser. The refrigerant, from state point 1 to point 2 rejects heat to the surroundings in the discharge line. At point 3, the main cycle refrigerant leaves the main cycle condenser as a high pressure, saturated liquid which enters the subcooler. In the subcooler, it is cooled below the saturated liquid state at a constant pressure, and enters the main cycle expansion valve. At point 5 it leaves the expansion valve as a low quality vapor and enters the evaporator, where it is evaporated at a constant pressure to the saturated vapor state.

The subcooler cycle refrigerant after cooling the main cycle refrigerant in the subcooler, leaves as a low pressure, low temperature, saturated vapor at state point 9 and enters the subcooler cycle compressor at state point 10. The refrigerant from state point 9 to point 10 takes heat from the surroundings. At point 11, it leaves the

compressor as a superheated vapor and enters the subcooler cycle condenser. The refrigerant from state point 11 to 12 rejects heat to the surrounding in the discharge line of the subcooler. At point 13 it leaves the condenser as a saturated liquid and enters the subcooler cycle expansion valve. At point 8 it leaves the expansion valve as a low quality vapor, and enters the subcooler.

4.1 Analysis of the Cycle

Referring to the main cycle loop in Fig. 4.1, from the first law of thermodynamics and the fact that the change in internal energy is zero for a cyclic process, we can write

$$(\dot{Q}_{cond}^{main} + \dot{Q}_{cond}^{loss,main}) - (\dot{Q}_{evap}^{main} + \dot{Q}_{evap}^{loss,main}) + \dot{Q}^{sub} + \dot{Q}_{W}^{loss,main} = \dot{W}^{main} \qquad (4.1)$$

Since entropy is a state function, its net change over the cycle is zero. Therefore, the contributions to the entropy generation are from heat trasfer (at the condenser, evaporator and the subcooler) and the entropy generation due to non-isentropic compression and expansion in the compressor and the expansion valve, respectively. It can be expressed as

$$\frac{(\dot{Q}_{cond}^{main} + \dot{Q}_{cond}^{loss,main})}{T_{cond}^{main}} - \frac{(\dot{Q}_{evap}^{main} + \dot{Q}_{evap}^{loss,main})}{T_{evap}^{main}} - (\dot{m}c_p)_{ref}^{main} ln[\frac{T^{out,sub}}{T_{cond}^{main}}] = \dot{S}_{igen}^{main} \qquad (4.2)$$

The heat transfer to and from the cycle occur by convection to flowing fluid streams having finite mass flow rates and specific heats. Therefore, the rate of heat transfer to the cycle at a low temperature in the main cycle evaporator can be written as

$$\dot{Q}_{evap}^{main} = (\varepsilon \dot{C})_{evap}^{main}(T_{evap}^{in.main} - T_{evap}^{main}) \tag{4.3}$$

Similarly the rate of heat transfer between the refrigeration cycle and the sink in the main cycle condenser is

$$\dot{Q}_{cond}^{main} = (\varepsilon \dot{C})_{cond}^{main}(T_{cond}^{main} - T_{cond}^{in.main}) \tag{4.4}$$

The rate of heat transfer between the main cycle refrigerant and the subcooler cycle refrigerant in the subcooler can be written as [49]

$$\dot{Q}^{sub} = (\dot{m}c_p)_{ref}^{main}(T_{cond}^{main} - T^{out.sub}) \tag{4.5}$$

Similarly for the subcooler loop all the equations describing the various processes in the cycle can be written as

$$(\dot{Q}_{cond}^{sub} + \dot{Q}_{cond}^{loss.sub}) - (\dot{Q}^{sub} + \dot{Q}^{loss.sub}) + \dot{Q}_{W}^{loss.sub} = \dot{W}^{sub} \tag{4.6}$$

$$\frac{(\dot{Q}_{cond}^{sub} + \dot{Q}_{cond}^{loss.sub})}{T_{cond}^{sub}} - \frac{(\dot{Q}^{sub} + \dot{Q}^{loss.sub})}{T^{sub}} = \dot{S}_{igen}^{sub} \tag{4.7}$$

$$\dot{Q}_{cond}^{sub} = (\varepsilon \dot{C})_{cond}^{sub}(T_{cond}^{sub} - T_{cond}^{in.main}) \tag{4.8}$$

$$\dot{Q}^{sub} = (\dot{m}c_p)_{ref}^{main}(\varepsilon)^{sub}(T_{cond}^{main} - T^{sub}) \tag{4.9}$$

Defining the COP_{total} as refrigerating effect over the net work input, we have

$$COP_{total} = \frac{\dot{Q}_{evap}^{main}}{\dot{W}^{main} + \dot{W}^{sub}} \tag{4.10}$$

substituting the expressions of $\dot{W}^{main}$ and $\dot{W}^{sub}$ from Eqs (4.1) and (4.6) in the above equation and expressing refrigeration temperatures in terms of the more readily available coolant temperatures, one obtains an analytical formula for the COP, as a function of cooling capacity, coolant temperatures, heat exchanger characteristics, heat leak terms, internal cycle losses and the exit temperature of the main cycle refrigerant from the subcooler, as

$$\frac{1}{COP} = -1$$

$$+\frac{(\dot{Q}_{cond}^{loss,main} - (\varepsilon\dot{C})_{cond}^{main} T_{cond}^{in,main})(\dot{S}_{igen}^{main} + (\dot{m}c_p)_{ref}^{main} ln[\frac{T^{out,sub}}{T_{cond}^{main}}] + \frac{\dot{Q}_{evap}^{main} + \dot{Q}_{evap}^{loss,main}}{T_{evap}^{in,main} - \frac{Q_{evap}^{main}}{(\varepsilon\dot{C})_{evap}^{main}}})}{\dot{Q}_{evap}^{main}(\dot{S}_{igen}^{main} + \frac{\dot{Q}_{evap}^{main} + \dot{Q}_{evap}^{loss,main}}{T_{evap}^{in,main} - \frac{Q_{evap}^{main}}{(\varepsilon\dot{C})_{evap}^{main}}} - (\varepsilon\dot{C})_{cond}^{main} + (\dot{m}c_p)_{ref}^{main} ln[\frac{T^{out,sub}}{T_{cond}^{main}}])}$$

$$+\frac{(\dot{Q}_{cond}^{loss,sub} - (\varepsilon\dot{C})_{cond}^{sub} T_{cond}^{in,main})(\dot{S}_{igen}^{sub} + \frac{\dot{Q}^{sub} + \dot{Q}^{loss,sub}}{T_{cond}^{main} - \frac{Q^{sub}}{(\dot{m}C_p)_{ref}^{main}(\varepsilon)^{sub}}})}{\dot{Q}_{evap}^{main}(\dot{S}_{igen}^{sub} + \frac{\dot{Q}^{sub} + \dot{Q}^{loss,sub}}{T_{cond}^{main} - \frac{Q^{sub}}{(\dot{m}c_p)_{ref}^{main}(\varepsilon)^{sub}}} - (\varepsilon\dot{C})_{cond}^{sub})}$$

$$+\frac{\dot{Q}_{\dot{W}}^{loss,main} - \dot{Q}_{evap}^{loss,main}}{\dot{Q}_{evap}^{main}} + \frac{\dot{Q}_{\dot{W}}^{loss,sub} - \dot{Q}^{loss,sub}}{\dot{Q}_{evap}^{main}} \qquad (4.11)$$

Equation (4.11) gives the COP_{total} of the system for one set of input data. The required input data can be measured experimentally from an actual working system or calculated from a thermodynamic model that is discussed in section (4.3). Table 4.1 and 4.2 shows the required input data obtained from the thermodynamic model of the system. The value of COP_{total} obtained from Eq. (4.11) using the input data given in Table 4.1 was found to be 2.4833 which is exactly equal to the value

Table 4.1: Input data to be used in Eq. (4.11) for plotting Fig. 4.3(a), obtained from the thermodynamic model.

Cooling capacity of the main cycle evaporator	$(\dot{Q}_{evap}^{main})$	25.0 kW
Heat leak into the suction line of the main cycle	$(\dot{Q}_{evap}^{loss,main})$	0.0 W
Heat leak from the discharge line of the main cycle	$(\dot{Q}_{cond}^{loss,main})$	0.0 W
Heat leak from the compressor shell of the main cyclecompressor	$(\dot{Q}_{W}^{loss,main})$	0.0 W
Effectiveness and capacitance rate product for the main cycle evaporator	$(\varepsilon\dot{C})_{evap}^{main}$	5.0 kW/K
Effectiveness and capacitance rate product for the main cycle condenser	$(\varepsilon\dot{C})_{cond}^{main}$	4.0 kW/K
Internal entropy generation due to non isentropic compression and expansion in the main cycle	$(\dot{S}_{gen}^{main})$	12.413 W/K
Coolant temperature at the inlet of the main cycle evaporator	$(T_{evap}^{in,main})$	0.0^oC
Coolant temperature at the inlet of the main cycle condenser	(T_{cond}^{in})	45.0^oC
Temperature of the main cycle refrigerant after exiting the subcooler	$(T^{out,sub})$	36.511^oC
Refrigerant temperature at the main cycle condenser	(T_{cond}^{main})	52.511^oC
Mass flow rate and the specific heat product of the main cycle refigerant	$((\dot{m}c_p)_{ref}^{main})$	265.8437 W/K
Mass flow rate and the Effectiveness-specific heat product of the main cycle refigerant	$(\dot{m}c_p)_{ref}^{main}(\varepsilon)^{sub}$	230.0 W/K
Cooling capacity of the subcooler	$(\dot{Q}^{sub})$	4253.5 W
Heat leak into the suction line of the subcooler cycle	$(\dot{Q}^{loss,sub})$	0.0 W
Heat leak from the discharge line of the subcooler cycle	$(\dot{Q}_{cond}^{loss,sub})$	0.0 W
Heat leak from the compressor shell of the subcooler cycle compressor	$(\dot{Q}_{W}^{loss,sub})$	0.0 W
Effectiveness and capacitance rate product for the subcooler cycle condenser	$(\varepsilon\dot{C})_{cond}^{sub}$	270.0 W/K
Internal entropy generation due to non isentropic compression and expansion in the subcooler cycle	$(\dot{S}_{gen}^{sub})$	1.06867 W/K

Table 4.2: Input data to be used in Eq. (4.11) for plotting Fig. 4.3(b), obtained from the thermodynamic model.

Cooling capacity of the main cycle evaporator	$(\dot{Q}_{evap}^{main})$	25.0 kW
Heat leak into the suction line of the main cycle	$(\dot{Q}_{evap}^{loss,main})$	0.0 W
Heat leak from the discharge line of the main cycle	$(\dot{Q}_{cond}^{loss,main})$	0.0 W
Heat leak from the compressor shell of the main cyclecompressor	$(\dot{Q}_{W}^{loss,main})$	0.0 W
Effectiveness and capacitance rate product for the main cycle evaporator	$(\varepsilon\dot{C})_{evap}^{main}$	5.0 kW/K
Effectiveness and capacitance rate product for the main cycle condenser	$(\varepsilon\dot{C})_{cond}^{main}$	4.0 kW/K
Internal entropy generation due to non isentropic compression and expansion in the main cycle	$(\dot{S}_{gen}^{main})$	3.13717 W/K
Coolant temperature at the inlet of the main cycle evaporator	$(T_{evap}^{in,main})$	0.0°C
Coolant temperature at the inlet of the main cycle condenser	(T_{cond}^{in})	45.0°C
Temperature of the main cycle refrigerant after exiting the subcooler	$(T^{out,sub})$	35.749°C
Refrigerant temperature at the main cycle condenser	(T_{cond}^{main})	51.749°C
Mass flow rate and the specific heat product of the main cycle refigerant	$((\dot{m}c_p)_{ref}^{main})$	262.965 W/K
Mass flow rate and the Effectiveness-specific heat product of the main cycle refigerant	$(\dot{m}c_p)_{ref}^{main}(\varepsilon)^{sub}$	230.0 W/K
Cooling capacity of the subcooler	$(\dot{Q}^{sub})$	4711.55 W
Heat leak into the suction line of the subcooler cycle	$(\dot{Q}^{loss,sub})$	0.0 W
Heat leak from the discharge line of the subcooler cycle	$(\dot{Q}_{cond}^{loss,sub})$	0.0 W
Heat leak from the compressor shell of the subcooler cycle compressor	$(\dot{Q}_{W}^{loss,sub})$	0.0 W
Effectiveness and capacitance rate product for the subcooler cycle condenser	$(\varepsilon\dot{C})_{cond}^{sub}$	270.0 W/K
Internal entropy generation due to non isentropic compression and expansion in the subcooler cycle	$(\dot{S}_{gen}^{sub})$	0.316124 W/K

obtained from the thermodynamic model. Therefore, the analytical expression in Eq. (4.11) and the thermodynamic model are correct and hence they can be used for design and performance evaluation purpose. It should be noted that the heat leak terms are neglected in the above comparison because they do not contribute much towards the overall system performance [15].

Figure 4.3 shows the characteristic performance curves ($1.0/COP$ vs $1.0/\dot{Q}_{evap}^{main}$) of the system. The plots are drawn for the set of input data given in Table 4.1 and Table 4.2. The design point is also shown in the figure, where for Fig. 4.3(a) the design point is ($COP = 2.4833$). Notice that the design point is located away from the minimum point because of the losses mainly due to non-isentropic compression in the compressors of the system. However the design point is at the minimum point ($COP = 3.726$) when the efficiency of the compressors is assumed to be 100 percent, as shown in Fig. 4.3(b). The plots are hypothetical curves drawn for a constant $T_{evap}^{in,main}$ and a range of main cycle evaporator capacity ($\dot{Q}_{evap}^{main}$). We note that the shape of the curves is similar to the one obtained for a simple cycle discussed by Gordon et al. [15].

The figure shows that COP is increasing with evaporator capacity upto the minimum point on the curve. In this region, the irreversible losses are mainly due to fluid friction (some times referred to as isentropic losses) in the compressors and the expansion valves. While at evaporator capacities greater than the minimum

point. COP decreases significantly because of the losses due to the finite rate of heat transfer in the heat exchangers of the system. It should be noted that the performance of the system in the light of various losses of the system is similar to the performance of a simple cycle discussed by Gordon and Choon [16].

4.2 Prediction of Optimum Subcooler Saturation Temperature

The performance of a mechanical subcooling system is controlled mostly by the subcooler temperature T^{sub}, as reported by Thornton et al. [28]. Mechanical subcooling allows the main cycle refrigerant to enter the main cycle evaporator with a lower quality (point 5), see Fig. 4.2, compared with a typical simple vapor-compression cycle (point 3'). The lower quality of the refrigerant at the evaporator inlet corresponds to an increase in the refrigeration capacity per unit mass of refrigerant circulated in the main cycle. However it should be noted that the increase in refrigeration capacity is not without cost since there are additional components in the system. Neglecting losses to the environment, an energy balance on the subcooler indicates that the amount of subcooling provided to the main cycle must equal the heat addition to the subcooling cycle evaporator. The heat addition to the subcooling cycle evaporator must be rejected in the subcooling cycle condenser at the cost of the work consumed in the subcooling cycle compressor. It should be emphasized

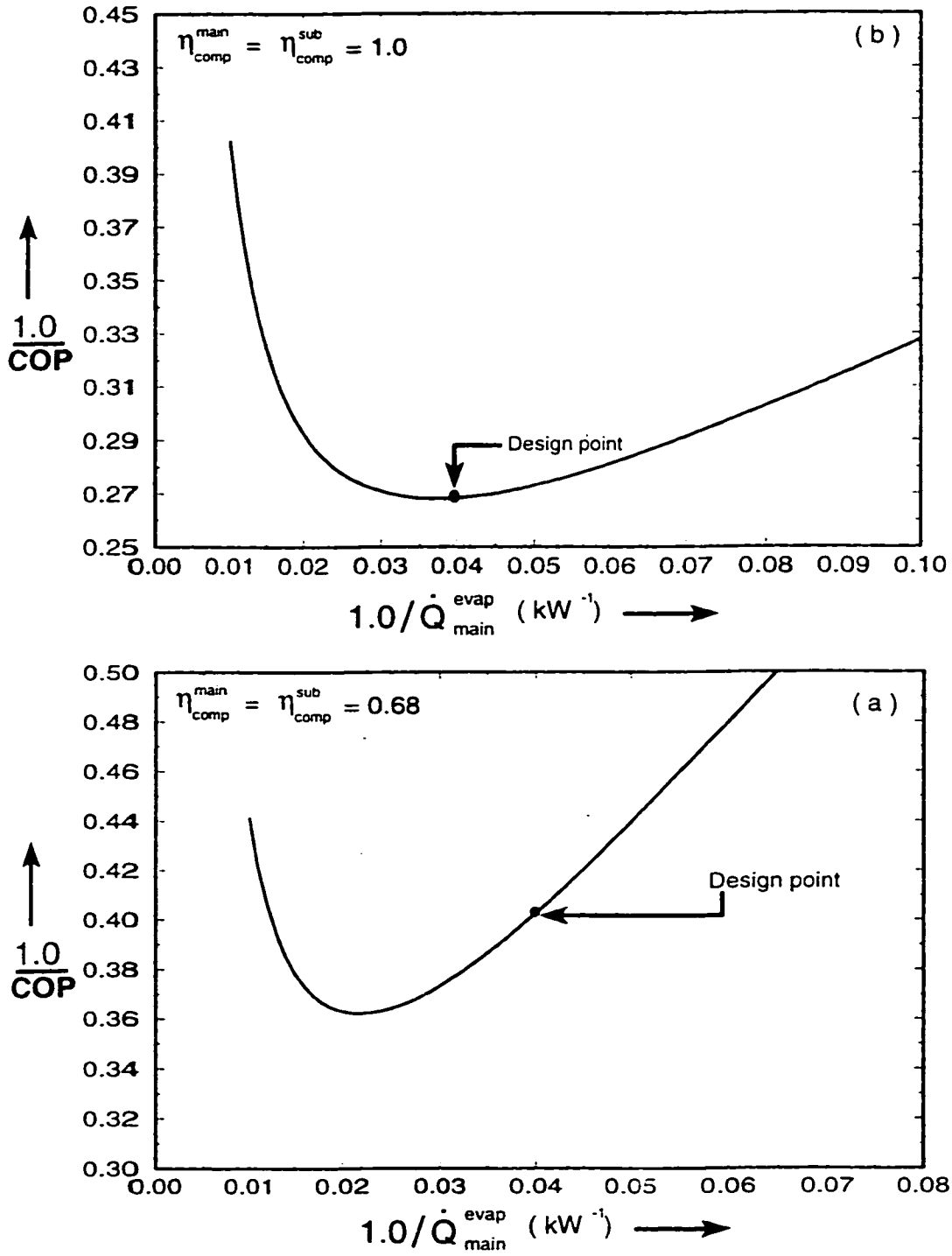

Figure 4.3: Performance curves of a dedicated mechanical subcooling system, for an input data given in Table 4.1 and Table 4.2

that there is an 'optimum' temperature for the subcooling cycle evaporator at which the COP_{total} of the cycle is maximized. This 'optimum' temperature can be investigated by expressing the overall COP_{total} of the system in terms of the subcooler cycle temperature T^{sub} and other variables as

$$COP_{total} = \frac{1 + X(T_{cond}^{main} - T^{sub})}{\frac{(T_{cond}^{in} - T_{evap}^{in,main}) + (\Delta T_m)}{T_{evap}^{in,main} - (\Delta T_m)} + \frac{X(T_{cond}^{main} - T^{sub})(\Delta TT_s)}{T_{cond}^{in} - (\Delta TT_s)}} \tag{4.12}$$

where in the above equation, the parameter X is defined as a measure of the relative size and performance of the subcooler, expressed as

$$X = \frac{(\varepsilon \dot{C})_{evap}^{sub}}{\dot{Q}_{evap}^{main,nosub}} \tag{4.13}$$

and

$$(\Delta T_m) = \dot{Q}_{evap}^{main} \left[\frac{1}{(\varepsilon \dot{C})_{evap}^{main}} + \frac{1}{(\varepsilon \dot{C})_{cond}^{main}} \right] \tag{4.14}$$

$$(\Delta T_s) = Q^{sub} \left[\frac{1}{(\varepsilon \dot{C})_{evap}^{sub}} + \frac{1}{(\varepsilon \dot{C})_{cond}^{sub}} \right] \tag{4.15}$$

$$T_{cond}^{main} = T_{cond}^{in} + \frac{\dot{Q}_{evap}^{main}}{(\varepsilon \dot{C})_{cond}^{main}} \left[\frac{T_{cond}^{in}}{T_{evap}^{in,main} - (\Delta T_m)} \right] \tag{4.16}$$

$$(\Delta TT_s) = (\Delta T_s) + (T_{cond}^{in} - T_{cond}^{main}) \tag{4.17}$$

It should be noted that Eq. (4.12) considers the irreversible losses in all the heat exchangers. However, when we consider $(\varepsilon \dot{C})_{cond}^{sub}$, $(\varepsilon \dot{C})_{cond}^{main}$, $(\varepsilon \dot{C})_{evap}^{main}$ to be very large, it gives losses in the subcooler only. Substituting the above values in Eqs. (4.14)-(4.17), we get

$$(\Delta T_m) = 0.0. \tag{4.18}$$

$$(\Delta T_s) = \frac{\dot{Q}^{sub}}{(\varepsilon \dot{C})^{sub}_{evap}} = (T^{main}_{cond} - T^{sub}). \tag{4.19}$$

$$T^{main}_{cond} = T^{in}_{cond}. \tag{4.20}$$

and

$$(\Delta TT_s) = (\Delta T_s). \tag{4.21}$$

Substituting the above values in Eq. (4.12) we get

$$COP_{total} = \frac{1 + N(T^{in}_{cond} - T^{sub})}{\frac{T^{in}_{cond} - T^{in,main}_{evap}}{T^{in,main}_{evap}} + N\frac{(T^{in}_{cond} - T^{sub})^2}{T^{sub}}} \tag{4.22}$$

which is exactly the same equation as that discussed by Thornton et al. [28].

Figure 4.4 shows the plot of Eq. (4.12), given as COP_{total} vs. the subcooling saturation temperature T_{sub} and the subcooler parameter N which defines the relative size of the subcooler, for the following set of input data. $T^{in,main}_{evap} = -43.0\ ^oC$, $T^{in}_{cond} = 37.0\ ^oC$, $\dot{Q}^{main}_{evap} = 53.0\ kW$, $(\varepsilon \dot{C})^{main}_{evap} = 5.0\ kW/K$, $(\varepsilon \dot{C})^{main}_{cond} = 6.0\ kW/K$ and $(\varepsilon \dot{C})^{sub}_{cond} = (\dot{m}c_p)^{main}_{ref}(\varepsilon)^{sub}$. As expected, the figure shows that the COP_{total} increases with the increase in the value of the subcooler parameter N. The figure also shows that for the given operating condition, there is a subcooler saturation temperature where the performance of the system is maximum, however, this subcooler temperature increases with the parameter N. It should be noted that these plots do not demonstrate the increase in COP_{total} over the main cycle COP with no subcooling. To show the predicted improvement in performance of

a mechanical subcooling refrigeration system with respect to the single stage cycle. the curves are plotted in a normalized form defined as

$$COPN = \frac{COP_{total}}{COP_{main}}. \tag{4.23}$$

similarly a reduced subcooler saturation temperature θ is defined as

$$\theta = \frac{T^{sub} - T^{main}_{evap}}{T^{main}_{cond} - T^{main}_{evap}} \tag{4.24}$$

Figure 4.5 shows the corresponding plot of Fig. 4.4 between the normalized coefficient of performance, $COPN$ and the reduced temperature θ. In both these plots T_{sub} was varied from $T^{in,main}_{evap}$ to T^{in}_{cond}, hence θ varies between 0 and 1.0, and for the range of θ between 0.9 and 1.0, for all values of N, $COPN$ is approximately equal to one, showing that when the subcooling cycle evaporator temperature T_{sub} is close to the inlet temperature to the main cycle condenser, then there is no temperature difference between the flow streams in the subcooler. Therefore, there will be no subcooling provided to the main cycle and consequently no work performed by the subcooling cycle compressor. The overall cycle will then act like one cycle operating between $T^{in,main}_{evap}$ and T^{in}_{cond}, and there will be no advantage of using the mechanical subcooling. On the other hand, for the range of θ, between 0.0 and 0.5, for all values of the subcooler parameter N, $COPN$ is less than one, showing that when the subcooling evaporator temperature is less than the average of T^{main}_{evap} and T^{main}_{cond}, the maximum amount of subcooling is being performed and the thermal lift of the subcooling cycle is more than the main cycle loop. The subcooling cycle compressor

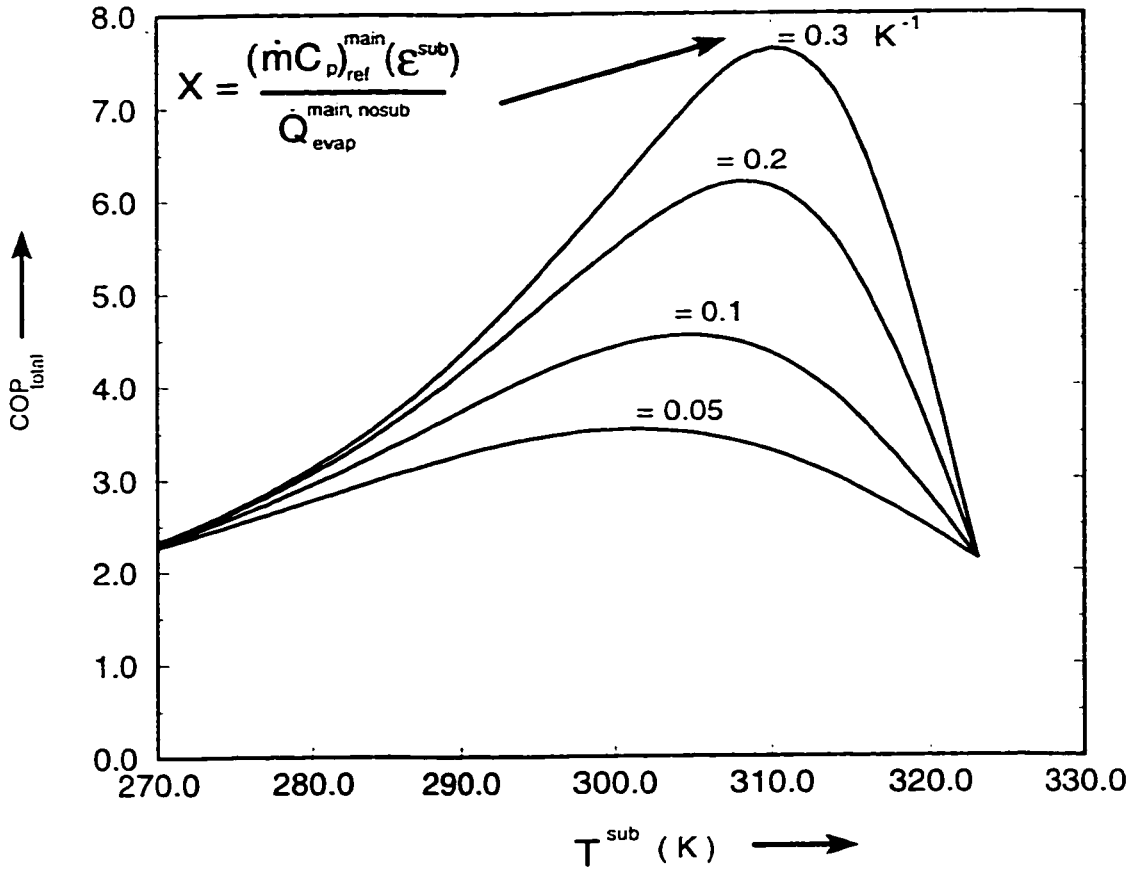

Figure 4.4: Variation of COP_{total} with the T^{sub} for a completely irreversible temperature-dependent mechanical subcooling system

consumes more power, and the advantage of using dedicated mechanical subcooling is destroyed and therefore the $COPN$ of the system reduces. In between these two extremes, there is an optimum T^{sub}, at which $COPN$ is maximum.

as shown in Fig. 4.5. Fig. 4.6 shows the plots between COP_{total} vs T_{sub} and the subcooler parameter N for an ideal temperature-dependent mechanical subcooling system (refer to Eq. (4.22). It should be noted that in an ideal temperature model there are irreversible losses only in the subcooler of the system. Comparison of Fig. 4.4 and Fig. 4.6 shows that COP_{total} is improved remarkably if the irreversibilities in the heat exchangers (main cycle condenser and evaporator, and subcooler cycle condenser) are removed. Also, we note that for the case of an ideal mechanical subcooling system the optimum value of T_{sub} is less than that for the irreversible mechanical subcooling system discussed earlier in Fig. 4.4 for the same set of input conditions.

The corresponding normalized plots, that is, $COPN$ vs the reduced temperature θ and the subcooler parameter N are shown in Fig. 4.7. In this figure following set of input data is considered: $T_{evap}^{in,main} = -43.0\ ^oC$, $T_{cond}^{in} = 37.0\ ^oC$ and $\dot{Q}_{evap}^{main} = 53.0\ kW$. As expected, the figure shows that $COPN$ is more than one for all values of θ because of the fact that the irreversible losses in the main cycle condenser and evaporator in addition to the subcooler cycle condenser are neglected.

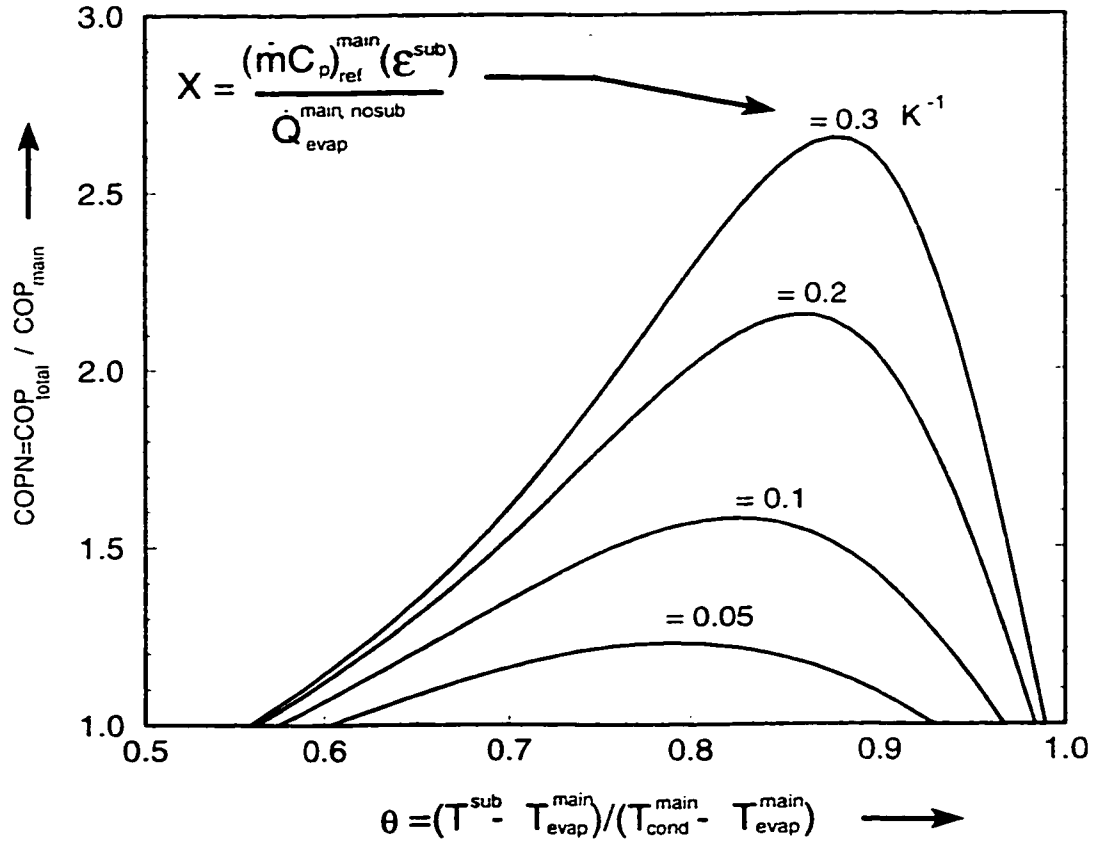

Figure 4.5: Variation of $COPN$ with θ for a completely irreversible temperature-dependent mechanical subcooling system

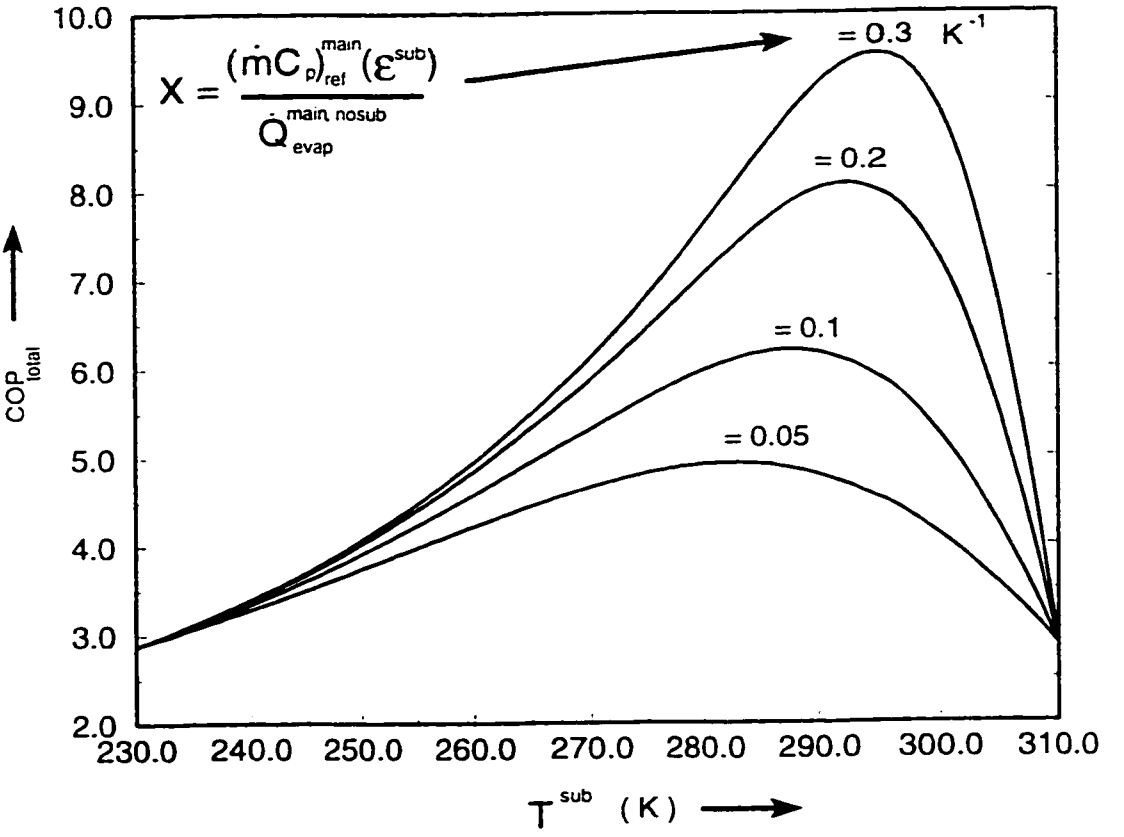

Figure 4.6: Variation of COP_{total} with T^{sub} for an ideal temperature-dependent mechanical subcooling system: irreversible losses only in the subcooler

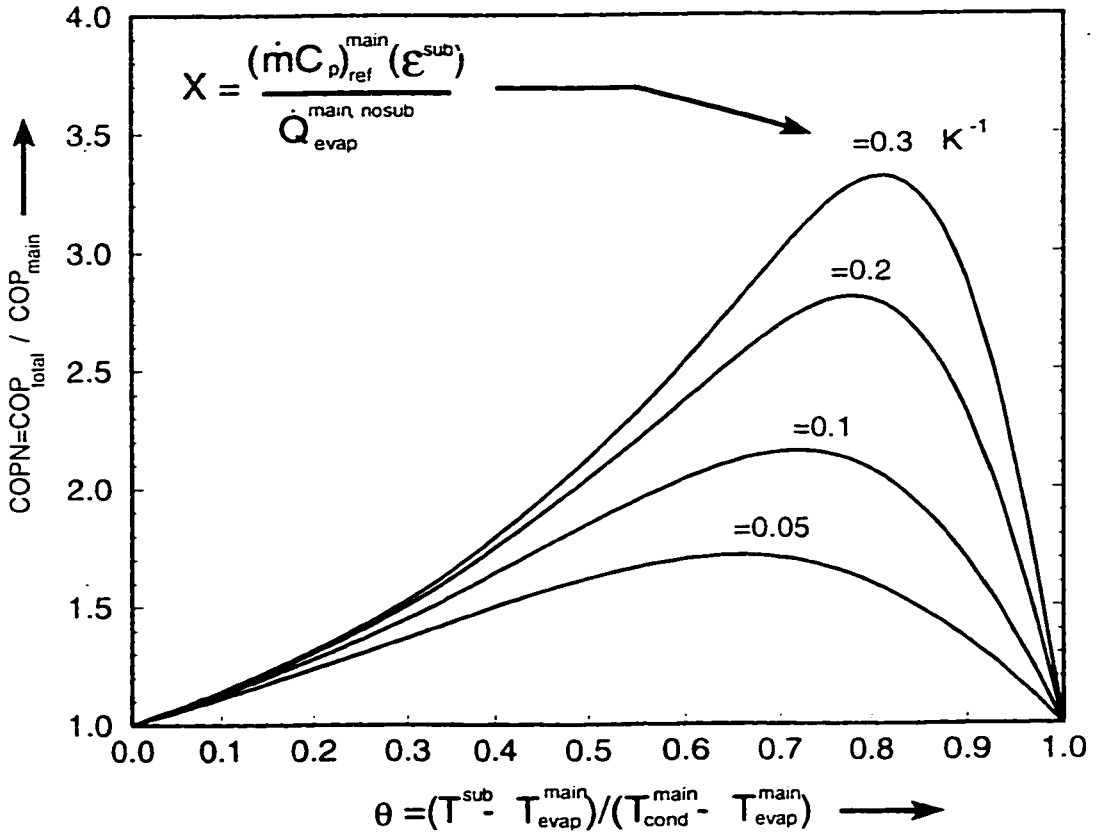

Figure 4.7: Variation of $COPN$ with θ for an ideal temperature-dependent mechanical subcooling system: irreversible losses only in the subcooler

4.3 A Finite Time Thermodynamic Model of the System

As mentioned earlier, the heat transfer to and from the cycle occur by convection to flowing fluid streams having finite mass flow rates and specific heats. Therefore, the rate of heat transfer to the cycle in the main cycle evaporator can be expressed in terms of temperature, mass flow rates, and change in specific enthalpy of the refrigerant, given by

$$\dot{Q}_{evap}^{main} = (\varepsilon \dot{C})_{evap}^{main}(T_{evap}^{in,main} - T_{evap}^{main}) = \dot{m}_{ref}^{main}(h_6 - h_5). \tag{4.25}$$

Similarly the rate of heat transfer between the refrigeration cycle and the sink in the main cycle condenser is expressed as

$$\dot{Q}_{cond}^{main} = (\varepsilon \dot{C})_{cond}^{main}(T_{cond}^{main} - T_{cond}^{in,main}) = \dot{m}_{ref}^{main}(h_2 - h_3). \tag{4.26}$$

In the subcooler, the rate of heat transfer between the main cycle refrigerant and the subcooler cycle refrigerant is given by

$$\dot{Q}^{sub} = (\dot{m}C_p)_{ref}^{main}(T_{cond}^{main} - T^{out,sub}) = \dot{m}_{ref}^{main}(h_3 - h_4). \tag{4.27}$$

The compressor operation is described in terms of an isentropic efficiency η_{comp}^{main} as described in [50], so that the power requirement for the main cycle compressor is given by

$$\dot{W}^{main} = \dot{m}_{ref}^{main}(h_1 - h_7) = \frac{\dot{W}_s^{main}}{\eta_{comp}^{main}} \tag{4.28}$$

Assuming that an amount of $\dot{Q}_{evap}^{loss,main}$ of heat, leaks into the suction line of the main cycle compressor, which can be expressed as

$$\dot{Q}_{evap}^{loss,main} = \dot{m}_{ref}^{main}(h_7 - h_6). \tag{4.29}$$

Similarly assuming that an amount of $(\dot{Q}_{cond}^{loss,main} + \dot{Q}_{W}^{loss,main})$ of heat leaks from the discharge line and compressor shell given by

$$\dot{Q}_{cond}^{loss,main} + \dot{Q}_{W}^{loss,main} = \dot{m}_{ref}^{main}(h_1 - h_2). \tag{4.30}$$

For the subcooler cycle loop, the rate of heat transfer between the subcooler cycle refrigerant and the main cycle refrigerant in the subcooler can be written in terms of temperatures, the mass flow rates, and specific enthalpy of the refrigerant, expressed as

$$\dot{Q}^{sub} = (\dot{m}c_p)_{ref}^{main}(\varepsilon)^{sub}(T_{cond}^{main} - T^{sub}) = \dot{m}_{ref}^{sub}(h_9 - h_8). \tag{4.31}$$

Similarly for the subcooling cycle condenser we have,

$$\dot{Q}_{cond}^{sub} = (\varepsilon\dot{C})_{cond}^{sub}(T_{cond}^{sub} - T_{cond}^{in,main}) = \dot{m}_{ref}^{sub}(h_{12} - h_{13}) \tag{4.32}$$

The work input to the subcooler cycle compressor is given by

$$\dot{W}^{sub} = \dot{m}_{ref}^{sub}(h_{11} - h_{10}) = \frac{\dot{W}_s^{sub}}{\eta_{comp}^{sub}} \tag{4.33}$$

Assuming that an amount of $\dot{Q}_{evap}^{loss,sub}$ of heat leaks into the suction line of the subcooler cycle, which can be expressed as

$$\dot{Q}_{loss}^{sub} = \dot{m}_{ref}^{sub}(h_{10} - h_9). \tag{4.34}$$

Similarly assuming that an amount of $(\dot{Q}_{cond}^{loss,sub} + \dot{Q}_{W}^{loss,sub})$ of heat leaks from the discharge line and the compressor shell. This is given by

$$\dot{Q}_{cond}^{loss,sub} + \dot{Q}_{W}^{loss,sub} = \dot{m}_{ref}^{sub}(h_{11} - h_{12}) \tag{4.35}$$

The above equations have been solved numerically by using the thermodynamic property data for several different refrigerants. The flow chart representing the method of solving the equations is shown in Fig. 4.8, wherein the terms SATPRP and TRIAL represents the subroutines for calculating the refrigerant saturated and vapor properties, respectively. These subroutines need any two independent intensive properties of the refrigerant to find other properties at a given state. For this purpose, a computer program, originally developed by Kartsounes and Erth [43] and modified by Fisher and Rice [44] and Khan and Zubair [46], have been used. The program gives the COP_{total} and all the other parameters of the system for the following set of input data: $\dot{Q}_{evap}^{main}$, $(\varepsilon\dot{C})_{cond}^{main}$, $(\varepsilon\dot{C})_{evap}^{main}$, T_{cond}^{in}, $T_{evap}^{in,main}$, $AMTS$ and $(\varepsilon)^{sub}$.

Figure 4.9(b) shows the plot of COP_{total} vs the subcooler saturation temperature T^{sub} and the subcooler parameter X, using the output from the above described thermodynamic model, for the input data given in Table 4.1. The design point (COP_{total} = 3.73) is the same point as discussed earlier in Fig. 4.3. The figure shows that for the given input conditions there is an optimum subcooler saturation temperature at which COP_{total} is maximum. We note that the property-dependent

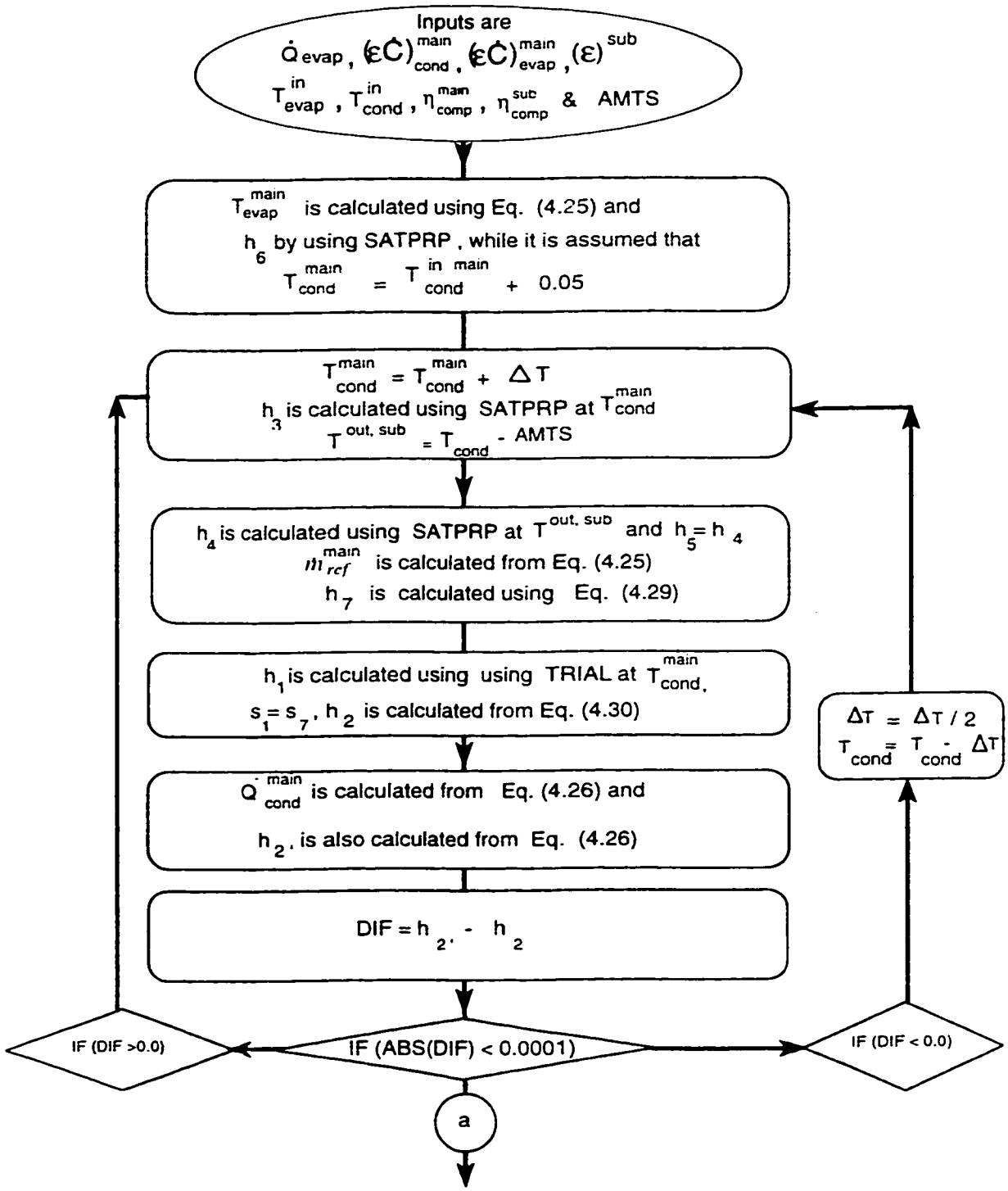
Inputs are
$\dot{Q}_{evap}$, $(\varepsilon\dot{C})^{main}_{cond}$, $(\varepsilon\dot{C})^{main}_{evap}$, $(\varepsilon)^{sub}$
T^{in}_{evap} , T^{in}_{cond} , η^{main}_{comp} , η^{sub}_{comp} & AMTS
T^{main}_{evap} is calculated using Eq. (4.25) and
h_6 by using SATPRP , while it is assumed that
$T^{main}_{cond} = T^{in\ main}_{cond} + 0.05$
$T^{main}_{cond} = T^{main}_{cond} + \Delta T$
h_3 is calculated using SATPRP at T^{main}_{cond}
$T^{out,\ sub} = T_{cond}$ - AMTS
h_4 is calculated using SATPRP at $T^{out,\ sub}$ and $h_5 = h_4$
$\dot{m}^{main}_{ref}$ is calculated from Eq. (4.25)
h_7 is calculated using Eq. (4.29)
h_1 is calculated using using TRIAL at T^{main}_{cond},
$s_1 = s_7$, h_2 is calculated from Eq. (4.30)
$\dot{Q}^{main}_{cond}$ is calculated from Eq. (4.26) and
$h_{2'}$ is also calculated from Eq. (4.26)
DIF = $h_{2'}$ - h_2
IF (DIF >0.0)
IF (ABS(DIF) < 0.0001)
IF (DIF < 0.0)
$\Delta T = \Delta T / 2$
$T_{cond} = T_{cond} - \Delta T$
a

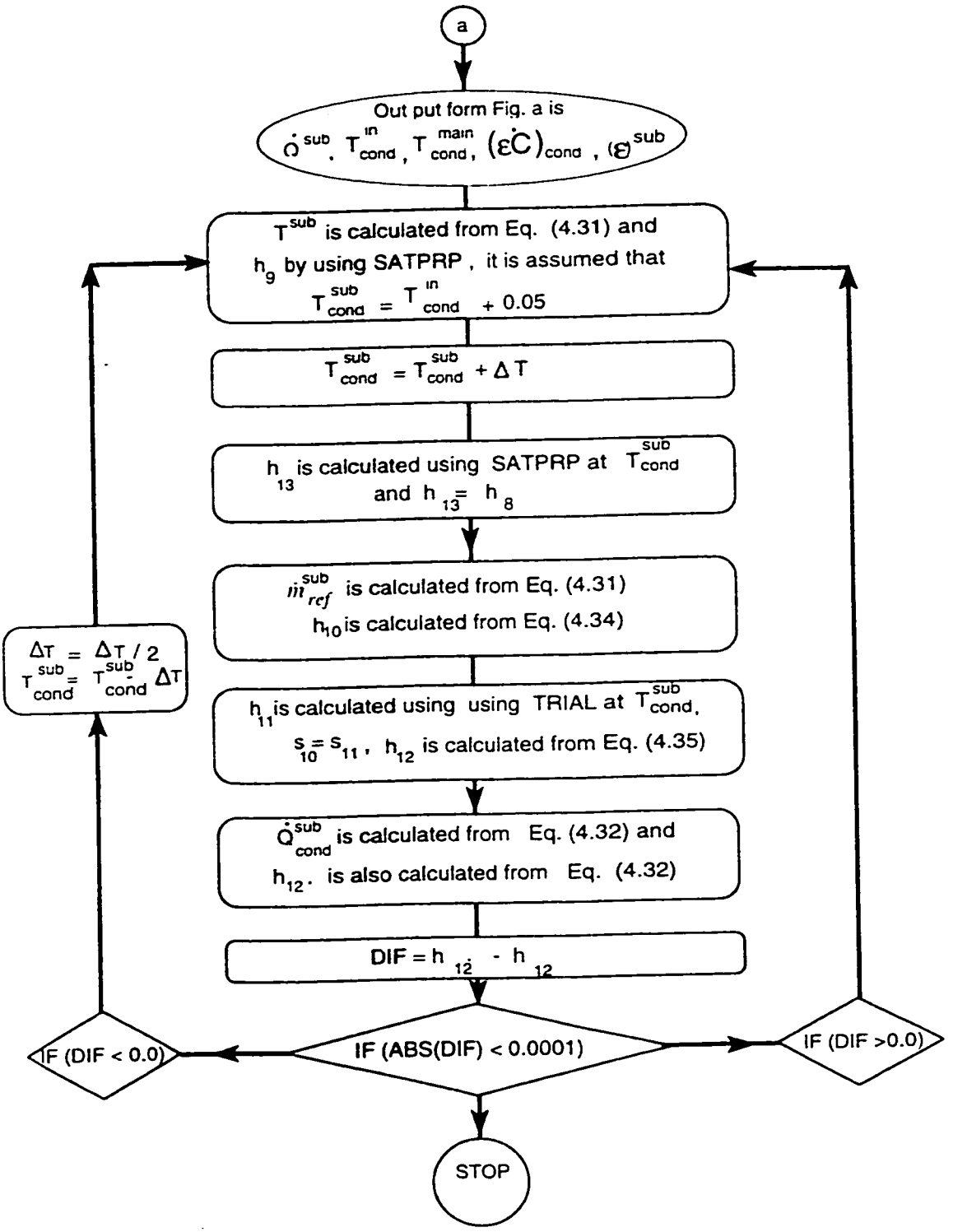

Figure 4.8: Flow chart for a thermodynamic model of a dedicated mechanical subcooling system

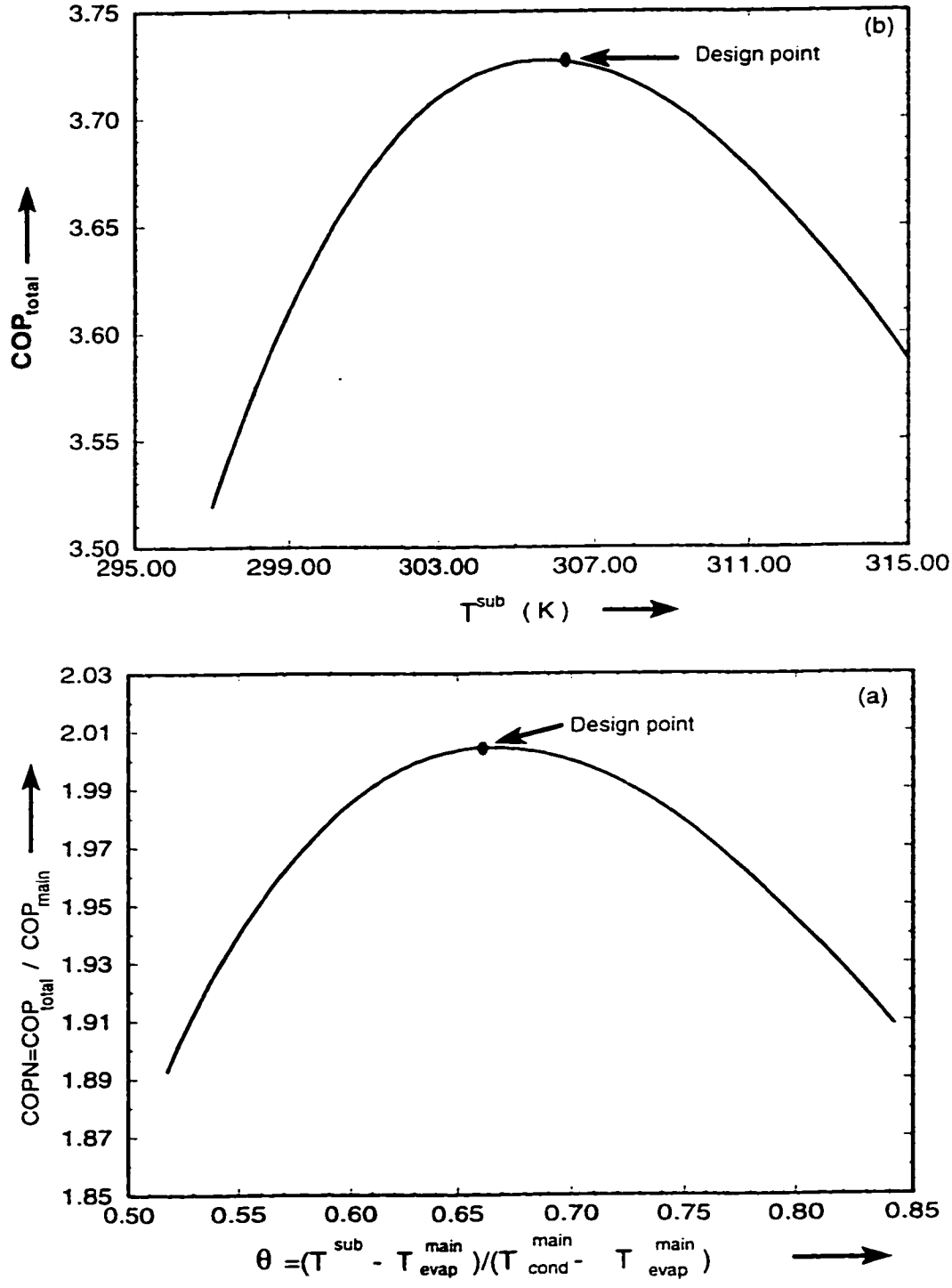

Figure 4.9: Variations of $COPN$ with θ (a) and of COP_{total} with T^{sub} (b) for the property-dependent model

model predicts the same relationship between COP_{total}, subcooler saturation temperature T_{sub} and the subcooler parameter X, as that predicted by the temperature-dependent model (refer to Figs 4.4-4.7).

Figures 4.4-4.7 are obtained by using the analytical expression in Eq. (4.12) and are as such dependent upon temperatures only. These plots will remain same for different types of refrigerants used in a mechanical subcooling system. However these plots can also be obtained from the thermodynamic model discussed in this section. In this regard Fig. 4.10 shows a plot of COP_{total} vs the reduced subcooler saturation temperature θ and the subcooler parameter X of the property-dependent and the temperature-dependent ideal mechanical subcooling vapor compression refrigeration system with irreversible losses only in the subcooler and using $R-134a$ as the refrigerant. These plots are drawn for the following set of input data $T_{evap}^{in,main} = 0.0\ ^oC$, $T_{cond}^{in} = 40.0\ ^oC$ and $\dot{Q}_{evap}^{main} = 30.0\ kW$. The figure shows that the shape of the curves for the two models are similar and the difference in the values of COP_{total} is mainly due to the non-isentropic expansion in the expansion valves of the property-dependent model.

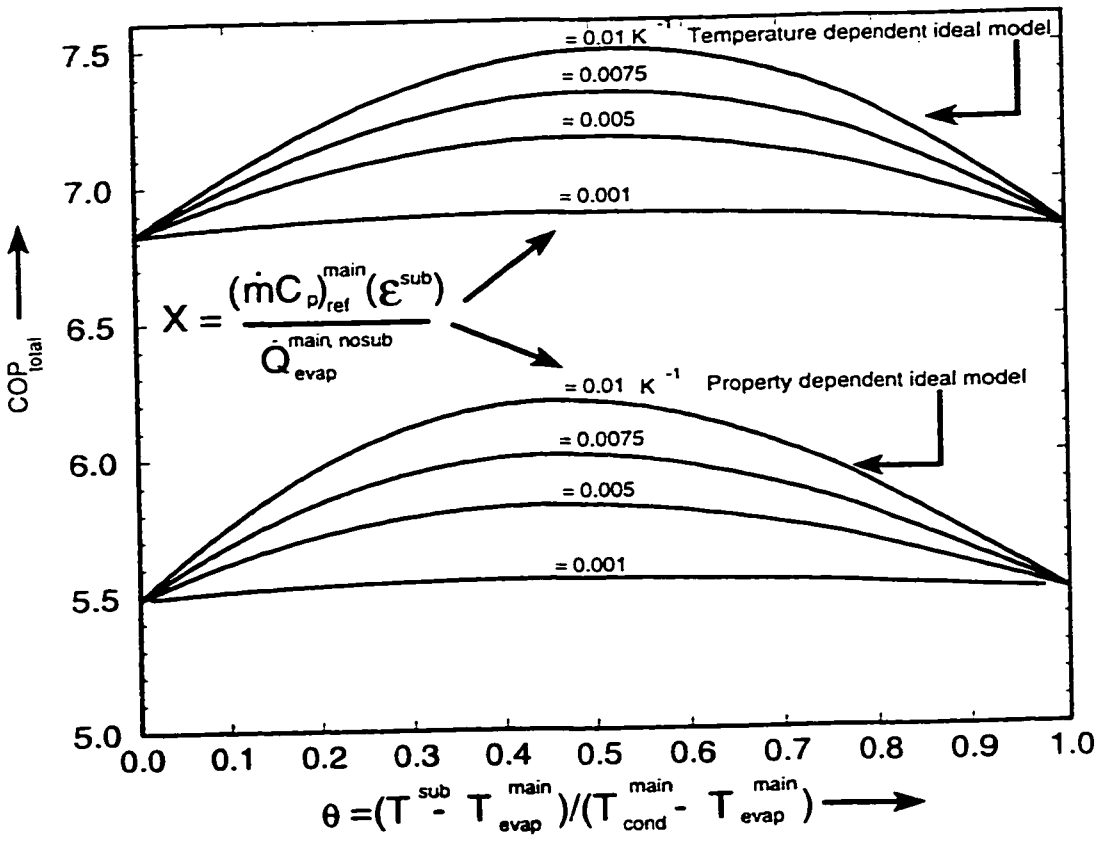

Figure 4.10: Variation of COP_{total} with θ for an ideal temperature-dependent and property-dependent mechanical subcooling system: irreversible losses only in the subcooler

4.4 Optimum Distribution of Heat Exchanger Areas

The design of mechanical subcooling refrigeration system involves proper selection of the external stream capacitance rates and the heat exchanger size. The heat exchanger effectiveness given by ε represents the heat exchanger surface area. The product $(\varepsilon\dot{C})$ of all the heat exchangers of the system is an expensive commodity and it determines the overall cost of the system. Increasing the size of the heat exchanger increases the overall performance of the system but it also increase the cost of the system. hence a compromise is sought between the first cost and the operating cost of the system. Dedicated mechanical subcooling system. in general. has four heat exchangers. two each. in the main and subcooling cycles. The total heat exchanger area for each loop can be defined in terms of the heat exchanger inventory. given by

$$\kappa^{main} = (\varepsilon\dot{C})^{main}_{cond} + (\varepsilon\dot{C})^{main}_{evap} \tag{4.36}$$

$$\kappa^{sub} = (\varepsilon\dot{C})^{sub}_{cond} + (\dot{m}c_p)^{main}_{ref}(\varepsilon)^{sub} \tag{4.37}$$

The κ values given by the above equation may be considered as the design constraint and the problem involved in the optimization is to allocate the total heat exchanger area of each cycle between the two heat exchangers in each cycle so that maximum performance of the system is obtained. The above problem can be solved by using the thermodynamic model presented earlier in section (4.3). the model simulates the

working of an actual reciprocating systems very closely.

To investigate the effect of relative size of heat exchangers, the following dimensionless heat exchanger parameters are defined to study the performance of the system:

$$f_h^{main} = \frac{(\varepsilon \dot{C})_{cond}^{main}}{(\varepsilon \dot{C})_{cond}^{main} + (\varepsilon \dot{C})_{evap}^{main}} \tag{4.38}$$

$$f_h^{sub} = \frac{(\varepsilon \dot{C})_{cond}^{sub}}{(\varepsilon \dot{C})_{cond}^{sub} + (\dot{m} c_p)_{ref}^{main} (\varepsilon)^{sub}} \tag{4.39}$$

A set of sample plots, shown in Fig. 4.11(a), is drawn between COP_{total} and the main cycle dimensionless heat exchanger parameter (f_h^{main}) using the output from the thermodynamic model, for the following set of input data and using $R-134a$ as the refrigerant: $\dot{Q}_{evap}^{main} = 30.0\ kW$, $(\varepsilon \dot{C})_{cond}^{sub} = 0.35\ kW/K$, $(\dot{m} c_p)_{ref}^{main} (\varepsilon)^{sub} = 0.15\ kW/K$, $\eta_{comp}^{main} = 0.65$, $\eta_{comp}^{sub} = 0.70$, $T_{evap}^{in,main} = 273.0\ K$, $T_{cond}^{in} = 313.0\ K$. The plots are drawn for different values of the main cycle thermal inventory (κ^{main}). The corresponding variation of the various temperatures of the system for $\kappa^{main} = 10.0\ kW/K$ is shown in Fig. 4.11(b). As expected the figure shows that as the value of κ^{main} is increased the COP_{total} of the system increases. The subcooler temperature T^{sub} and the T_{cond}^{sub} more or less remains constant with the change in the heat exchanger area of the main cycle. We note that the difference between T_{cond}^{in} and T_{cond}^{main} decreases with increase in the value of f_h^{main} because the area of the main cycle condenser is increased and hence the heat transfer in the main cycle

condenser takes place across a lower temperature difference, resulting in reduced irreversible losses due to heat transfer. However the difference between T_{evap}^{main} and $T_{evap}^{in.main}$ increases with the increase in the value of f_h^{main}, because the area of the main cycle evaporator is reduced and hence the heat transfer in the main cycle evaporator takes place across a higher temperature difference, resulting in an increased losses due to the irreversible heat transfer. In between these two extremes, there lies an optimum distribution of the heat exchanger area at which COP_{total} is maximum. This optimum point is shown in Fig. 4.11(a) for different values of κ^{main}.

Figure 4.12(a) shows plots of $COPN$ vs the subcooler cycle heat exchanger parameter (f_h^{sub}) and the subcooler thermal inventory κ^{sub} using the output from the thermodynamic model, for the following set of input data and using $R-134a$ as the refrigerant $\dot{Q}_{evap}^{main} = 30.0\,kW$, $(\varepsilon\dot{C})_{cond}^{main} = 4.3\,kW/K$, $(\varepsilon\dot{C})_{evap}^{main} = 5.7\,kW/K$, $\eta_{comp}^{main} = 0.65$, $\eta_{comp}^{sub} = 0.70$, $T_{evap}^{in.main} = 273.0\,K$, $T_{cond}^{in} = 313.0\,K$. The corresponding variation of the temperatures of the system for $\kappa^{sub} = 0.45\,kW/K$ is shown in Fig. 4.12(b). As expected, the value of $COPN$ increases with the thermal inventory κ^{sub}. The figure shows that the temperatures of the main cycle remains constant with the variation of the heat exchanger area of the subcooler cycle. It should be noted that T_{cond}^{main} is the external fluid to the subcooler. The difference between T^{sub} and T_{cond}^{main}, increases as the value of f_h^{sub} increases due to the reduction in area of the subcooler. Hence the heat transfer in the subcooler takes place at a higher

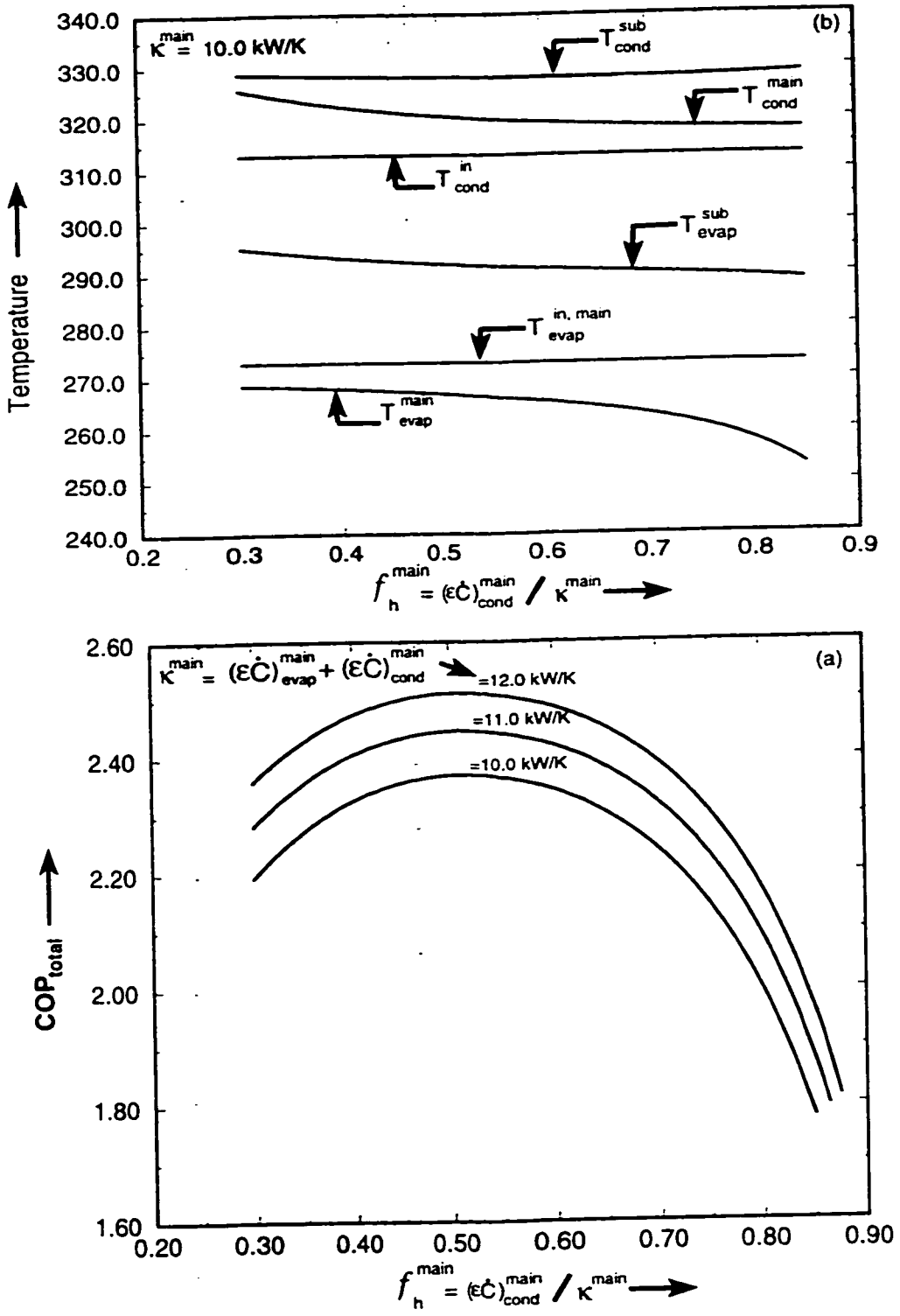

Figure 4.11: Variation of COP_{total} (a) and of operating temperatures (b) with f_h^{main} for the following input data: $\dot{Q}^{main}_{evap} = 30.0\ kW$, $(\varepsilon\dot{C})^{sub}_{cond} = 0.35\ kW/K$, $(\dot{m}c_p)^{main}_{ref}(\varepsilon)^{sub} = 0.15\ kW/K$, $\eta^{main}_{comp} = 0.65$, $\eta^{sub}_{comp} = 0.70$, $T^{in,main}_{evap} = 273.0\ K$, $T^{in}_{cond} = 313.0\ K$.

temperature difference, resulting in the increased irreversible losses due to heat transfer. However the difference between T^{in}_{cond} and T^{sub}_{cond}, decreases as the value of f^{sub}_h increases due to the increase in the area of the subcooling cycle condenser, thus the heat transfer in the subcooling cycle condenser takes place at a reduced temperature difference, resulting in a relatively low irreversible losses due to heat transfer. Similar to the main cycle loop, there is an optimum value of f^{sub}_h at which COP is maximum. The optimum value is shown in Fig. 4.12(a) for different values of κ^{sub}.

Figure 4.11(a) shows that for a given value of the main cycle heat exchanger inventory (κ^{main}) there is an optimum value of f^{main}_h at which COP_{total} of the system is maximum, when all other input parameters of the system are kept constant. Similarly, Fig. 4.12(a) shows that for a given value of the subcooler cycle heat exchanger inventory (κ^{sub}), there is an optimum value of f^{sub}_h at which COP_{total} is maximum, when all other input parameters of the system are kept constant. Hence it can be concluded that there is only one optimum value of f^{main}_h and f^{sub}_h for a given values of κ^{sub} and κ^{main} at which COP_{total} is maximum. Figure 4.13(a) shows a normalized plot of COP as a function of reduced subcooler saturation temperature θ obtained from the thermodynamic model for the following input conditions: $\dot{Q}^{main}_{evap} = 30.0\ kW$, $T^{in,main}_{evap} = 273.0\ K$, $T^{in}_{cond} = 313.0\ K$, $\kappa^{main} = 10.0\ kW/K$, $\kappa^{sub} = 0.5\ kW/K$ and using $R-134a$ as the refrigerant. The figure shows that for the best operation of the system at the given input conditions we

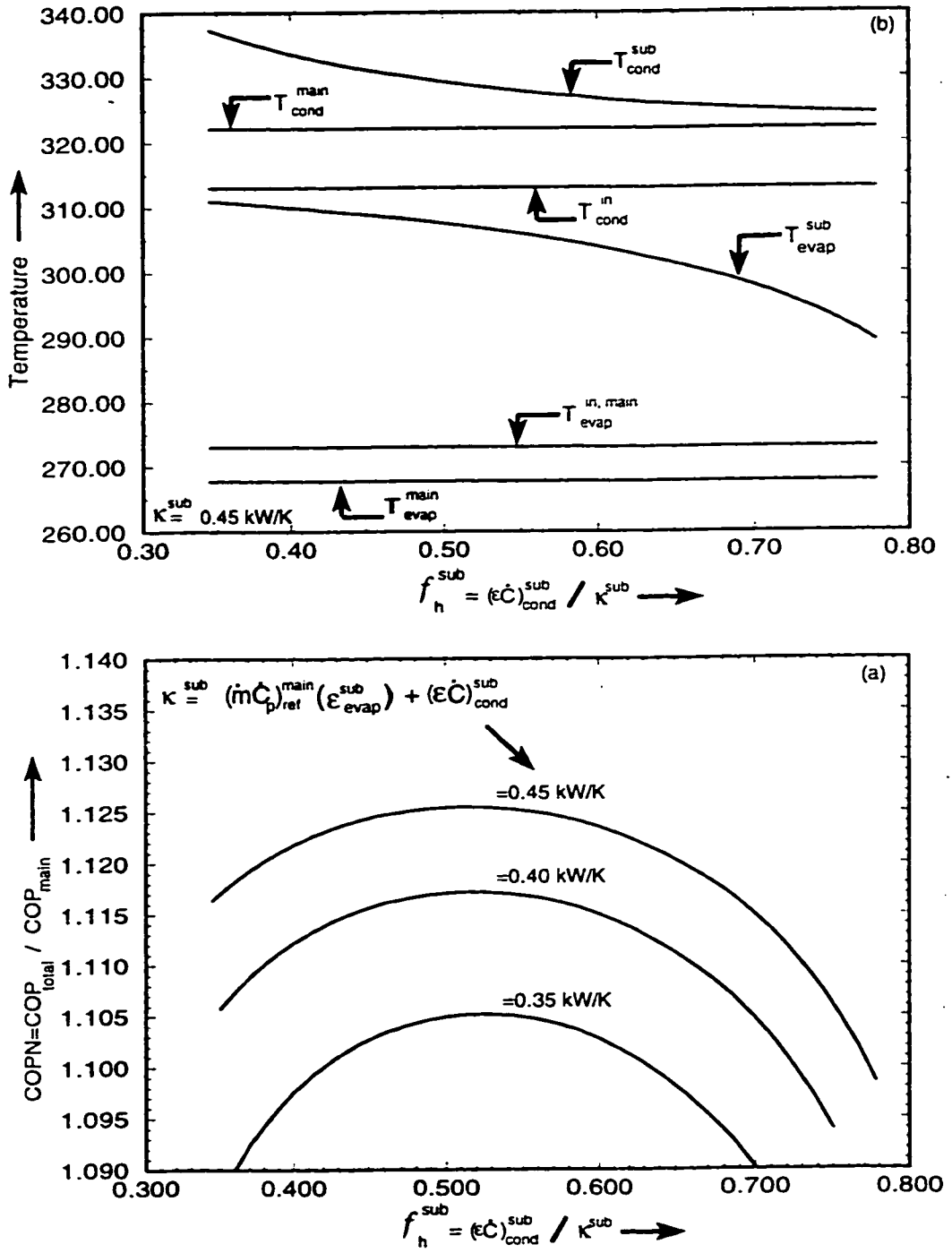

Figure 4.12: Variations of $COPN$ (a) and of operating temperatures (b) with f_h^{sub} for the input data: $\dot{Q}_{evap}^{main} = 30.0\ kW$, $(\varepsilon\dot{C})_{cond}^{main} = 4.3\ kW/K$, $(\varepsilon\dot{C})_{evap}^{main} = 5.7\ kW/K$, $\eta_{comp}^{main} = 0.65$, $\eta_{comp}^{sub} = 0.70$, $T_{evap}^{in,main} = 273.0\ K$, $T_{cond}^{in} = 313.0\ K$

should have $\theta = 0.65$, which gives $T^{sub}_{.} = 28.9\ ^{o}C$. Also it was found that the heat exchanger area distribution for the above set of conditions should be such that $f_h^{main} = 0.514$ and $f_h^{sub} = 0.52$. It should be noted that in this figure for every value of reduced subcooler saturation temperature θ, an optimum value of f_h^{main} and f_h^{sub} is calculated that gives the maximum COP. However, for the range of reduced temperature θ considered in this study, the global maximum normalized COP is ($COP.N = 1.135$) at $\theta = 0.65$.

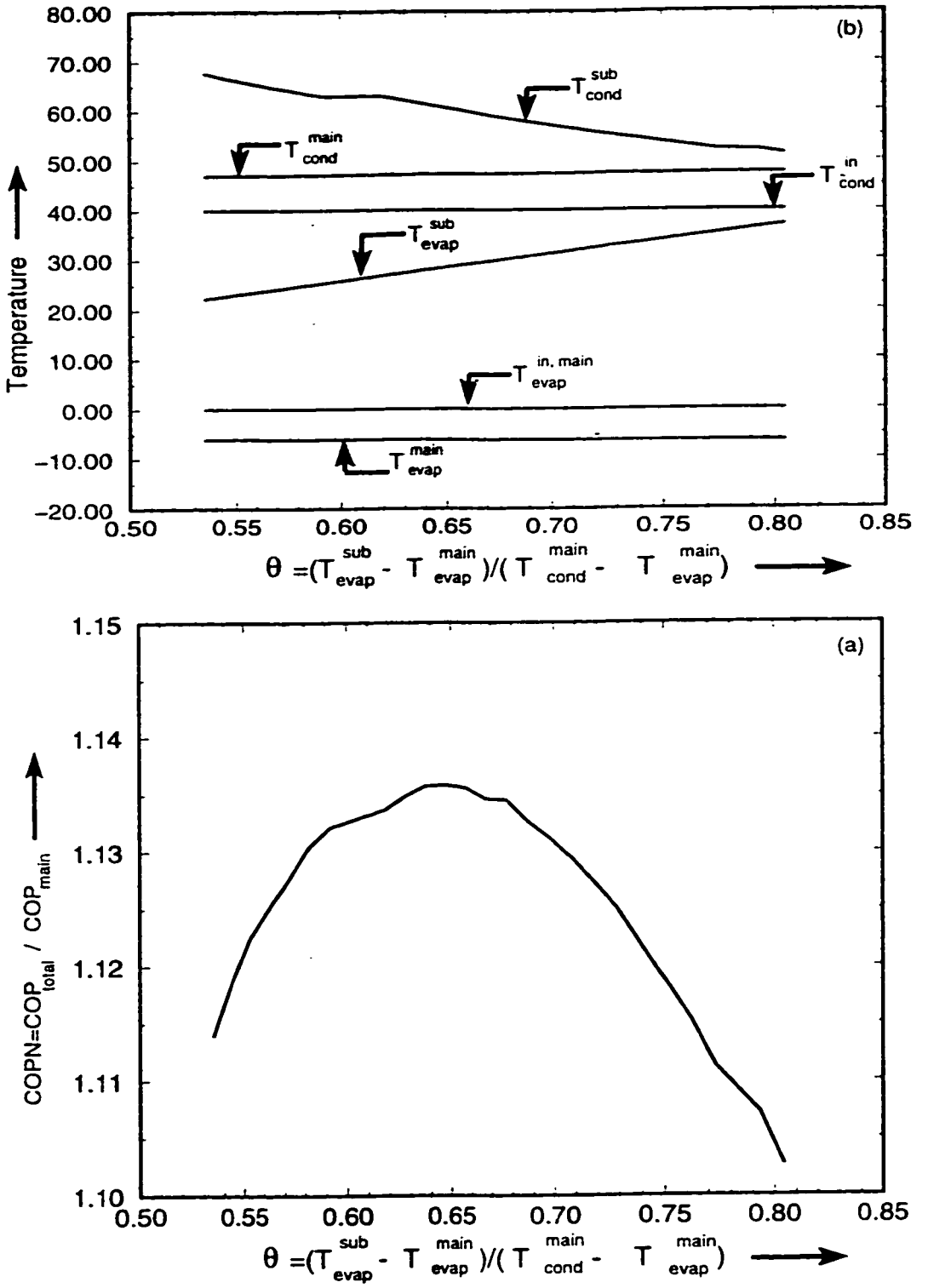

Figure 4.13: Variation of $COPN$ (a) and of operating temperatures (b) with θ for the following input data: $\dot{Q}_{evap}^{main} = 30.0\ kW$, $T_{evap}^{in,main} = 273.0\ K$, $\eta_{comp}^{main} = 0.65$, $\eta_{comp}^{sub} = 0.70$, $T_{cond}^{in} = 313.0\ K$, $\kappa^{main} = 10.0\ kW/K$, $\kappa^{sub} = 0.5\ kW/K$

Chapter 5

Thermodynamic Analysis of an Integrated Mechanical Subcooling Vapor Compression Refrigeration System

The major components of an integrated mechanical subcoling vapor compression refrigeration system includes two reciprocating compressors, two expansion valves, condenser, evaporator, receiver and a subcooler. The system consists of two simple cycles coupled to each other via a subcooler as shown in Fig. 5.1, while its pressure enthalpy diagram is shown in Fig. 5.2. The bigger cycle is known as the main cycle and the smaller cycle is known as the subcooler cycle. The two cycles have

a common condenser, and the components of the two cycles are connected in a closed loop through a piping system that has heat transfer with the surroundings. The figure shows that the main cycle refrigerant leaves the main cycle evaporator at state point 1 as a low pressure, low temperature, saturated vapor and enters the main cycle compressor at state point 2. The refrigerant, from state point 1 to point 2 takes heat from the surroundings in the suction line. At state point 3 it leaves the compressor as a high temperature, high pressure, superheated vapor. The refrigerant, from state point 3 to point 4 rejects heat to the surroundings in the discharge line. At state point 4 it mixes with the subcooler cycle refrigerant coming from the subcooler cycle compressor and attains the state point 13, and the mixture enters the condenser. The mixture after leaving the condenser is collected in the receiver. Some of this liquid refrigerant mixture is extracted from the receiver and is expanded in the expansion valve of the subcooler cycle and is then passed through the subcooler. The remaining liquid refrigerant in the receiver enters the subcooler, where it is cooled below the saturated liquid state at a constant pressure to state point 6 by the subcooler cycle refrigerant. It enters the main cycle expansion vavle and at point 7 it leaves the expansion valve as a low quality vapor and enters the evaporator. In the evaporator, it is evaporated at a constant pressure to the saturated vapor state.

The subcooler cycle refrigerant after cooling the main cycle refrigerant in the

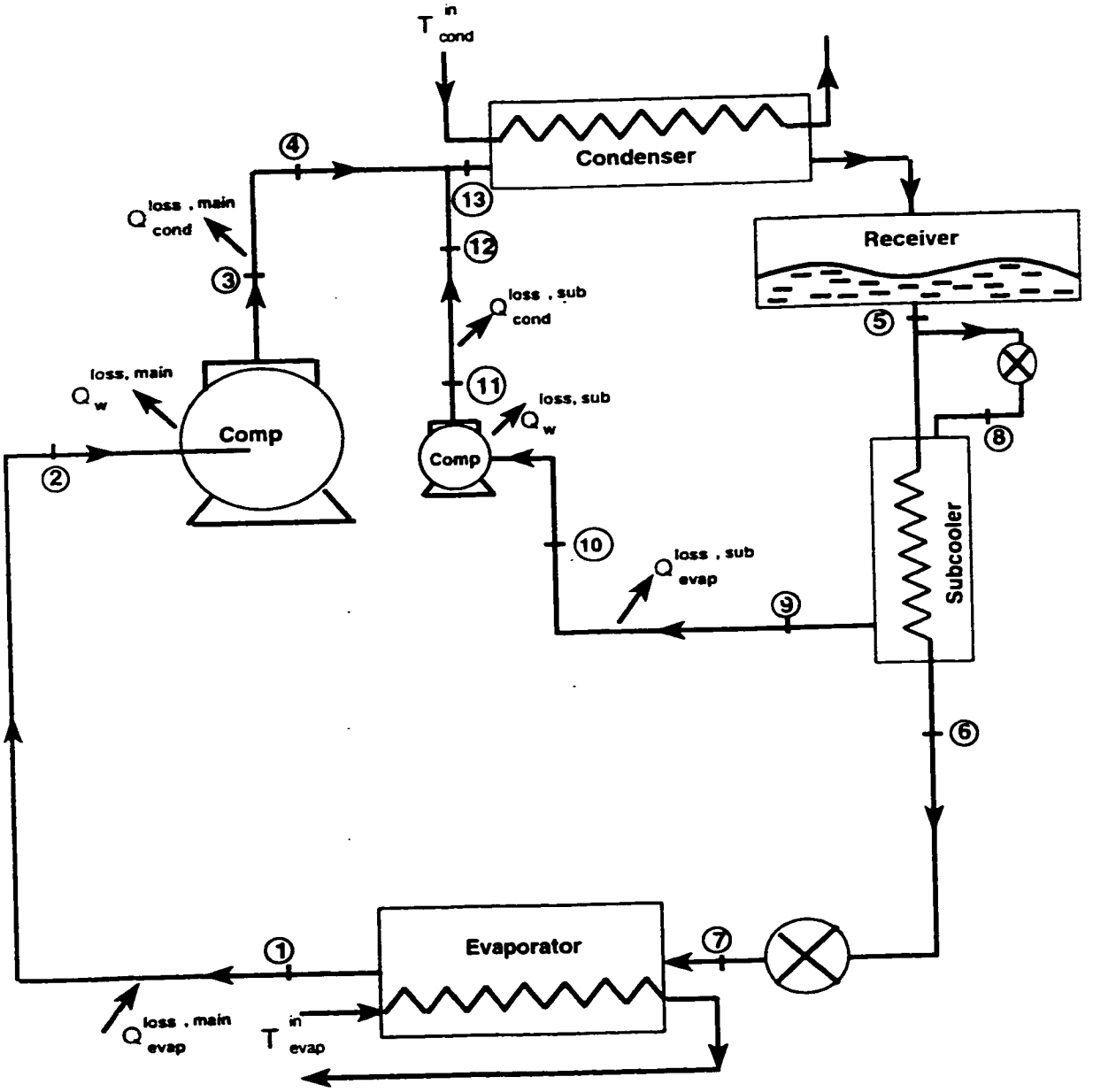

Figure 5.1: Schematic diagram of an integrated mechanical subcooling refrigeration cycle.

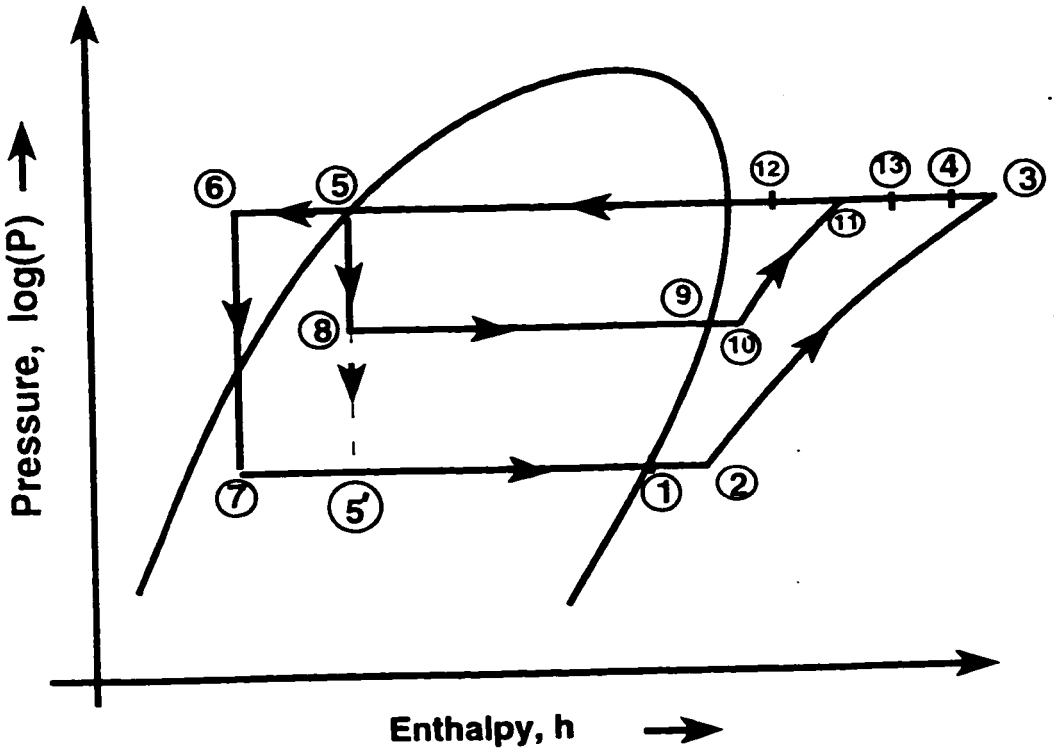

Figure 5.2: Pressure-enthalpy diagram of an integrated mechanical subcooling refrigeration cycle.

subcooler, leaves as a low pressure, low temperature, saturated vapor at state point 9 and enters the subcooler cycle compressor at state point 10. The refrigerant from state point 9 to point 10 takes heat from the surroundings. At state point 11, it leaves the compressor as a superheated vapor where it is mixed with the main cycle refrigerant coming from the main cycle compressor, and attains the state point of 13.

5.1 Analysis of the Cycle

Referring to the complete cycle shown in Fig. 5.1, from the first law of thermodynamics and the fact that the change in internal energy is zero for a cyclic process, we can write

$$\dot{W}^{main} + \dot{W}^{sub} = (\dot{Q}_{cond} + \dot{Q}_{cond}^{loss,main} + \dot{Q}_{W}^{loss,main} + \dot{Q}_{W}^{loss,sub} + \dot{Q}_{cond}^{loss,sub}) - (\dot{Q}_{evap}^{main} + \dot{Q}_{evap}^{loss,main} + \dot{Q}^{loss,sub}) \quad (5.1)$$

Since entropy is a state function, it's net change over the cycle is zero. Therefore, the contributions to the internal entropy generation are from heat trasfer (at the condenser, evaporator, the subcooler) and the entropy generation due to non-isentropic compression and expansion in the compressors and the expansion valve of the system, respectively. In addition, there is also a contribution to the entropy generation due to the mixing of the refrigerants after exiting their respective compressors, shown

in Fig. 5.1. The internal entropy generation can be expressed as

$$\dot{S}_{igen}^{total} = \frac{\dot{Q}_{cond}}{T_{cond}} - \frac{(\dot{Q}_{evap}^{main} + \dot{Q}_{evap}^{loss.main})}{T_{evap}^{main}} - (\dot{m}c_p)_{ref}^{main}.ln[\frac{T^{out.sub}}{T_{cond}}] - (\dot{m}c_p)_{ref}^{main}.ln[\frac{T_{13}}{T_3}] - \frac{(\dot{Q}^{sub} + \dot{Q}^{loss.sub})}{T^{sub}} - (\dot{m}c_p)_{ref}^{sub}.ln[\frac{T_{13}}{T_{11}}] \quad (5.2)$$

The heat transfer to and from the cycle occur by convection to the flowing fluid streams having finite mass flow rates and specific heats. Therefore, the rate of heat transfer to the cycle at a low temperature in the main cycle evaporator can be written as

$$\dot{Q}_{evap}^{main} = (\varepsilon\dot{C})_{evap}^{main}(T_{evap}^{in.main} - T_{evap}^{main}). \quad (5.3)$$

Similarly the rate of heat transfer between the refrigeration cycle and the sink in the main cycle condenser is

$$\dot{Q}_{cond} = (\varepsilon\dot{C})_{cond}(T_{cond} - T_{cond}^{in}). \quad (5.4)$$

Substituting the expressions of $(\dot{W}^{main} + \dot{W}^{sub})$ from Eq. (5.1) in the above equation and expressing refrigeration temperatures in terms of the more readily available coolant temperatures, one obtains an analytical formula for the COP, as a function of cooling capacity, coolant temperatures, heat exchanger characteristics, heat leak terms, internal cycle losses and the exit temperature of the main cycle refrigerant from the subcooler, as

$$\frac{1}{COP} = -1$$

$$+\frac{(\dot{Q}_{cond}^{loss.main}+\dot{Q}_{11}^{loss.main}+\dot{Q}_{11}^{loss.sub}+\dot{Q}_{cond}^{loss.sub})}{\dot{Q}_{evap}^{main}}$$

$$+\frac{X1}{X2}$$

$$-\frac{\dot{Q}_{evap}^{loss.main}+\dot{Q}^{loss.sub}}{\dot{Q}_{evap}^{main}} \tag{5.5}$$

where in the above equation we have.

$$\begin{aligned} X1 \;=\; & (\varepsilon\dot{C})_{cond}(T_{cond}^{in}) \\ & (\dot{S}_{igen}^{total}+\frac{(\dot{Q}_{evap}^{main}+\dot{Q}_{evap}^{loss.main})}{(T_{evap}^{in}-\frac{\dot{Q}_{evap}^{main}}{(\varepsilon\dot{C})_{evap}^{main}})}+(\dot{m}c_p)_{ref}^{main}.ln[\frac{(T^{out.sub})(T_{i3})}{(T_{cond})(T_3)}]+ \\ & \frac{(\dot{Q}^{sub}+\dot{Q}^{loss.sub})}{T^{sub}}+(\dot{m}c_p)_{ref}^{sub}.ln[\frac{T_{13}}{T_{11}}]) \end{aligned} \tag{5.6}$$

$$\begin{aligned} X2 \;=\; & \dot{Q}_{evap}^{main}((\varepsilon\dot{C})_{cond}-(\dot{S}_{igen}^{total}+ \\ & \frac{(\dot{Q}_{evap}^{main}+\dot{Q}_{evap}^{loss.main})}{(T_{evap}^{in}-\frac{\dot{Q}_{evap}^{main}}{(\varepsilon\dot{C})_{evap}^{main}})}+(\dot{m}c_p)_{ref}^{main}.ln[\frac{(T^{out.sub})(T_{i3})}{(T_{cond})(T_3)}]+ \\ & \frac{(\dot{Q}^{sub}+\dot{Q}^{loss.sub})}{T^{sub}}+(\dot{m}c_p)_{ref}^{sub}.ln[\frac{T_{13}}{T_{11}}])) \end{aligned} \tag{5.7}$$

Equation (5.5) gives the COP_{total} of the system for one set of input data. The required input data can be measured experimentally from an actual system or calculated from a thermodynamic model that is discussed in section (5.3). Tables 5.1

and 5.2 shows the required input data obtained from the thermodynamic model of the system. The value of COP_{total} obtained from Eq. (5.5) for Fig. 5.3(a), using the input data given in Table 5.1 was found to be 2.763, which is exactly equal to the value obtained from the thermodynamic model. Therefore, the analytical expression in Eq. (5.5) and the thermodynamic model are correct and hence they can be used for design and performance evaluation purpose. It should be noted that the heat leak terms are neglected in the above comparison because they do not contribute much towards the overall system performance as reported by Gordon et al. [15].

Figure 5.3 shows the characteristic performance curves ($1.0/COP$ vs $1.0/\dot{Q}_{evap}$) of the system. The plots are drawn using the input data given in Tables 5.1 and 5.2. The design point is also shown in the figure, where for Fig. 5.3(a) the design point is ($COP = 2.763$). Notice that the design point is located away from the minimum point because of the losses mainly due to non-isentropic compression in the compressors of the system. However the design point is at the minimum point ($COP = 4.1297$) when the efficiency of the compressors is assumed to be 100 percent, as shown in Fig. 5.3(b). The plots are hypothetical curves drawn for a constant T^{in}_{evap} and a range of LP cycle evaporator capacity ($\dot{Q}_{evap}$). We note that the shape of the curves is similar to the one obtained for a simple cycle discussed by Gordon et al. [15]. The figures shows that the COP is increasing with evaporator capacity upto the minimum point on the curve. In this region, the irreversibilities losses are

Table 5.1: Input data to be used in Eq. (5.5) for drawing Fig. 5.3(a). obtained from the thermodynamic model.

Cooling capacity of the main cycle evaporator	$(\dot{Q}_{evap}^{main})$	30.0 kW
Heat leak into the suction line of the main cycle	$(\dot{Q}_{evap}^{loss.main})$	0.0 W
Heat leak from the discharge line of the main cycle	$(\dot{Q}_{cond}^{loss.main})$	0.0 W
Heat leak from the compressor shell of the main cyclecompressor	$(\dot{Q}_{W}^{loss.main})$	0.0 W
Effectiveness and capacitance rate product for the main cycle evaporator	$(\varepsilon\dot{C})_{evap}^{main}$	5000.0 W/K
Effectiveness and capacitance rate product for the main cycle condenser	$(\varepsilon\dot{C})_{cond}^{main}$	5.5000.0 W/K
Internal entropy generation due to non isentropic compression and expansion in the complete cycle	$(\dot{S}_{igen}^{total})$	13.958 W/K
Coolant temperature at the inlet of the main cycle evaporator	$(T_{evap}^{in.main})$	0.0°C
Coolant temperature at the inlet of the condenser	(T_{cond}^{in})	40.0°C
Temperature of the main cycle refrigerant after exiting the subcooler	$(T^{out.sub})$	34.653°C
Refrigerant temperature at the main cycle condenser	(T_{cond}^{main})	46.653°C
Subcooler saturation temperature	T^{sub}	30.507°C
Mass flow rate and specific heat product of the main cycle refigerant	$((\dot{m}c_p)_{ref}^{main})$	309.46 W/K
Mass flow rate and specific heat product of the subcoler cycle refigerant	$((\dot{m}c_p)_{ref}^{sub})$	182.33 W/K
Cooling capacity of the subcooler	$(\dot{Q}^{sub})$	3713 W
Heat leak into the suction line of the subcooler cycle	$(\dot{Q}^{loss.sub})$	0.0 W
Heat leak from the discharge line of the subcooler cycle	$(\dot{Q}_{cond}^{loss.sub})$	0.0 W
Heat leak from the compressor shell of the subcooler cycle compressor	$(\dot{Q}_{W}^{loss.sub})$	0.0 W
Temperature at state point 13	T_{13}	54.717°C
Temperature at state point 3	T_3	57.9699°C
Temperature at state point 11	T_{11}	49.196°C

Table 5.2: Input data to be used in Eq (5.5) for drawing Fig. 5.3(b), obtained from the thermodynamic model.

Cooling capacity of the main cycle evaporator	$(\dot{Q}_{evap}^{main})$	30.0 kW
Heat leak into the suction line of the main cycle	$(\dot{Q}_{evap}^{loss,main})$	0.0 W
Heat leak from the discharge line of the main cycle	$(\dot{Q}_{cond}^{loss,main})$	0.0 W
Heat leak from the compressor shell of the main cyclecompressor	$(\dot{Q}_{W}^{loss,main})$	0.0 W
Effectiveness and capacitance rate product for the main cycle evaporator	$(\varepsilon\dot{C})_{evap}^{main}$	5.0 kW/K
Effectiveness and capacitance rate product for the main cycle condenser	$(\varepsilon\dot{C})_{cond}^{main}$	5.50 kW/K
Internal entropy generation due to non isentropic compression and expansion in the complete cycle	$(\dot{S}_{igen}^{total})$	3.517 W/K
Coolant temperature at the inlet of the main cycle evaporator	$(T_{evap}^{in,main})$	$0.0°C$
Coolant temperature at the inlet of the condenser	(T_{cond}^{in})	$40.0°C$
Temperature of the main cycle refrigerant after exiting the subcooler	$(T^{out,sub})$	$34.039°C$
Refrigerant temperature at the main cycle condenser	(T_{cond}^{main})	$46.039°C$
Subcooler saturation temperature	T^{sub}	$30.029°C$
Mass flow rate and specific heat product of the main cycle refigerant	$((\dot{m}c_p)_{ref}^{main})$	306.85 W/K
Mass flow rate and specific heat product of the subcoler cycle refigerant	$((\dot{m}c_p)_{ref}^{sub})$	195.85 W/K
Cooling capacity of the subcooler	$(\dot{Q}^{sub})$	3682.20 W
Heat leak into the suction line of the subcooler cycle	$(\dot{Q}^{loss,sub})$	0.0 W
Heat leak from the discharge line of the subcooler cycle	$(\dot{Q}_{cond}^{loss,sub})$	0.0 W
Heat leak from the compressor shell of the subcooler cycle compressor	$(\dot{Q}_{W}^{loss,sub})$	0.0 W
Temperature at state point 13	T_{13}	$52.1038°C$
Temperature at state point 3	T_3	$54.3529°C$
Temperature at state point 11	T_{11}	$48.58°C$

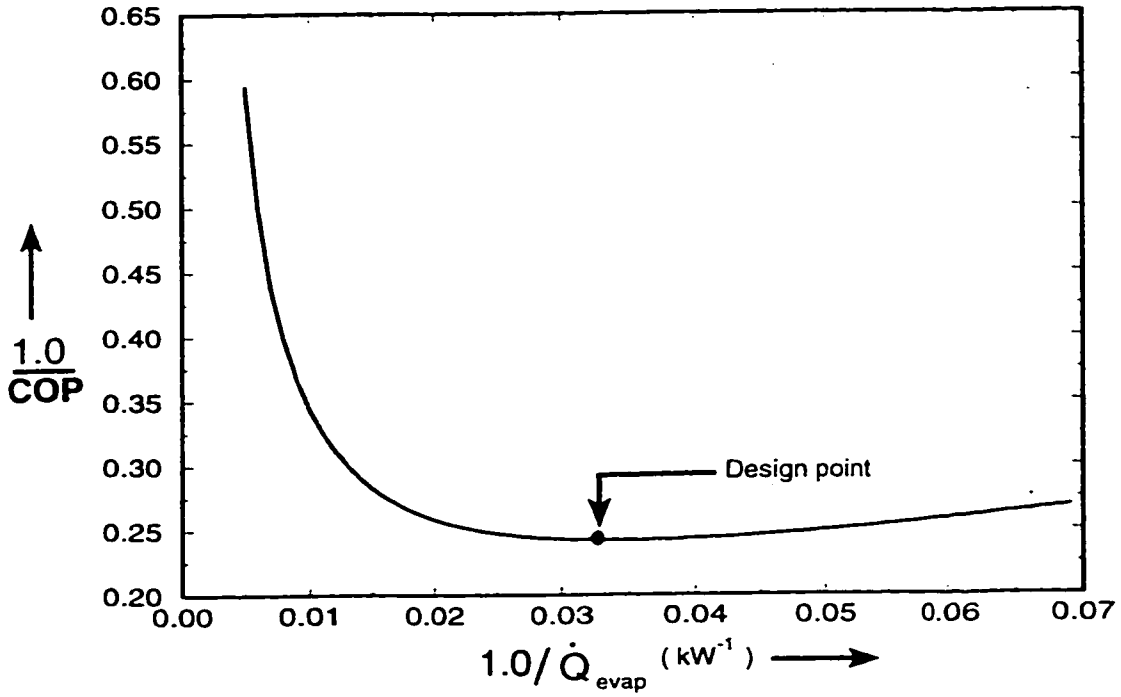

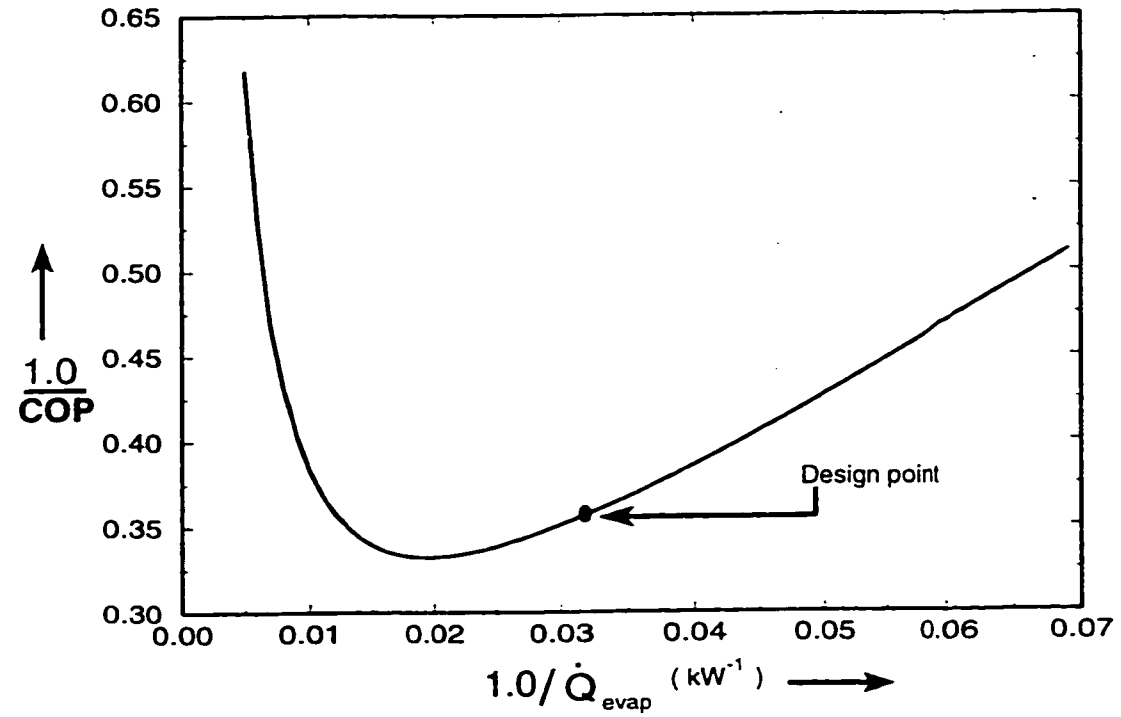

Figure 5.3: Performance curves of an integrated mechanical subcooling vapor compression refrigeration system. for an input data given in Tables 5.1 and 5.2.

mainly due to fluid friction (some times referred to as non-isentropic losses) in the compressor and the expansion valve. While at evaporator capacities greater than the minimum point, COP decreases significantly because of the losses due to the finite rate of heat transfer in the heat exchangers of the system. It should be noted that the performance of the system in the light of various irreversible losses of the system is similar to the performance of a simple cycle discussed by Gordon and Choon [16].

5.2 Prediction of Optimum Subcooler Saturation Temperature

Figure 5.1 shows that the main cycle refrigerant and the subcooler cycle refrigerant mix with each other at state point 13, after leaving their respective compressors. The mixture then rejects heat in the condenser at almost at a constant temperature T_{cond}. It can be deduced that each cycle refrigerant uses a fraction of the total condenser area for rejecting it's heat. To investigate the fraction of area utilized by each refrigerant, a factor defined as the subcooler heat rejection factor is defined as follows

$$f_{rejection} = \frac{(\varepsilon \dot{C})^{sub}_{cond}}{(\varepsilon \dot{C})^{main}_{cond} + (\varepsilon \dot{C})^{sub}_{cond}} \tag{5.8}$$

where $((\varepsilon\dot{C})^{main}_{cond} + (\varepsilon\dot{C})^{sub}_{cond})$ is the total thermal inventory of the condenser $(\varepsilon\dot{C})_{cond}$. The individual areas can be expressed in terms of the total area as follows

$$(\varepsilon\dot{C})^{sub}_{cond} = f_{rejection}(\varepsilon\dot{C})_{cond} \tag{5.9}$$

$$(\varepsilon\dot{C})^{main}_{cond} = (1.0 - f_{rejection})(\varepsilon\dot{C})_{cond} \tag{5.10}$$

It should be noted that the performance of the integrated system is also controlled by the subcooler cycle temperature T^{sub}. It is expected that there is an optimum subcooler temperature at which the overall coefficient of performance of the cycle COP_{total} is maximized. This optimum temperature can be investigated by expressing COP_{total} of the system in terms of the subcooler saturation temperature T^{sub} and other variables of the system as

$$COP_{total} = \frac{1 + X(T_{cond} - T^{sub})}{\frac{(T^{in}_{cond} - T^{in,main}_{evap}) + (\Delta T_m)}{T^{in,main}_{evap} - (\Delta T_m)} + \frac{X(T_{cond} - T^{sub})(\Delta TT_s)}{T^{in}_{cond} - (\Delta TT_s)}} \tag{5.11}$$

where in the above equation, we have subcooler parameter given by

$$X = \frac{(\varepsilon\dot{C})^{sub}_{evap}}{\dot{Q}^{main,nosub}_{evap}}, \tag{5.12}$$

and various temperatures as

$$(\Delta T_m) = \dot{Q}^{main}_{evap}\left[\frac{1}{(\varepsilon\dot{C})^{main}_{evap}} + \frac{1}{(1.0 - f_{rejection})(\varepsilon\dot{C})_{cond}}\right] \tag{5.13}$$

$$(\Delta T_s) = Q^{sub}\left[\frac{1}{(\varepsilon\dot{C})^{sub}_{evap}} + \frac{1}{f_{rejection}(\varepsilon\dot{C})_{cond}}\right] \tag{5.14}$$

$$T_{cond} = T^{in}_{cond} + \frac{\dot{Q}^{main}_{evap}}{(1.0 - f_{rejection})(\varepsilon\dot{C})_{cond}}\left[\frac{T^{in}_{cond}}{T^{in,main}_{evap} - (\Delta T_m)}\right] \tag{5.15}$$

$$(\Delta TT_s) = (\Delta T_s) + T_{cond}^{in} - T_{cond} \tag{5.16}$$

It should be noted that Eq. (5.11) represents a completely irreversible temperature-dependent integrated mechanical subcooling model.

To show the predicted improvement in performance of a mechanical subcooling refrigeration system with respect to the single stage cycle, the curves are ploted in a normalized form defined as

$$COPN = \frac{COP_{total}}{COP_{main}}. \tag{5.17}$$

Similarly a reduced subcooler saturation temperature θ is defined as

$$\theta = \frac{T^{sub} - T_{evap}^{main}}{T_{cond} - T_{evap}^{main}} \tag{5.18}$$

Figure 5.4(a) shows the plot of normalized coefficient of performance ($COPN$) and the reduced subcooler saturation temperature (θ). The plots are obtained by using Eq. (5.11) for the following set of input data: $T_{evap}^{in,main} = 0.0\ ^oC$, $T_{cond}^{in} = 40.0\ ^oC$, $\dot{Q}_{evap}^{main} = 30.0\ kW$, $(\varepsilon\dot{C})_{evap}^{main} = 5000.0\ W/K$, $(\varepsilon\dot{C})_{cond} = 5500.0\ W/K$. In these plots θ varies between T_{evap}^{main} and T_{cond}. It can be seen from the plots that maximum $COPN$ occurs at approximately $\theta = 0.5$, and it almost remains constant for all the values of the subcooler cycle heat exchanger parameter X. For θ lower than 0.5, the difference between T_{sub} and T_{evap}^{main} is less and hence maximum amount of subcooling is being performed: in this case the thermal lift of the subcooling cycle

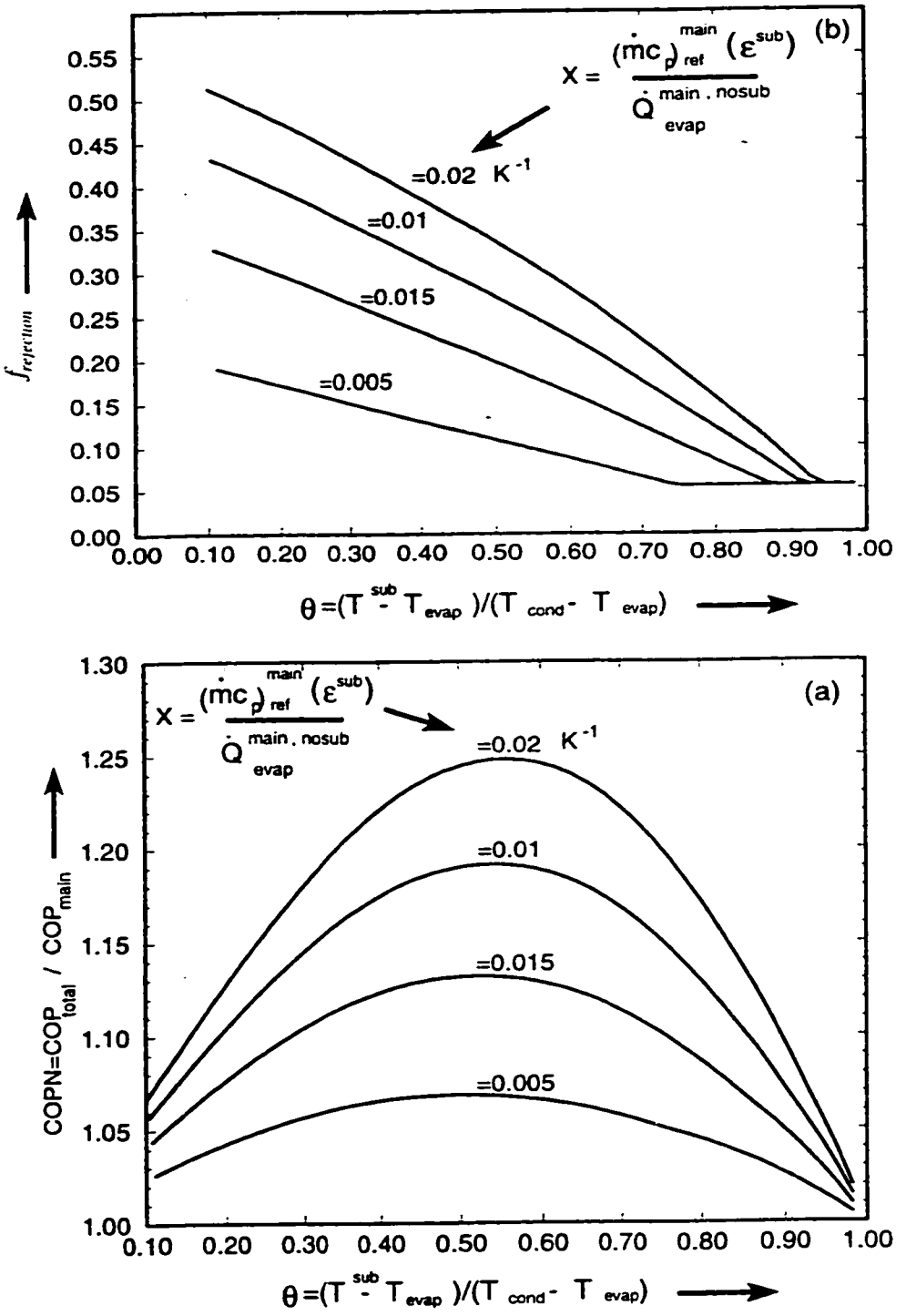

Figure 5.4: Variations of $COPN$ (a) and the subcooler heat rejection factor $f_{rejection}$ (b) with θ for a completely irreversible temperature dependent integrated mechanical subcooling system.

is close to that of the main cycle. Therefore, the subcooling cycle compressor consumes more power, and the advantage of using integrated mechanical subcooling is destroyed and the $COP.N$ of the system reduces. For θ greater than 0.5, the difference between T_{sub} and T_{cond} is less and hence a relatively low amount of subcooling is being performed and the overall cycle behaves very close to a simple cycle, thus the value of $COP.N$ is lower than the maximum possible value. In between these two extremes, there is an optimum T^{sub} at which $COP.N$ is maximum, as shown in the figure.

Figure 5.4(b) shows the variation of the subcooler heat rejection factor $f_{rejection}$ with the reduced subcooler temperature θ. It can be seen from the plots that at higher values of θ, the amount of subcooling performed is lower and hence the amount of heat to be rejected by the subcooler cycle refrigerant is also low. Therefore, it uses a small fraction of the condenser area, however as the value of θ reduces, the amount of subcooling performed is higher: thereby requiring more subcooler compressor work and hence the amount of heat to be rejected by the subcooler cycle refrigerant is relatively high. Therefore, it uses a large fraction of the condenser area. Also, for a given value of θ the heat rejection factor increases with the value of N since subcooling increases with the subcooler heat exchanger parameter N.

Figure 5.5(a) shows the effect of condenser coolant inlet temperature (T^{in}_{cond}) on

the subcooler heat rejection factor $f_{rejection}$ for constant values of other system parameters. The figure shows that for higher values of T_{cond}^{in} and particularly at low values of θ, the heat rejection factor $f_{rejection}$ increases, since the amount of subcooling increases: thereby requiring more subcooler compressor work and therefore an increase in heat rejection factor for the subcooling cycle. Also, the figure shows that at higher values of θ, for all the values of T_{cond}^{in}, the amount of subcooling performed is lower and hence the amount of heat to be rejected by the subcooler cycle refrigerant is relatively low. Therefore, it uses a small fraction of the condenser area.

Figure 5.5(b) shows the effect of evaporator coolant inlet temperature T_{evap}^{in} on the subcooler heat rejection factor $f_{rejection}$ for constant values of other system parameters. Similar to Fig. 5.4(a), this figure also shows that for lower values of T_{evap}^{in} and particularly at low values of θ, the heat rejection factor $f_{rejection}$ increases, since the amount of subcooling increases; thereby requiring more subcooler compressor work and hence increase in heat rejection factor for the subcooling cycle. Also, the figure shows that at higher values of θ and almost for all the values of T_{evap}^{in}, the amount of subcooling performed is lower and hence the amount of heat to be rejected by the subcooler cycle refrigerant is relatively low. Therefore, it uses a small fraction of the condenser area, however as described earlier that as the value of θ reduces, the amount of subcooling performed is higher and hence the amount of heat to be rejected by the subcooler cycle refrigerant is relatively high. Therefore it

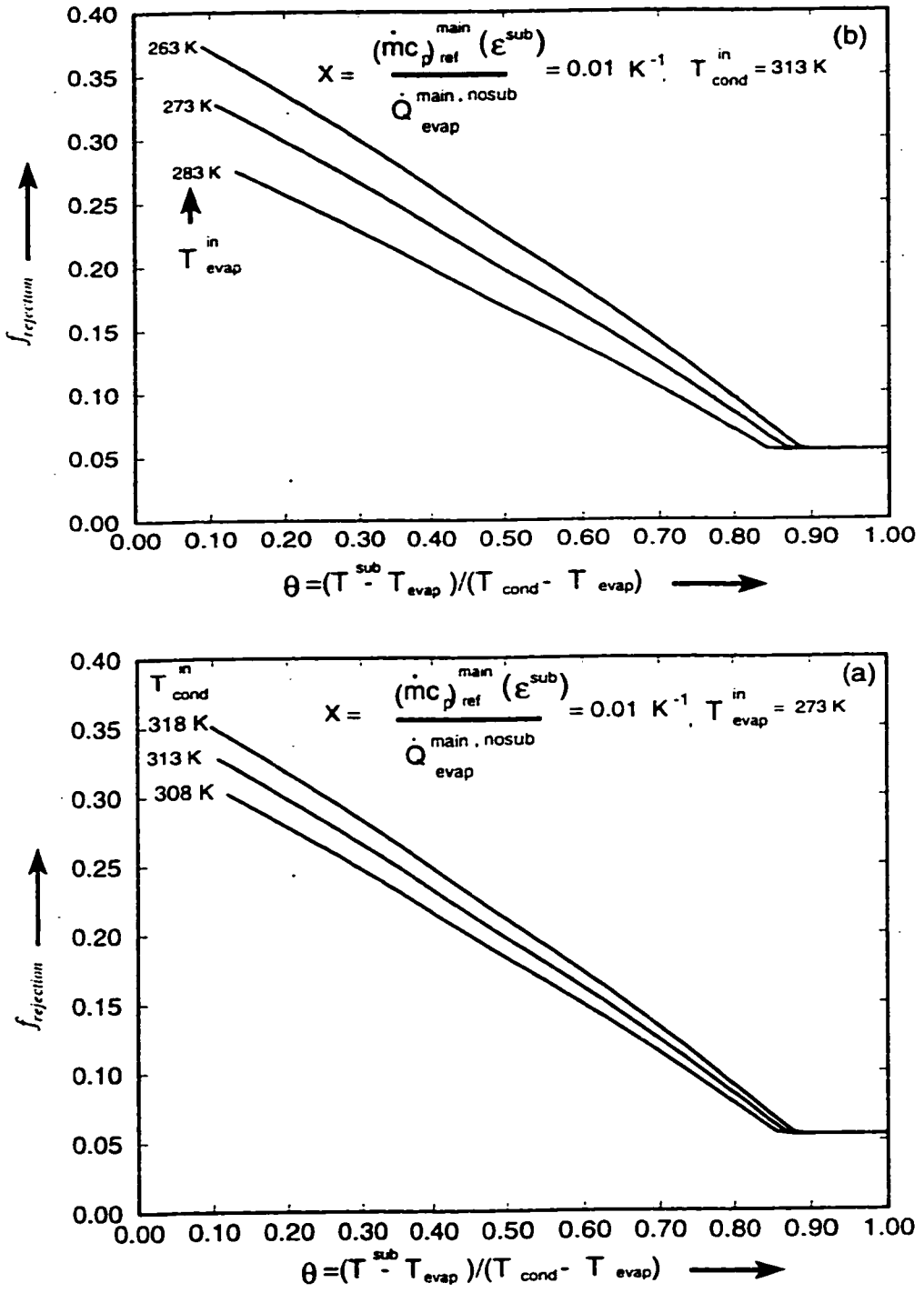

Figure 5.5: Variations of heat rejection factor $f_{rejection}$ for various T^{in}_{cond} (a) and for various T^{in}_{evap} (b) with θ.

uses a large fraction of the condenser area.

5.3 A Finite Time Thermodynamic Model of the System

The rate of heat transfer to the cycle in the main cycle evaporator can be expressed in terms of temperature, mass flow rates, and change in enthalpy of the refrigerant as

$$\dot{Q}_{evap}^{main} = (\varepsilon \dot{C})_{evap}^{main}(T_{evap}^{in,main} - T_{evap}^{main}) = \dot{m}^{main}(h_1 - h_7). \tag{5.19}$$

The compressor operation is described in terms of an isentropic efficiency η_{comp}^{main}, so that the power requirement for the main cycle compressor is given by

$$\dot{W}^{main} = \dot{m}^{main}(h_3 - h_2) = \frac{\dot{W}_s^{main}}{\eta_{comp}^{main}}. \tag{5.20}$$

In the subcooler, the rate of heat transfer between the main cycle refrigerant and the one flowing through the subcooler is given by

$$\dot{Q}^{sub} = (\dot{m}C_p)^{main}(T_{cond} - T^{out,sub}) = \dot{m}^{main}(h_5 - h_6). \tag{5.21}$$

Assuming that an amount of $\dot{Q}_{evap}^{loss,main}$ of heat, leaks into the suction line of the main cycle compressor, which can be expressed as

$$\dot{Q}_{evap}^{loss,main} = \dot{m}^{main}(h_2 - h_1). \tag{5.22}$$

Similarly assuming that an amount of $(\dot{Q}_{cond}^{loss,main} + \dot{Q}_{W}^{loss,main})$ of heat leaks from the discharge line and compressor shell given by

$$\dot{Q}_{cond}^{loss,main} + \dot{Q}_{W}^{loss,main} = \dot{m}_{ref}^{main}(h_3 - h_4). \tag{5.23}$$

For the subcooler cycle loop, the rate of heat transfer between the refrigerant flowing through the subcooler and that coming from the condenser is given as

$$\dot{Q}^{sub} = (\dot{m}C_p)_{ref}^{main}(\varepsilon)^{sub}(T_{cond} - T^{sub}) = \dot{m}^{sub}(h_9 - h_8). \tag{5.24}$$

The work input to the subcooler cycle compressor is given by

$$\dot{W}^{sub} = \dot{m}_{ref}^{sub}(h_{11} - h_{10}) = \frac{\dot{W}_s^{sub}}{\eta_{comp}^{sub}}. \tag{5.25}$$

Assuming that an amount of $\dot{Q}_{evap}^{loss,sub}$ of heat leaks in to the suction line of the subcooler cycle, we get

$$\dot{Q}_{loss}^{sub} = \dot{m}_{ref}^{sub}(h_{10} - h_9). \tag{5.26}$$

Similarly assuming that an amount of $(\dot{Q}_{cond}^{loss,sub} + \dot{Q}_{W}^{loss,sub})$ of heat leaks from the discharge line and the compressor shell, expressed as

$$\dot{Q}_{cond}^{loss,sub} + \dot{Q}_{W}^{loss,sub} = \dot{m}_{ref}^{sub}(h_{11} - h_{12}). \tag{5.27}$$

The mixing of the main cycle refrigerant and the subcooler cycle refrigerant after leaving their respective compressors is given by

$$\dot{m}^{main}(h_4 - h_{13}) = \dot{m}^{sub}(h_{13} - h_{12}). \tag{5.28}$$

From the above equation, we get

$$h_{13} = \frac{(\dot{m}^{main} h_4 + \dot{m}^{sub} h_{12})}{(\dot{m}^{main} + \dot{m}^{sub})}. \tag{5.29}$$

The rate of heat transfer between the refrigeration cycle and the sink in the condenser is

$$\dot{Q}_{cond} = (\varepsilon \dot{C})_{cond}(T_{cond} - T_{cond}^{in.main}) = (\dot{m}^{main} + \dot{m}^{sub})(h_{13} - h_5). \tag{5.30}$$

The above equations have been solved numerically by using the thermodynamic property data for several different refrigerants. The flow chart representing the method of solving the equations is shown in Fig. 5.6, wherein the terms SATPRP and TRIAL represents the subroutines for calculating the refrigerant saturated and vapor properties, respectively. These subroutines need any two independent intensive properties of the refrigerant to find other properties at a given state. For this purpose, a computer program, originally developed by Kartsounes and Erth [43] and modified by Fisher and Rice [44] and Khan and Zubair [46], have been used. The program gives the COP_{total} as well as all the other important parameters of the system for the following set of input data: $\dot{Q}_{evap}^{main}$, $(\varepsilon \dot{C})_{cond}^{main}$, $(\varepsilon \dot{C})_{evap}^{main}$, T_{cond}^{in}, T_{evap}^{in} and $AMTS$.

Figure 5.7(a) shows the plot of $COPN$ vs the reduced subcooler saturation temperature θ and the heat exchanger thermal inventory parameter K, defined as

$$K = (\varepsilon \dot{C})_{evap} + (\varepsilon \dot{C})_{cond}. \tag{5.31}$$

The results shown in the figure are obtained from the above described thermodynamic model for $R-134a$ as the refrigerant, and having the following set of input data: $T_{evap}^{in,main} = 0.0\,^oC$, $T_{cond}^{in} = 40.0\,^oC$, $\eta_{comp}^{main} = 0.65$, $\eta_{comp}^{sub} = 0.7$, $(\dot{m}\dot{C}_p)_{ref}(\varepsilon^{sub}) = 0.1\ kW/K$ and $\dot{Q}_{evap}^{main} = 30.0\ kW$. Fig. 5.7(b) shows the corresponding variation of the system operating temperatures for $K = 12.5\ kW/K$. The figure shows that as the value of heat exchanger thermal inventory parameter K increases, the value of $COPN$ also increases, because as K increases the irreversible losses due to heat transfer decreases in the heat exchangers of the system, thus increasing the system performance. We note that the property-dependent model predicts the same relationship between $COPN$ and the reduced subcooler saturation temperature θ, as that discussed earlier by the temperature-dependent model. (refer to Fig. 5.4(a)). It should be noted that the heat leak terms are neglected in the above analysis because they do not contribute much towards the overall system performance (refer Gordon et al., (1996)). Referring to Fig. 5.7(b), we note that the condenser temperature more-or-less remains constant, however one would expect a variation in T_{cond}^{main} with the reduced subcooler saturation temperature θ. The calculations indicate a somewhat constant temperature varying between 319.42 and 319.33 K, which is mainly due to the fact that the variation in $\dot{Q}_{cond}$ is relatively small and moreover the value of $((\varepsilon\dot{C})_{cond} = 6.5\ kW/K)$ in the calculation of T_{cond}^{main} is high.

It should be emphasized that Figs. 5.4 and 5.5 are obtained by using the ana-

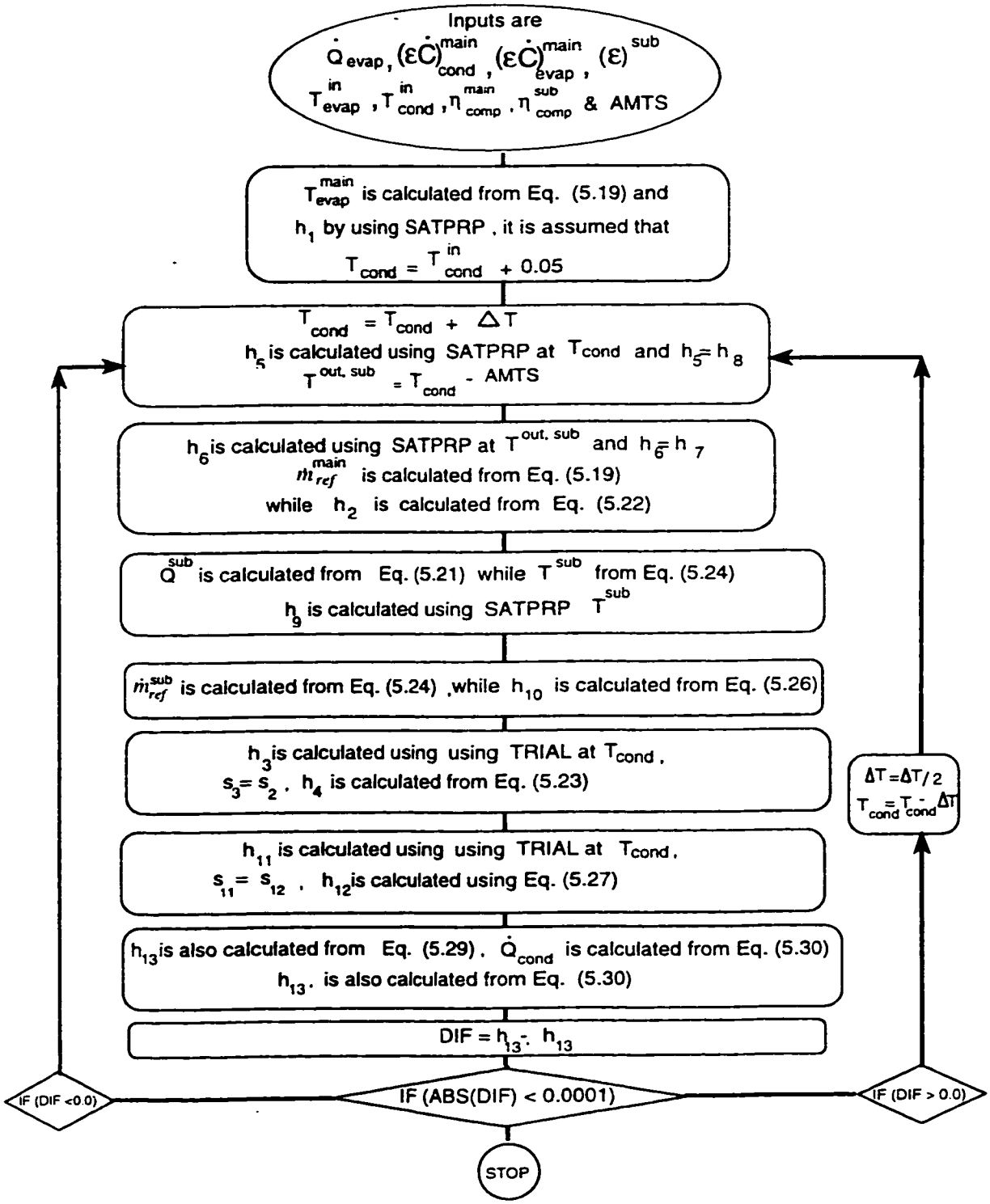

Figure 5.6: Flow chart for a thermodynamic model of an integrated mechanical subcooling system.

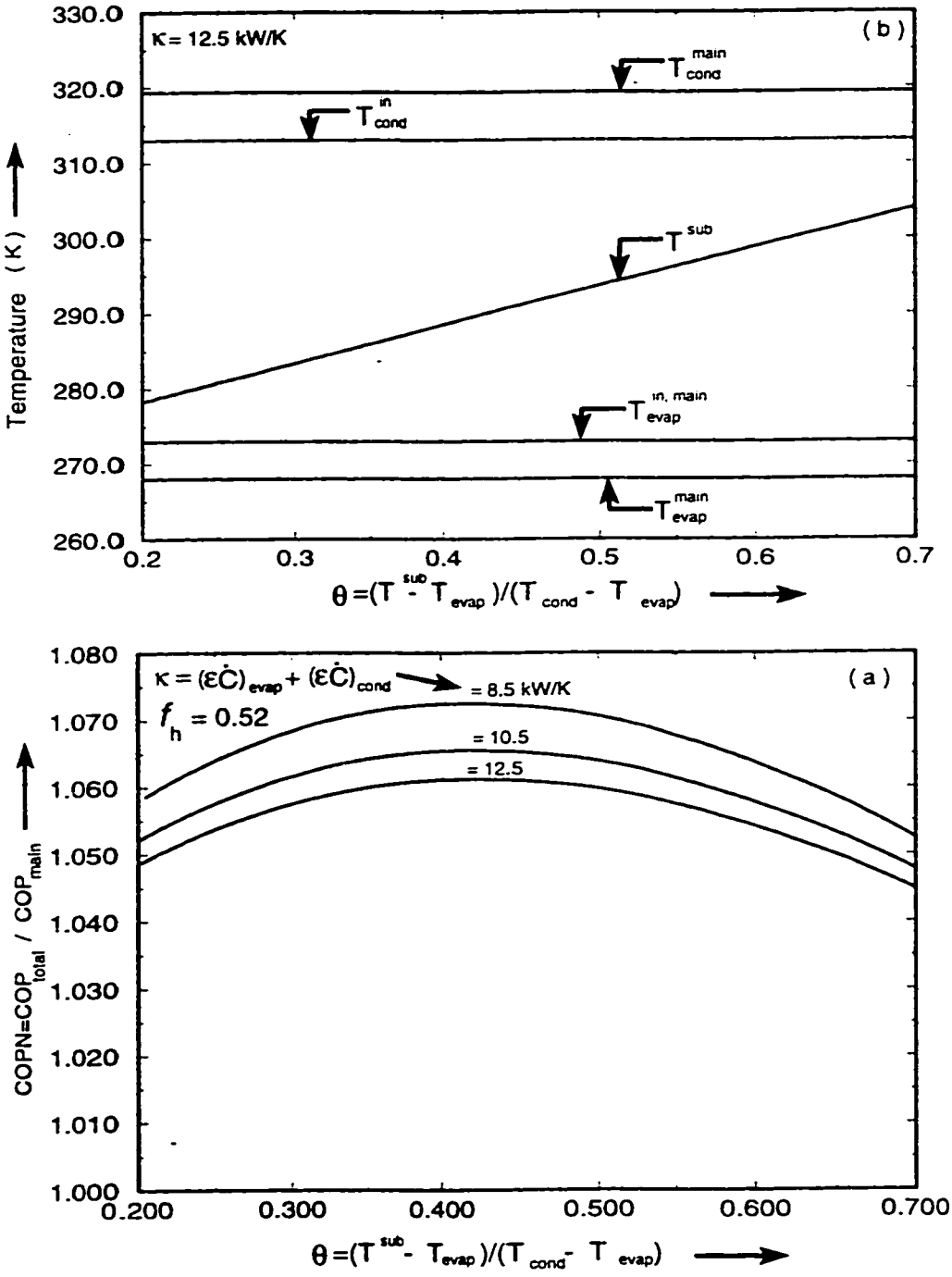

Figure 5.7: Variations of $COPN$ (a) and of operating temperatures (b) with θ for the following input data: $\dot{Q}_{evap}^{main} = 30.0\ kW$, $(\dot{m}c_p)_{ref}^{main}(\varepsilon)^{sub} = 0.1\ kW/K$, $\eta_{comp}^{main} = 0.65$, $\eta_{comp}^{sub} = 0.70$, $T_{evap}^{in,main} = 273.0\ K$, $T_{cond}^{in} = 313.0\ K$.

lytical expression given in Eq. (5.11) and are as such dependent upon temperature only. These plots will remain same for different types of refrigerants used in a given system. However similar type of plots can also be obtained from the thermodynamic model discussed in this section. In this regard, Fig. 5.8 shows the plot of COP_{total} vs the reduced subcooler saturation temperature θ and the subcooler parameter X of the property dependent and the temperature dependent ideal mechanical subcooling vapor compression refrigeration system with irreversible losses only in the subcooler and using $R-134a$ as the refrigerant. The plots are drawn for the following set of input data: $T^{in}_{evap} = 0.0\ ^oC$, $T^{in}_{cond} = 40.0\ ^oC$ and $\dot{Q}^{main}_{evap} = 30.0\ kW$. The figure shows that the shape of the curves for the two models are similar and the difference in the values of COP_{total} is mainly due to non-isentropic expansion in the expansion valves of the property dependent model.

5.4 Optimum Distribution of the Heat Exchanger Areas

The total heat exchanger area defined by Eq. (5.31) is considered as the design constraint, therefore the problem involved in the optimization is how to allocate the total heat exchanger area between the condenser and the evaporator of the cycle. To investigate the effect of relative size of heat exchangers, the following dimensionless

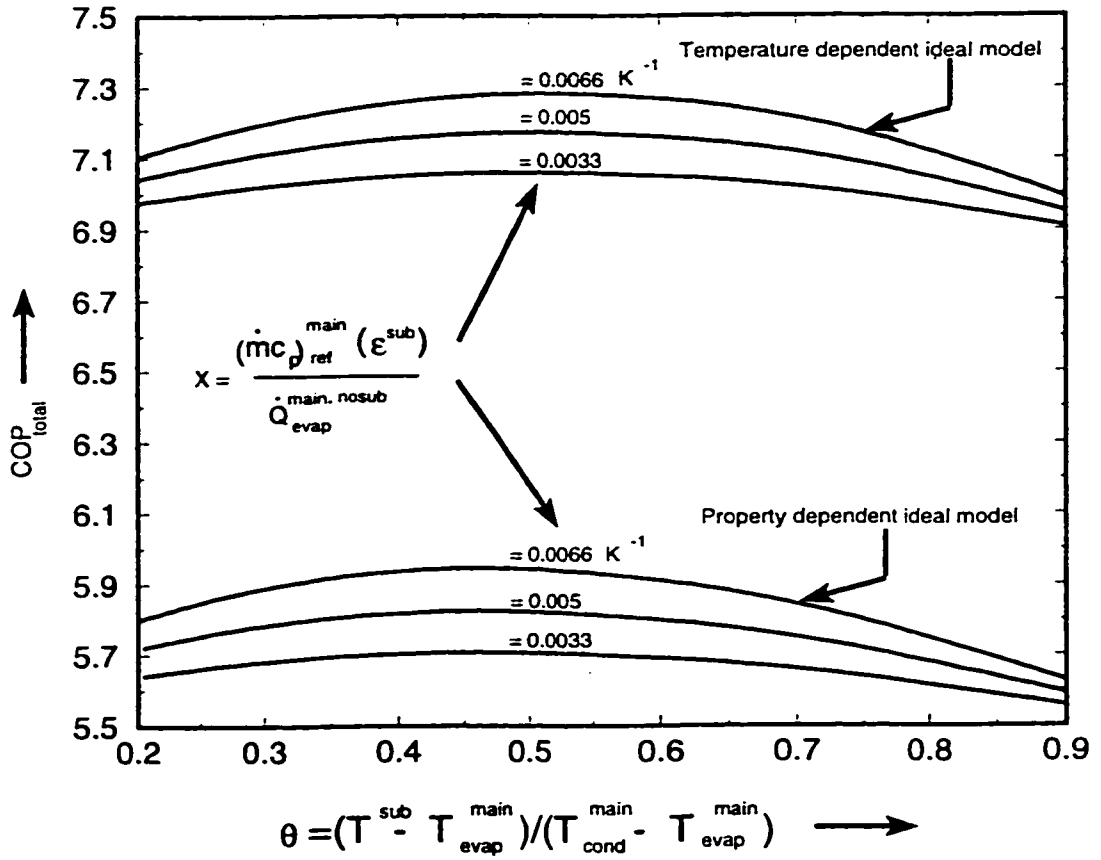

Figure 5.8: Variation of COP_{total} with θ for an ideal temperature dependent and property dependent mechanical subcooling system: irreversible losses only in the subcooler.

heat exchanger parameter is defined to study the performance of the system:

$$f_h = \frac{(\varepsilon \dot{C})_{cond}}{(\varepsilon \dot{C})_{cond} + (\varepsilon \dot{C})_{evap}} \tag{5.32}$$

A set of sample plots, shown in Fig. 5.9(a), is drawn between COP_{total} and the dimensionless heat exchanger parameter (f_h) using the output from the model: for the following set of input data and using $R-134a$ as the refrigerant: $\dot{Q}_{evap}^{main} = 30.0\ kW$, $T_{evap}^{in,main} = 273.0\ K$, $T_{cond}^{in} = 313.0\ K$, $K = 10.0\ kW/K$, $\eta_{comp}^{main} = 0.65$, $\eta_{comp}^{sub} = 0.7$. The plots are drawn for different values of the parameter $(\dot{m}C_p)_{ref}^{main}(\varepsilon)^{sub}$ and for each value of the dimensionless heat exchanger parameter (f_h): the most optimum value of the subcooler saturation temperature T^{sub} is calculated as shown in Fig. 5.7(a). For better explanation of the plots, the variation of system temperatures are shown in Fig. 5.9(b) for $(\dot{m}C_p)_{ref}^{main}(\varepsilon)^{sub} = 0.2\ kW/K$. The figure shows that COP_{total} is maximum at about $f_h = 0.55$, for all the curves. The difference between the T_{cond}^{in} and T_{cond} is higher at low values of the parameter f_h, therefore the heat transfer in the condenser takes place with higher temperature difference resulting in higher irreversible losses due to finite rate of heat transfer and these losses decrease as f_h increases. However, the difference between $T_{evap}^{in,main}$ and T_{evap}^{main} increases as f_h increases and the heat transfer in the evaporator takes place at a higher temperature difference, resulting in an increase in irreversible losses due to the finite rate of heat transfer. At $f_h = 0.55$, the temperature difference in the evaporator and the condenser is minimum, hence COP_{total} is maximum at this point.

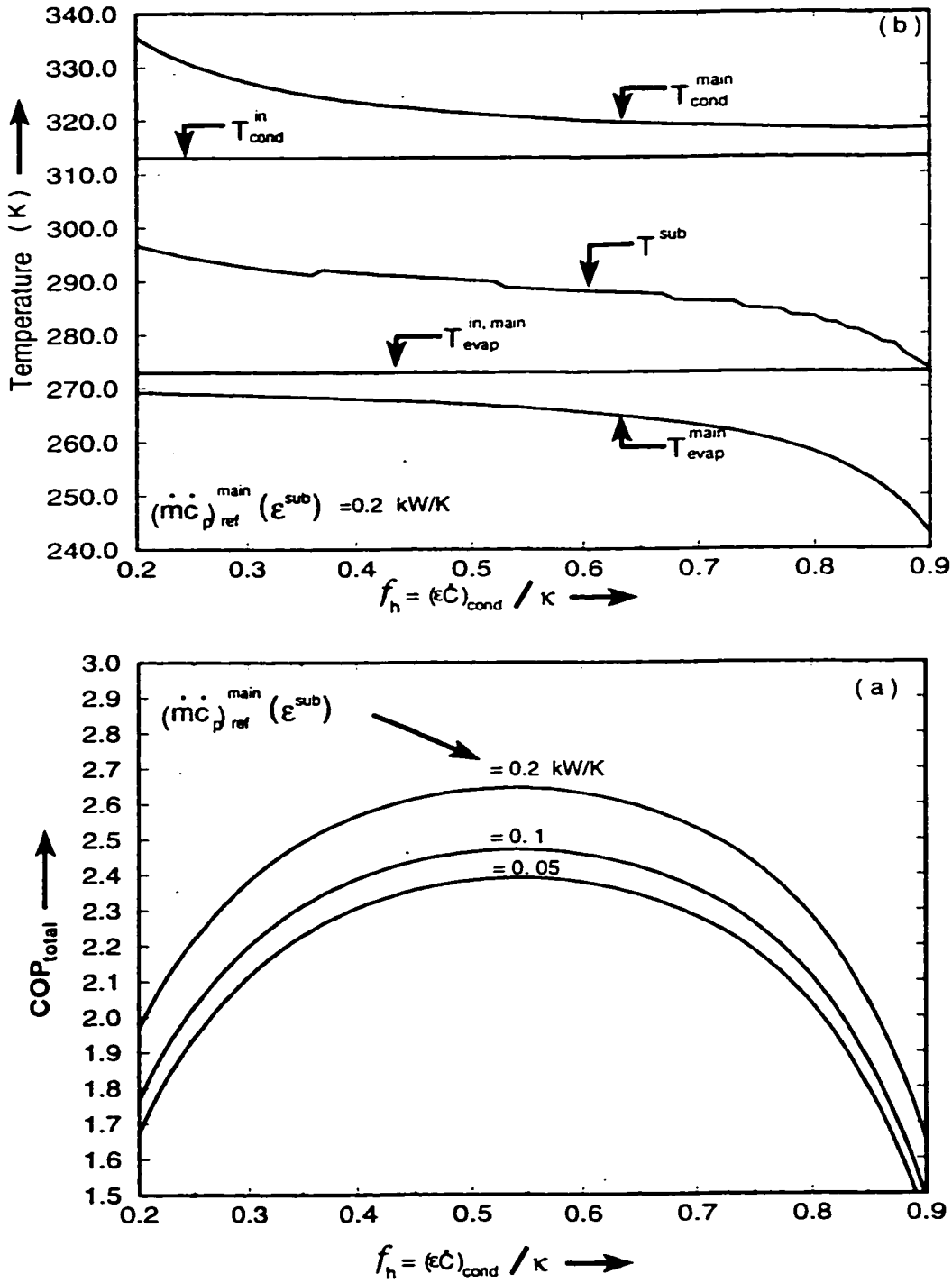

Figure 5.9: Variation of COP_{total} (a) and of operating temperatures (b) with f_h for the input data: $\dot{Q}_{evap}^{main} = 30.0\ kW$, $\eta_{comp}^{main} = 0.65$, $\eta_{comp}^{sub} = 0.70$, $T_{evap}^{in,main} = 273.0\ K$, $T_{cond}^{in} = 313.0\ K$.

It should also be noted that the heat transfer in the subcooler takes place through the temperature difference between T_{cond}^{main} and T_{sub}, and the figure shows that this temperature difference is approximately constant for all values of f_h.

Chapter 6

Thermodynamic Analysis of a Two-Stage Vapor Compression Refrigeration System

The major components of a two stage vapor compression refrigeration system includes two reciprocating compressors, two expansion valves, a condenser, an evaporator and a flash tank. The system consists of two simple cycles, (HP cycle and LP cycle) coupled to each other via a flash tank as shown in Fig. 6.1, while the pressure-enthalpy diagram is shown in Fig. 6.2. The components of the system are connected in a closed loop through a piping system that has heat transfer with the surroundings. The figure shows that the LP cycle refrigerant leaves the evaporator at state point 2 as a low pressure, saturated vapor and enters the LP cycle

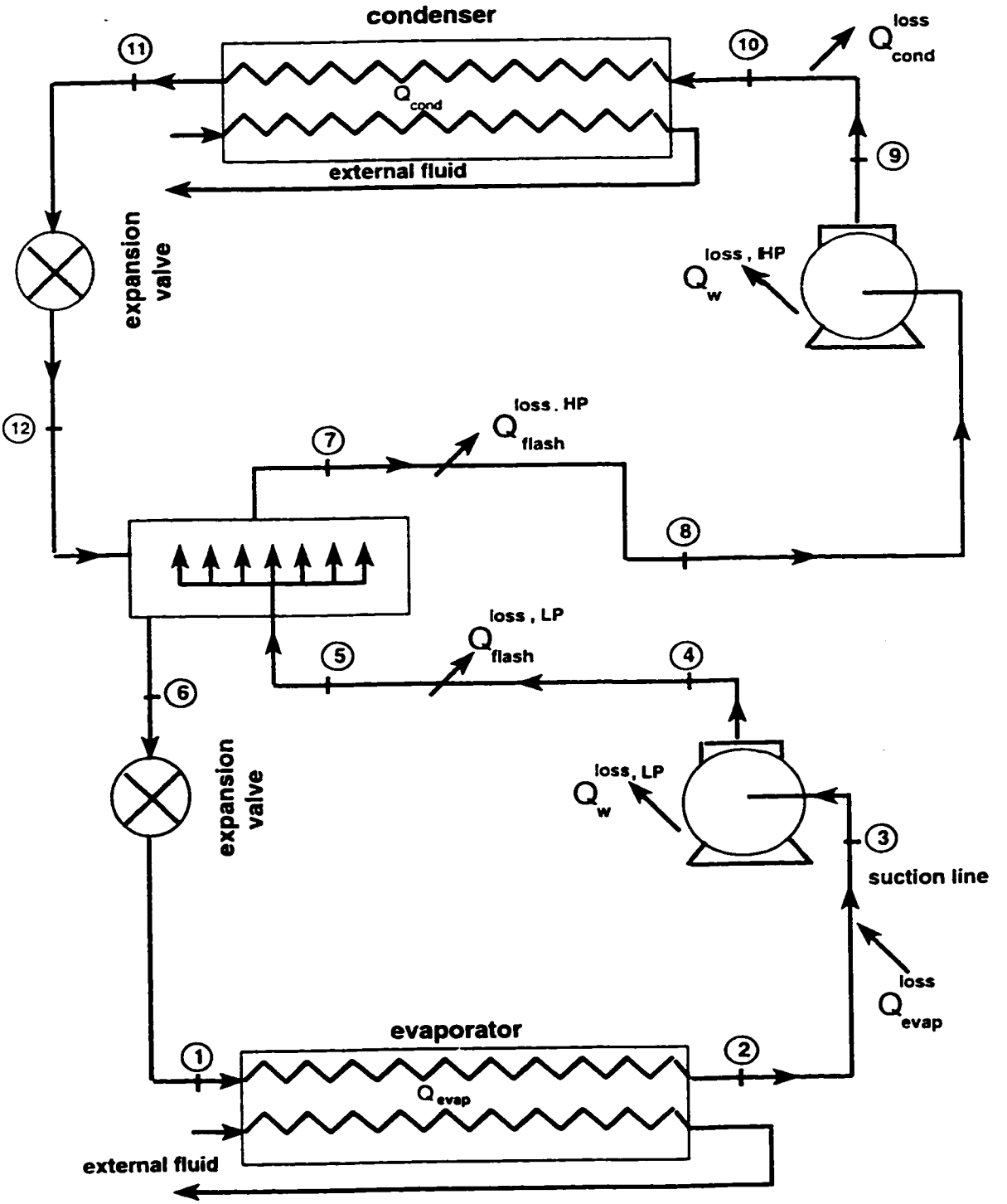

Figure 6.1: Schematic diagram of a two stage vapor compression refrigeration system.

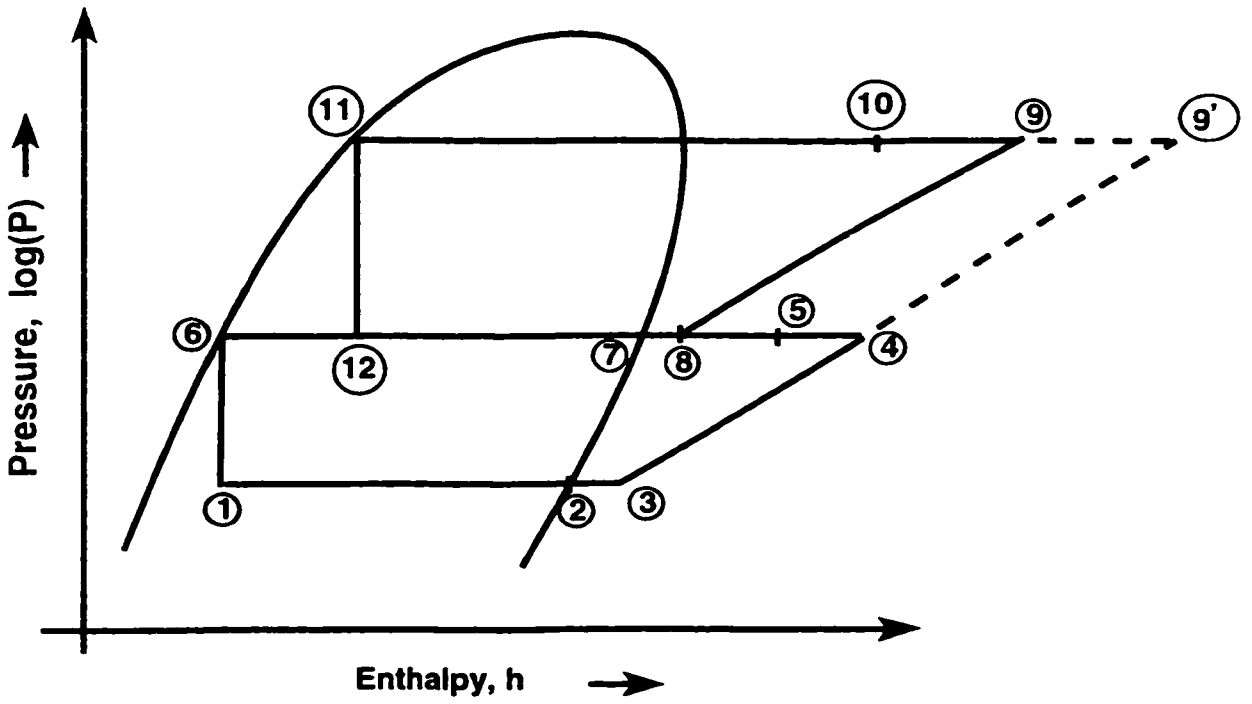

Figure 6.2: Pressure-enthalpy diagram of a two stage vapor compression refrigeration system.

compressor at state point 3. The refrigerant, from state point 2 to point 3 takes heat from the surroundings in the suction line. The refrigerant from the suction line at state point 3 is compressed by the LP cycle compressor to the saturation pressure of the flash intercooler, also known as interstage pressure. At state point 4, it leaves the compressor as a high temperature, high pressure, superheated vapor and enters the flash intercooler. Notice that the refrigerant form state point 4 to point 5 rejects heat to the surroundings in the discharge line before entering the flash intercooler. In the flash intercooler, the vapor bubbles through the liquid refrigerant and is desuperheated by the evaporation of the relatively cold liquid in the flash intercooler. The flash vapor formed by the throttling process (state point 11 to 12), in addition to the vapor formed by the evaporation of the cold liquid in the flash intercooler and the desuperheated vapor from the LP cycle are compressed in the HP compressor of the HP cycle. The vapor undergoes heat transfer with the surroundings form state point 7 to point 8, in the suction line of the HP compressor. At state point 9, it leaves the compressor as a high pressure, superheated vapor and enters the condenser. The refrigerant, from state point 9 to point 10 rejects heat to the surroundings in the discharge line. At state point 11, the refrigerant leaves the condenser and enters the expansion valve of the HP cycle, at point 12 it leaves the valve as a low quality and at the interstage pressure. Saturated liquid (state point 6) at the interstage pressure is withdrawn form the flash intercooler and is expanded through the expansion valve of the LP cycle to the evaporator pressure

corresponding to state point 1.

6.1 Analysis of the Cycle

Referring to the LP cycle loop in Fig. 6.1. from the first law of thermodynamics and the fact that the change in internal energy is zero for a cyclic process. we can write

$$(\dot{Q}_{flash} + \dot{Q}_{flash}^{loss.LP}) - (\dot{Q}_{evap} + \dot{Q}_{evap}^{loss}) + \dot{Q}_{W}^{loss.LP} = \dot{W}^{LP} \tag{6.1}$$

Since entropy is a state function, it's net change over the cycle is zero. Therefore, the contributions to the entropy generation are from heat trasfer (at the flash intercooler and evaporator) and the entropy generation due to non-isentropic compression and expansion in the compressor and the expansion valve, respectively. It can be expressed as

$$\frac{(\dot{Q}_{flash} + \dot{Q}_{flash}^{loss,LP})}{T_{inst}} - \frac{(\dot{Q}_{evap} + \dot{Q}_{evap}^{loss})}{T_{evap}} = \dot{S}_{igen}^{LP} \tag{6.2}$$

The heat transfer to and from the cycle occur by convection to flowing fluid streams having finite mass flow rates and specific heats. Therefore, the rate of heat transfer to the cycle at a low temperature in the LP cycle evaporator can be written as

$$\dot{Q}_{evap} = (\varepsilon \dot{C})_{evap}(T_{evap}^{in} - T_{evap}) \tag{6.3}$$

Similarly the rate of heat transfer between the refrigeration cycle and the sink in the HP cycle condenser is

$$\dot{Q}_{cond} = (\varepsilon \dot{C})_{cond}(T_{cond} - T^{in}_{cond}) \tag{6.4}$$

Similarly for the HP cycle loop all the equations describing the various processes in the cycle can be written as

$$(\dot{Q}_{cond} + \dot{Q}^{loss}_{cond}) - (\dot{Q}^{flash} + \dot{Q}^{loss.HP}_{flash}) + \dot{Q}^{loss.HP}_{\dot{W}} = \dot{W}^{HP} \tag{6.5}$$

$$\frac{(\dot{Q}_{cond} + \dot{Q}^{loss}_{cond})}{T_{cond}} - \frac{(\dot{Q}_{flash} + \dot{Q}^{loss.HP}_{flash})}{T_{inst}} = \dot{S}^{HP}_{igen} \tag{6.6}$$

$$\dot{Q}_{cond} = (\varepsilon \dot{C})_{cond}(T_{cond} - T^{in}_{cond}) \tag{6.7}$$

Defining the COP_{total} as refrigerating effect over the net work input, we have

$$COP_{total} = \frac{\dot{Q}_{evap}}{\dot{W}^{HP} + \dot{W}^{LP}} \tag{6.8}$$

Substituting the expressions of $\dot{W}^{LP}$ and $\dot{W}^{HP}$ from Eqs (6.1) and (6.5) in the above equation and expressing refrigeration temperatures in terms of the more readily available coolant temperatures, one obtains an analytical formula for the COP, as a function of cooling capacity, coolant temperatures, heat exchanger characteristics, heat leak terms, internal cycle losses and the interstage temperature of the flash intercooler, as

$$\frac{1}{COP} = -1$$

$$+\frac{(T^{in}_{cond}(\dot{S}^{LP}_{igen}+\dot{S}^{HP}_{igen}+\frac{(\dot{Q}_{evap}+\dot{Q}^{loss}_{evap})}{(T^{in}_{evap}-\frac{\dot{Q}_{evap}}{(\dot{m}C)_{evap}})}-\frac{(\dot{Q}^{loss.LP}_{flash}-\dot{Q}^{loss.HP}_{flash})}{T_{inst}})-\dot{Q}^{loss}_{cond}}{\dot{Q}_{evap}(1.0-\frac{1.0}{(\dot{m}C)_{cond}}(\dot{S}^{LP}_{igen}+\dot{S}^{HP}_{igen}+\frac{(\dot{Q}_{evap}+\dot{Q}^{loss}_{evap})}{(T^{in}_{evap}-\frac{\dot{Q}_{evap}}{(\dot{m}C)_{evap}})}-\frac{(\dot{Q}^{loss.LP}_{flash}-\dot{Q}^{loss.HP}_{flash})}{T_{inst}}))}$$

$$+(\frac{\dot{Q}^{loss.LP}_{flash}+\dot{Q}^{loss.LP}_{W}-\dot{Q}^{loss}_{evap}}{\dot{Q}_{evap}})+(\frac{\dot{Q}^{loss}_{cond}+\dot{Q}^{loss.HP}_{W}-\dot{Q}^{loss.HP}_{flash}}{\dot{Q}_{evap}}) \qquad (6.9)$$

Equation (6.9) gives the COP_{total} of the system for one set of input data. The required input data can be measured experimentally from an actual system or calculated from a thermodynamic model that is discussed in section 5. Table 6.1 shows the required input data obtained from the thermodynamic model of the system. The value of COP_{total} for Fig. 6.3(a), obtained from Eq. (6.9) using the input data given in Table 6.1 was found to be 2.78 which is exactly equal to the value obtained from the thermodynamic model. Therefore, the analytical expression in equation (10) and the thermodynamic model are correct and hence they can be used for design and performance evaluation purpose. It should be noted that the heat leak terms are neglected in the above comparison because they do not contribute much towards the overall system performance [15].

Figure 6.3 shows the characteristic performance curve ($1.0/COP$ vs $1.0/\dot{Q}_{evap}$) of the system. The plots are drawn using the input data given in Table 6.1, in addition the data which is not common to the figures is shown on the respective

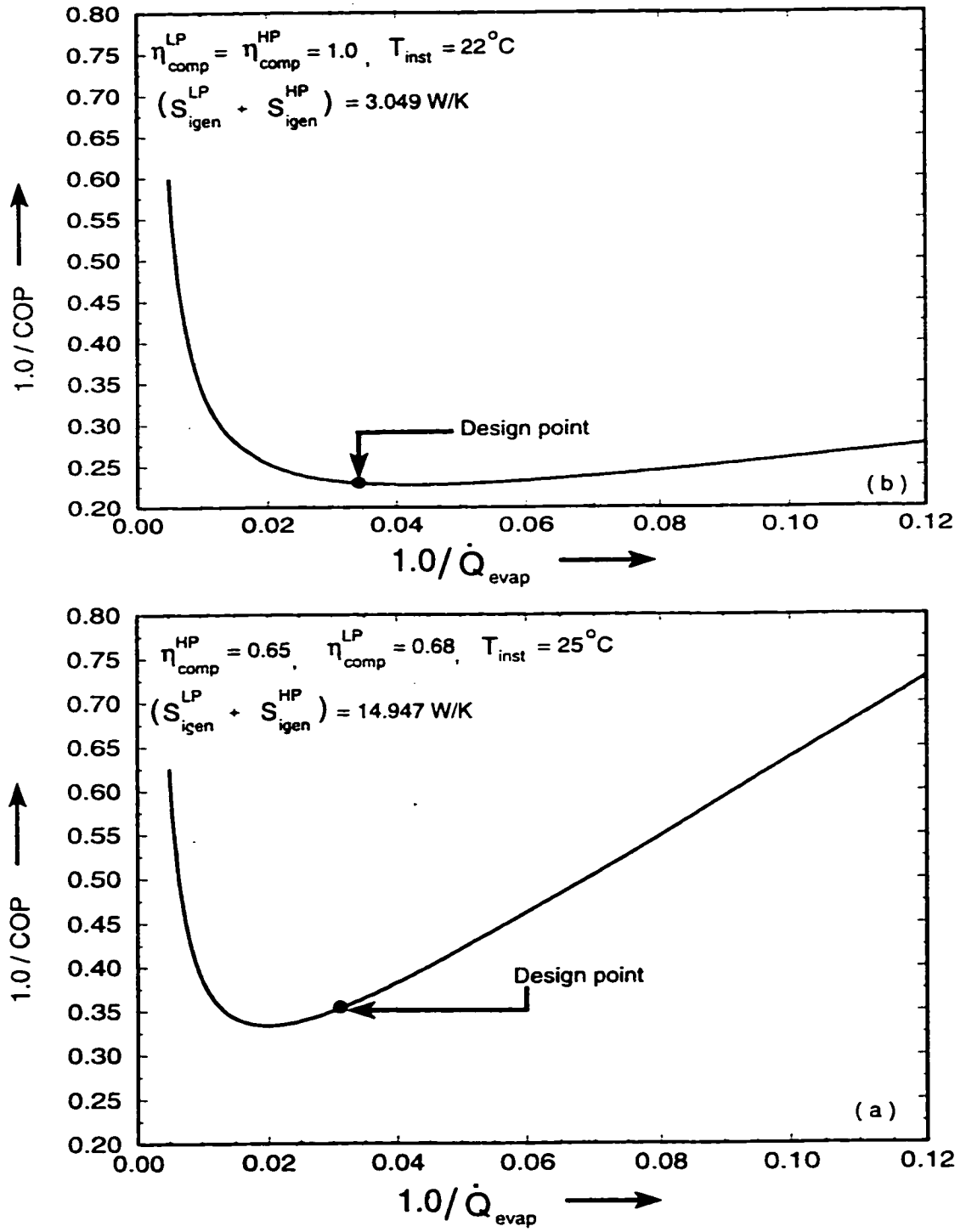

Figure 6.3: Performance curves for a two stage vapor compression refrigeration system.

Table 6.1: Input data to be used in Eq. (6.9). obtained from the thermodynamic model

Cooling capacity of the LP cycle evaporator	$(\dot{Q}_{evap})$	30000.0 W
Heat leak into the suction line of the LP cycle	$(\dot{Q}_{evap}^{loss})$	0.0 W
Heat leak from the discharge line of the LP cycle	$(\dot{Q}_{flash}^{loss.LP})$	0.0 W
Heat leak from the compressor shell of the LP cycle compressor	$(\dot{Q}_{W}^{loss.LP})$	0.0 W
Effectiveness and capacitance rate product for the LP cycle evaporator	$(\varepsilon\dot{C})_{evap}$	5000.0 W/K
Effectiveness and capacitance rate product for the HP cycle condenser	$(\varepsilon\dot{C})_{cond}$	5500.0 W/K
Coolant temperature at the inlet of the LP cycle evaporator	(T_{evap}^{in})	$0.0^{o}C$
Coolant temperature at the inlet of the HP cycle condenser	(T_{cond}^{in})	$40.0^{o}C$
Heat leak into the suction line of the HP cycle	$(\dot{Q}_{flash}^{loss,HP})$	0.0 W
Heat leak from the discharge line of the HP cycle	$(\dot{Q}_{cond}^{loss})$	0.0 W
Heat leak from the compressor shell of the HP cycle compressor	$(\dot{Q}_{W}^{loss.HP})$	0.0 W

plots. The design point is also shown in the figure, where for Fig. 6.3(a) the design point is ($COP = 2.78$). Notice that the design point is located away from the minimum point because of the losses mainly due to non-isentropic compression in the compressors of the system. However the design point is at the minimum point ($COP = 4.35$) when the efficiency of the compressors is assumed to be 100 percent, as shown in Fig. 6.3(b). The plots are a hypothetical curve drawn for a constant T^{in}_{evap} and a range of LP cycle evaporator capacity ($\dot{Q}_{evap}$). We note that the shape of the curve is similar to the one obtained for a simple cycle discussed by Gordon et al. [15]. The figure shows that COP is increasing with evaporator capacity upto the minimum point on the curve. In this region, the irreversible losses are mainly due to fluid friction (some times referred to as non-isentropic losses) in the compressor and the expansion valve. While at evaporator capacities greater than the minimum point, COP decreases significantly because of the losses due to the finite rate of heat transfer in the heat exchangers of the system. It should be noted that the performance of the system in the light of various irreversible losses of the system is similar to the performance of a simple cycle discussed by Gordon and Choon [16].

6.2 Prediction of Optimum Interstage Temperature

The performance of a two stage vapor-compression refrigeration system is controlled mostly by the interstage temperature (T_{inst}) of the flash intercooler. as reported by Zubair and Khan [27]. As discussed earlier. the multistage compression allows the total compression process to be performed very close to the saturation curve. compared with the typical simple-vapor compression cycle (process 3-9'). thereby. reducing the total compressor work. However it should be noted that the increase in performance of the system is not without cost since there are additional components in the system. The flash intercooler can be considered as a condenser for the the LP cycle and an evaporator for the HP cycle. The variation of the interstage temperature of the flash intercooler from the evaporating temperature (T_{evap}) of the LP cycle to the condensing temperature (T_{cond}) of the HP cycle causes the coefficient of performance of the LP cycle (COP^{LP}) to decrease and the coefficient of performance of the HP cycle (COP^{HP}) to increase. It should be emphasized that there is a particular interstage temperature of the flash intercooler at which $COP^{LP} = COP^{HP}$. This temperature can be investigated by expressing the overall coefficient of performance of the system (COP_{total}) in terms of T_{inst} and other

variables as

$$COP_{total} = \frac{1.0}{(\frac{T_{inst}-T^{in}_{evap}+(\Delta\ T^{LP})}{T^{in}_{evap}-(\Delta\ T^{LP})}) + (\frac{T^{in}_{cond}-T_{inst}+(\Delta\ T^{HP})}{T_{inst}-(\Delta\ T^{HP})})(\frac{T_{inst}}{T^{in}_{evap}-(\Delta\ T^{LP})})} \tag{6.10}$$

where in the above equation we have

$$(\Delta\ T^{LP}) = \dot{Q}_{evap}\left[\frac{1.0}{\varepsilon\dot{C}_{evap}}\right]. \tag{6.11}$$

$$\dot{Q}_{flash} = \dot{Q}_{evap}\left[\frac{T_{inst}}{T^{in}_{evap}-(\Delta\ T^{LP})}\right]. \tag{6.12}$$

$$(\Delta\ T^{HP}) = \dot{Q}_{flash}\left[\frac{1.0}{\varepsilon\dot{C}_{cond}}\right]. \tag{6.13}$$

Equation (6.10) can also be expressed in terms of the individual $COPs$ of the LP and the HP cycles as

$$COP_{total} = \left[\frac{1.0}{\frac{1.0}{COP^{LP}} + \frac{1.0}{COP^{HP}}(\frac{T_{inst}}{T^{in}_{evap}-(\Delta\ T^{LP})})}\right] \tag{6.14}$$

where

$$COP^{LP} = \frac{T^{in}_{evap}-(\Delta\ T^{LP})}{T_{inst}-T^{in}_{evap}+(\Delta\ T^{LP})} \tag{6.15}$$

and

$$COP^{HP} = \frac{T_{inst}-(\Delta\ T^{HP})}{T^{in}_{cond}-T_{inst}+(\Delta\ T^{HP})}. \tag{6.16}$$

It should be noted that Eq. (6.10) considers the irreversible losses due to rate of heat transfer in all the heat exchangers. However, when we consider $(\varepsilon\dot{C})_{cond}$ and $(\varepsilon\dot{C})_{evap}$ to be very large, we get

$$(\Delta\ T^{LP}) = 0.0 \tag{6.17}$$

and

$$(\Delta T^{HP}) = 0.0 \tag{6.18}$$

Substituting the above values in Eq. (6.10) we get

$$COP_{total} = \frac{T^{in}_{evap}}{T^{in}_{cond} - T^{in}_{evap}} \tag{6.19}$$

which is the Carnot cycle (COP). For better comparison of the twostage vapor compression refrigeration system with the corresponding simple system, the curves are plotted in a normalized form defined as

$$COPN = \frac{COP_{total}}{COP_{simple}} \tag{6.20}$$

where COP_{simple} is the COP of the corresponding simple cycle. Similarly a reduced interstage saturation temperature θ is defined as

$$\theta = \frac{T_{inst} - T^{in}_{evap}}{T^{in}_{cond} - T^{in}_{evap}} \tag{6.21}$$

Figure 6.4(a) shows the plot of coefficent of performances (COP_{total}, COP^{LP}, COP^{HP}) vs. the reduced interstage saturation temperature θ, for the following set of input data: $T^{in}_{evap} = 0.0\ ^oC$, $T^{in}_{cond} = 40.0\ ^oC$, $\dot{Q}_{evap} = 30.0\ kW$, $(\varepsilon\dot{C})^{HP}_{cond} = 5.5\ kW/K$ and $(\varepsilon\dot{C})_{evap} = 5.0\ kW/K$. As expected, the figure shows that COP^{LP} is decreasing with the reduced interstage temperature (θ) and COP^{HP} is increasing with θ. The figure also shows that the two $COPs$ are equal at $\theta = 0.48$, and the value of COP_{total} is constant throughout. Fig. 6.4(b) shows the corresponding variation of the system

operating temperatures. as can be seen from the figure that the temperature difference in the condenser and the evaporator of the system are constant for all values of θ. This demonstrates that the irreversible losses due to the rate of heat transfer in the heat exchangers remains constant for all values of the interstage saturation temperature. and hence there is no variation in COP_{total}. The above behavior of the COP is based on the fact that Eq. (6.10) includes only the irreversible losses due the heat transfer rate.

6.3 A Finite Time Thermodynamic Model of the System

As mentioned earlier, the heat transfer to and from the cycle occur by convection to flowing fluid streams having finite mass flow rates and specific heats. Therefore, the rate of heat transfer to the cycle in the LP cycle evaporator can be expressed in terms of temperature, mass flow rates, and change in enthalpy of the refrigerant. given by

$$\dot{Q}_{evap} = (\varepsilon \dot{C})_{evap}(T^{in}_{evap} - T_{evap}) = \dot{m}^{LP}(h_2 - h_1). \tag{6.22}$$

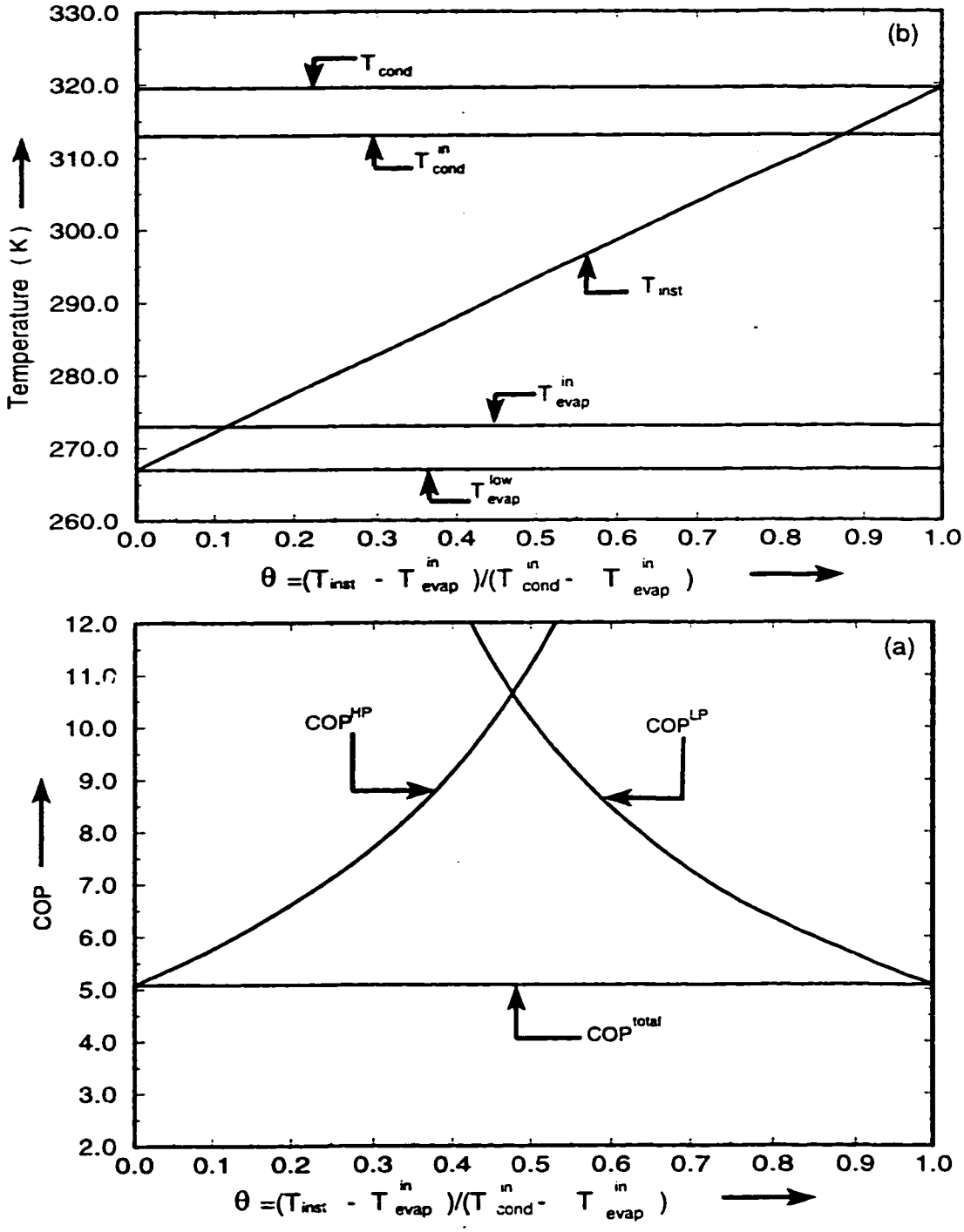

Figure 6.4: Variations of COP (a) and of operating temperatures (b) with (T_{inst}) for an irreversible temperature dependent two stage vapor compression system.

Similarly the rate of heat transfer between the refrigeration cycle and the sink in the HP cycle condenser is expressed as

$$\dot{Q}_{cond} = (\varepsilon \dot{C})_{cond}(T_{cond} - T_{cond}^{in}) = \dot{m}^{HP}(h_{10} - h_{11}). \tag{6.23}$$

In the flash intercooler, the rate of heat transfer between the LP cycle refrigerant and the HP cycle refrigerant is given by

$$\dot{Q}_{flash} = \dot{m}^{HP}(h_7 - h_{12}) = \dot{m}^{LP}(h_5 - h_6). \tag{6.24}$$

The compressor operation is described in terms of an isentropic efficiency η_{comp}^{LP}, so that the power requirement for the LP cycle compressor is given by

$$\dot{W}^{LP} = \dot{m}^{LP}(h_4 - h_3) = \frac{\dot{W}_s^{LP}}{\eta_{comp}^{LP}}. \tag{6.25}$$

Assuming that an amount of $\dot{Q}_{evap}^{loss}$ of heat, leaks into the suction line of the LP cycle compressor, which can be expressed as

$$\dot{Q}_{evap}^{loss} = \dot{m}^{LP}(h_3 - h_2). \tag{6.26}$$

Similarly assuming that an amount of $(\dot{Q}_{flash}^{loss,LP} + \dot{Q}_{W}^{loss,LP})$ of heat leaks from the discharge line and compressor shell given by

$$\dot{Q}_{flash}^{loss,LP} + \dot{Q}_{W}^{loss,LP} = \dot{m}^{LP}(h_4 - h_5). \tag{6.27}$$

The work input to the HP cycle compressor is given by

$$\dot{W}^{HP} = \dot{m}^{HP}(h_9 - h_8) = \frac{\dot{W}_s^{HP}}{\eta_{comp}^{HP}} \tag{6.28}$$

Assuming that an amount of $\dot{Q}_{flash}^{loss.HP}$ of heat leaks into the suction line of the HP cycle compressor, which can be expressed as

$$\dot{Q}_{flash}^{loss.HP} = \dot{m}^{HP}(h_8 - h_7). \tag{6.29}$$

Similarly assuming that an amount of $(\dot{Q}_{cond}^{loss} + \dot{Q}_{W}^{loss.HP})$ of heat leaks from the discharge line and the compressor shell of the HP cycle. This is given by

$$\dot{Q}_{cond}^{loss} + \dot{Q}_{W}^{loss.HP} = \dot{m}^{HP}(h_9 - h_{10}) \tag{6.30}$$

The above equations have been solved numerically by using the thermodynamic property data for several different refrigerants. The flow chart representing the method of solving the equations is shown in Fig. 6.5, wherein the terms SATPRP and TRIAL represents the subroutines for calculating the refrigerant saturated and vapor properties, respectively. These subroutines need any two independent intensive properties of the refrigerant to find other properties at a given state. For this purpose, a computer program, originally developed by Kartsounes and Erth [43] and modified by Fisher and Rice [44] and Khan and Zubair [46], have been used. The program gives the optimum COP_{total} and all the other parameters of the system for the following set of input data: $\dot{Q}_{evap}$, $(\varepsilon\dot{C})_{cond}$, $(\varepsilon\dot{C})_{evap}$, T_{cond}^{in}, T_{evap}^{in}, η_{comp}^{HP} and η_{comp}^{LP}.

Figure 6.6(b) shows the plot of COP_{total} vs the flash intercooler saturation temperature T_{inst} , using the output from the above described thermodynamic model.

for the input data given in Table 6.1. The design point ($COP_{total} = 2.78$) is the same point as discussed earlier in Fig. 6.3. The figure shows that for the given input conditions there is an optimum flash intercooler temperature at which COP_{total} is maximum. As expected, the property dependent model predicts different relationship between COP_{total} and the flash intercooler temperature T_{inst}, as that predicted by the temperature dependent model (refer to Fig. 6.4), since the property dependent model also considers the irreversible losses due to non-isentropic compression and expansion in the compressor and the expansion valve of the system, respectively.

Figure 6.7(a) shows the plot of COP_{total} vs the flash intercooler saturation temperature T_{inst} and the heat exchanger thermal inventory parameter (κ) defined as

$$\kappa = (\varepsilon \dot{C})_{cond} + (\varepsilon \dot{C})_{evap}, \tag{6.31}$$

using the output from the thermodynamic model, for the following set of input data: $\dot{Q}_{evap} = 30.0\ kW$, $(\varepsilon \dot{C})_{cond} = 5.5\ kW/K$, $(\varepsilon \dot{C})_{evap} = 5.0\ kW/K$, $T^{in}_{cond} = 40.0\ ^{o}C$, $T^{in}_{evap} = 0.0^{o}C$, $\eta^{HP}_{comp} = 0.65$ and $\eta^{LP}_{comp} = 0.68$. As expected, the figure shows that the performance of the system increases as the value of κ is increased, which is due to the fact that increase in the value of κ decreases irreversible losses due to the rate of heat transfer in the heat exchangers. We note that the property dependent model predicts an optimum flash intercooler temperature at which the overall coefficient of performance COP_{total} of the system is maximum, which is not

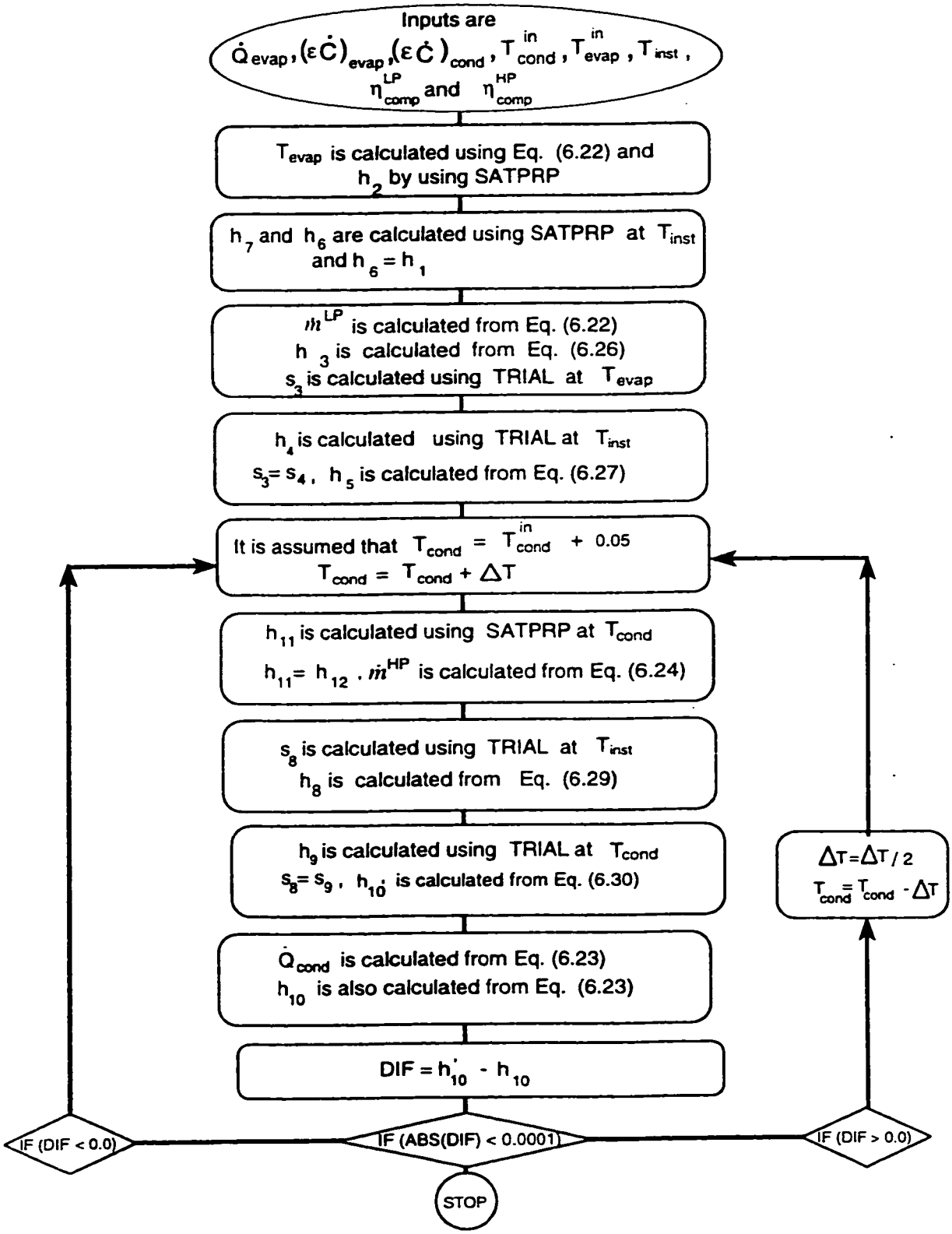

Figure 6.5: Flow chart for a two stage vapor compression refrigeration system.

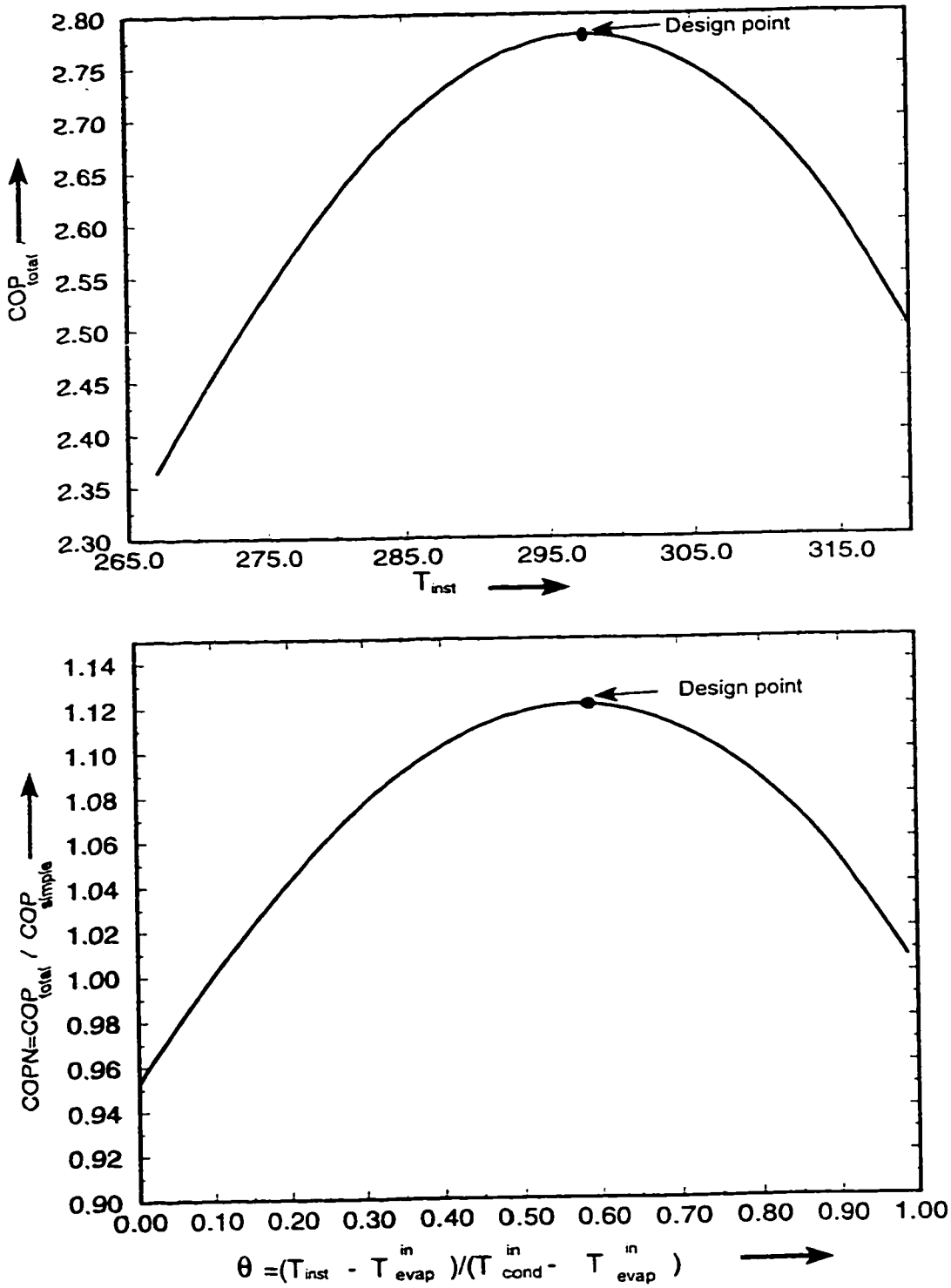

Figure 6.6: Variations of $COPN$ with (θ) (a) and of COP_{total} reduced (T_{inst}) (b) for the property dependent model.

predicted by the temperature dependent model (refer to Fig. 6.4). Fig. 6.7(b) shows the corresponding variation of system operating temperatures for $\kappa = 10.5\ kW/K$. Also, the condenser temperature and the evaporator temperature more-or-less remains constant, however one would expect a variation in T_{cond} with the reduced interstage temperature θ. The calculations indicates a somewhat constant temperature varying between 320.76 and 320.4166 K, which is mainly due to the fact that the variation in $\dot{Q}_{cond}$ is relatively less and the value of $(\varepsilon\dot{C})_{cond}$ in the calculation is high. This observation demonstrates that the contribution of ireversible losses due to rate of heat transfer in the heat exchangers, to the variation of COP_{total} with the reduced interstage temperature θ is negligible and that the optimum point occurs mainly due to the the non-isentropic compression and expansion in the compressors and the expansion valves of the system, respectively.

6.4 Optimum Distribution of Heat Exchanger Areas

The design of two stage refrigeration system involves proper selection of the external stream capacitance rates and the heat exchanger size. The heat exchanger effectiveness given by ε represents the heat exchanger surface area. The product $(\varepsilon\dot{C})$ of all the heat exchangers of the system is an expensive commodity and it determines

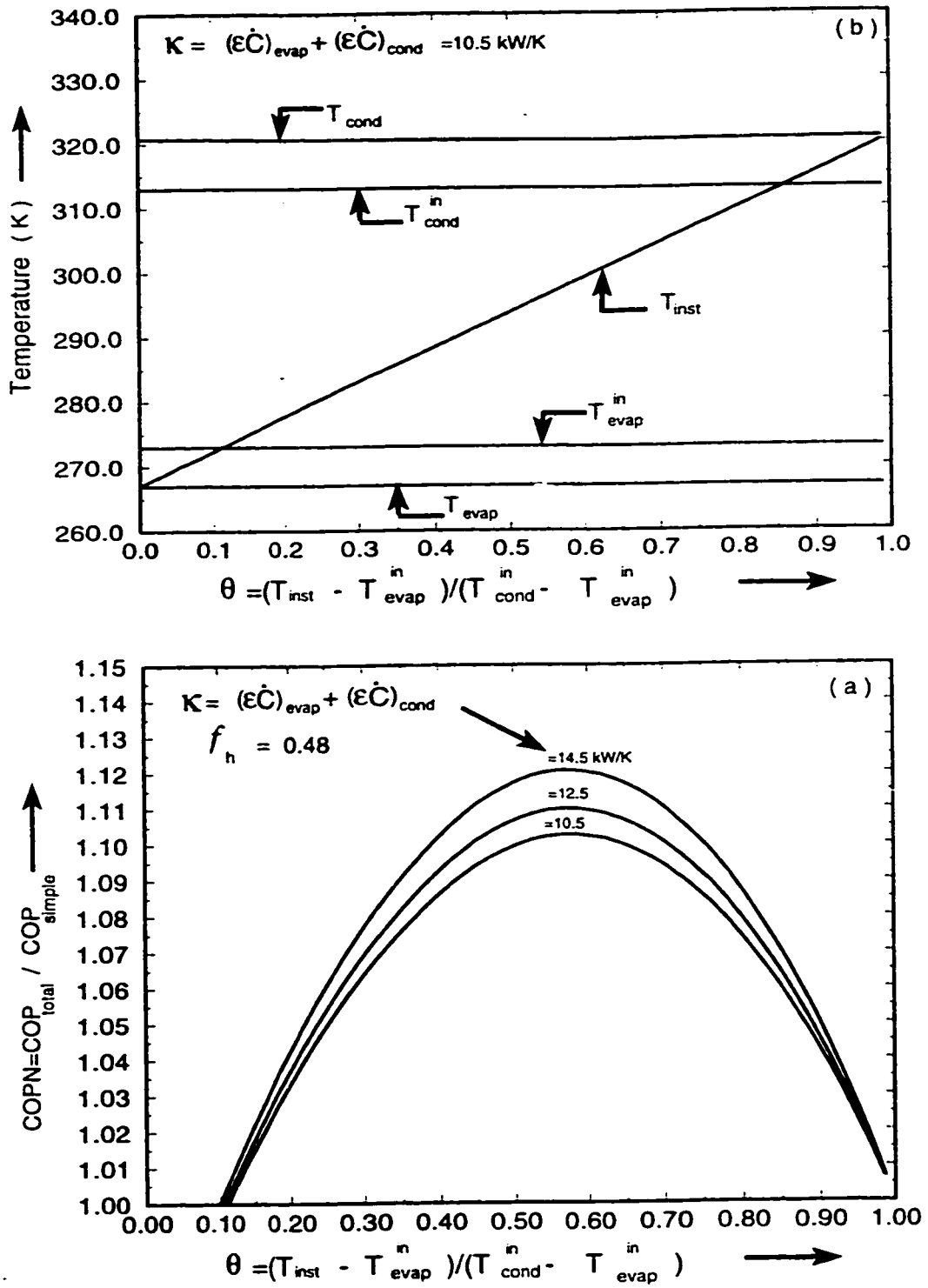

Figure 6.7: Variation of $COPN$ (a) and of operating temperatures (b) with (θ) for the following input data: $\dot{Q}_{evap} = 30.0\ kW$, $(\varepsilon\dot{C})_{cond} = 5.5\ kW/K$, $(\varepsilon\dot{C})_{evap} = 5.0\ kW/K$, $\eta^{LP}_{comp} = 0.68$, $\eta^{HP}_{comp} = 0.65$, $T^{in}_{evap} = 0.0\ ^oC$, $T^{in}_{cond} = 40.0\ ^oC$.

the overall cost of the system. Increasing the size of the heat exchanger increases the overall performance of the system but it also increase the cost of the system. hence a compromise is sought between the first cost and the operating cost of the system. As defined earlier, the thermal heat exchanger inventory parameter κ, may be considered as the design constraint and the problem involved in the optimization is to allocate the total heat exchanger area between the two heat exchangers (namely condenser and evaporator), so that maximum performance of the system is obtained. The above problem can be solved by using the thermodynamic model presented earlier in section 5, the model simulates the working of an actual reciprocating systems very closely.

To investigate the effect of relative size of heat exchangers, the following dimensionless heat exchanger parameter is defined to study the performance of the system:

$$f_h = \frac{(\varepsilon \dot{C})_{evap}}{(\varepsilon \dot{C})_{cond} + (\varepsilon \dot{C})_{evap}} \tag{6.32}$$

A set of sample plots, shown in Fig. 6.8(a), is drawn between COP_{total} and the dimensionless heat exchanger parameter (f_h) using the output from the thermodynamic model, for the following set of input data and using $R-134a$ as the refrigerant: $\dot{Q}_{evap} = 30.0\ kW$, $\eta^{LP}_{comp} = 0.65$, $\eta^{HP}_{comp} = 0.65$, $T^{in.}_{evap} = 0.0\ ^oC$, $T^{in}_{cond} = 40.0\ ^oC$. The plots are drawn for different values of the thermal heat exchanger inventory (κ). The corresponding variation of the various temperatures of the system for

$\kappa = 10.0\ kW/K$ is shown in Fig. 6.8(b). As expected, the figure shows that as the value of κ is increased the COP_{total} of the system increases, mainly because of the reduced irreversible losses due to the finite rate of heat transfer in the heat exchangers. We note that the difference between T^{in}_{cond} and T_{cond} increases with the value of f_h because the area of the HP cycle condenser is decreased and hence the heat transfer in the condenser takes place across a high temperature difference, resulting in reduced irreversible losses due to heat transfer. However the difference between T^{in}_{evap} and T_{evap} decreases with the increase in the value of f_h because the area of the evaporator is increased and hence the heat transfer in the evaporator takes place across a lowe temperature difference, resulting in reduced irreversible losses due to heat transfer. In between these two extremes, there lies an optimum distribution of heat exchanger area at which the COP_{total} is maximum. This optimum point is shown in Fig. 6.8(a) for different values of the heat exchanger thermal inventory parameter κ. It should be noted that in this figure for every value of the dimensionless heat exchanger parameter f_h an optimum value of T_{inst} is calculated that gives the maximum COP_{total} (refer to Fig. 6.7(a)). Therefore, the optimum point obtained in the figure is the global optimum for the given operating conditions.

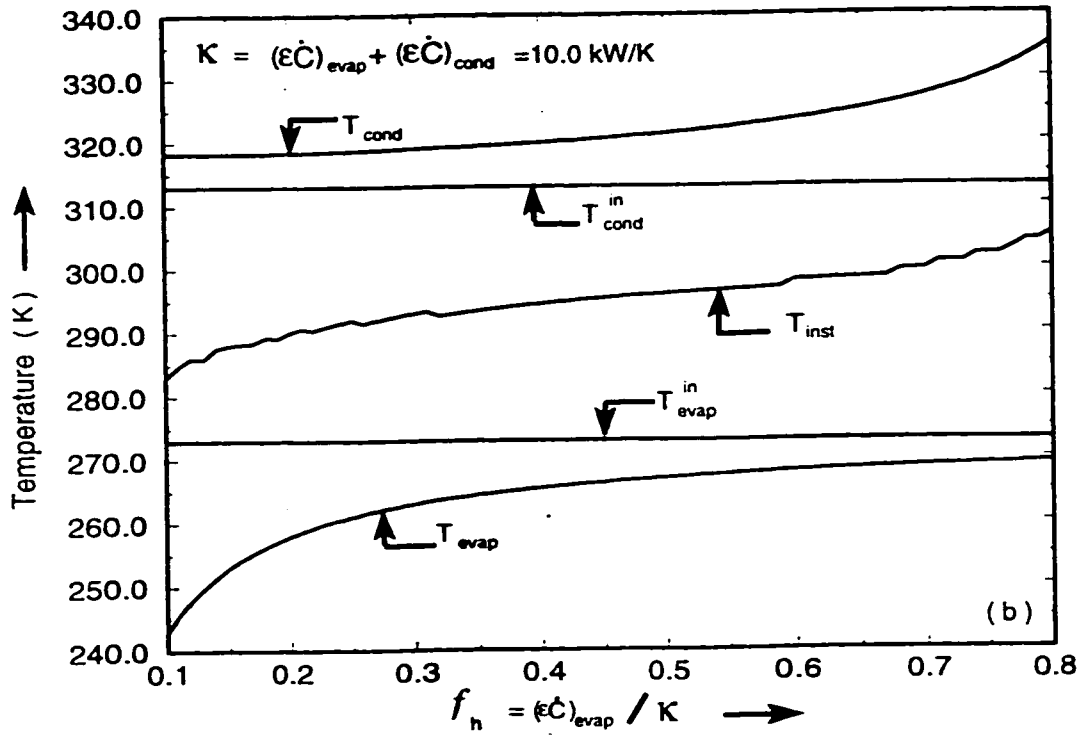

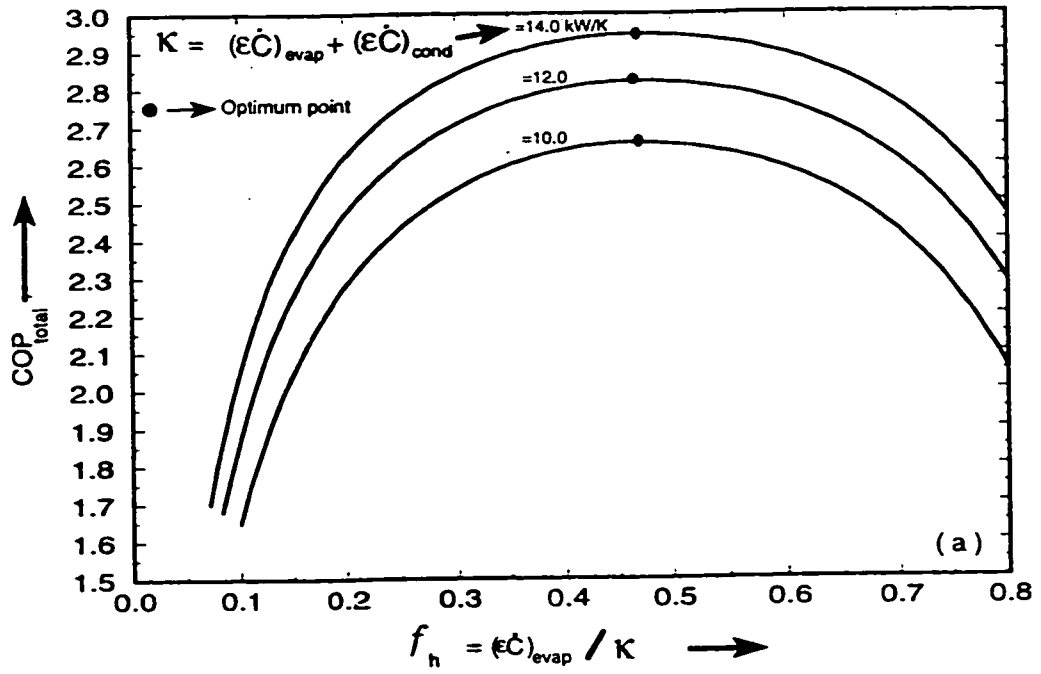

Figure 6.8: Variations of COP_{total} (a) and of operating temperatures (b) with (f_h) for the following input data: $\dot{Q}_{evap} = 30.0\ kW$, $\eta^{HP}_{comp} = 0.65$, $\eta^{LP}_{comp} = 0.65$, $T^{in}_{evap} = 0.0\ ^oC$, $T^{in}_{cond} = 40.0\ ^oC$.

Chapter 7

Conclusions and Recommendations

7.1 A Simple Vapor Compression Refrigeration System

The characteristic chiller performance curves of an actual simple reciprocating refrigeration system are explained by taking into account various losses of the system such as, the irreversibilities due to finite rate of heat transfer in the heat exchangers and the non-isentropic compression and expansion in the compressor and expansion valve of the system, respectively. The losses due to the irreversible rate of heat transfer dominates at high evaporator capacities and that due to the non-isentropic

compression and expansion are significant at low evaporator capacities.

The computer simulation of the reciprocating refrigeration system using thermodynamic model involves the use of actual refrigerant properties. Using such a model, the system COP and all other system parameters are calculated accurately (within ± 2.0 % of actual values). The model is demonstrated to be a useful tool for design and performance evaluation of reciprocating refrigeration systems. In this regard, the performance characteristics of a variable speed system are discussed with respect to irreversible losses in the heat exchangers and other non-isentropic losses. The effects of superheating and subcooling on the performance of the system indicate that superheating has more influence on the system performance.

Analysis of the simple reciprocating system using a thermodynamic model shows that for a given evaporator capacity, COP is maximum when the value of $(\varepsilon \dot{C})_{cond}$ is slightly more than that of $(\varepsilon \dot{C})_{evap}$. It is found that the results predicted from the thermodynamic model is true for actual systems as well, despite assuming constant inlet condenser and evaporator temperatures, the refrigeration capacity, and a constant compressor efficiency in the thermodynamic model. It should be noted that the definitive influences on the compressor efficiency of a reciprocating compressor is the suction-to-discharge pressure ratio, which would be useful to incorporate if the modelling is to take place over a wide range of condensing and evaporating

temperatures.

7.2 A Dedicated Mechanical Subcooling Vapor Compression Refrigeration System

The thermodynamic models are developed by considering the finite size of all components of the dedicated mechanical subcooling vapor compression system. The models developed include both the temperature dependent and the property dependent models. The performance evaluation of the system is investigated by considering the temperature model. It is demonstrated that the optimum subcooler temperature, at which the COP of the system is maximum, is a function of the subcooler parameter X and the reduced subcooler saturation temperature θ. This optimum temperature is found to be shifting closer to the condensation temperature of the main cycle condenser, particularly when the subcooler parameter X is increased.

The property dependent model showed the same trends as that predicted by the temperature model, that is, the existence of an optimum subcooling saturation temperature. In addition, the optimum distribution of total heat exchanger areas between the condenser and evaporator of each cycle (main and subcooler) of the system is also investigated. It is found that the COP of the system is maximum when a large fraction of the total area is allocated to the condenser as compared to

the evaporator of the main cycle. It is also demonstrated that this optimum occurs when the irreversibilities due to the finite rate of heat transfer in heat exchangers are minimum.

7.3 An Integrated Mechanical Subcooling Vapor Compression Refrigeration System

Thermodynamic models of an integrated mechanical subcooling vapor compression refrigeration system are developed to study the design and performance evaluation of the system. The models developed include both the temperature-dependent and the property-dependent models. The performance evaluation of the systems is investigated by considering the temperature-dependent model. It is demonstrated that the optimum subcooler saturation temperature at which COP of the system is maximum, is not a function of the subcooler heat exchanger parameter X. This optimum temperature is found to be about halfway between the condensation and the evaporation temperatures (i.e., $\theta = 0.50$) for almost all values of the parameters X.

The property dependent model showed the same trends as that predicted by the temperature model, that is, the existence of the optimum subcooler saturation

temperature. In addition, the optimum distribution of total heat exchanger areas between the condenser and the evaporator of the cycle is also investigated. It is found that COP of the system is maximum when a large fraction of the total area is allocated to the condenser of the cycle. It is also shown that this optimum distribution corresponds to the fact that the irreversibilities due to the finite rate of heat transfer in the heat exchangers are minimum at a maximum COP point.

7.4 Two-Stage Vapor Compression Refrigeration System

The thermodynamic models are developed by considering the finite size of all components of the two stage vapor compression refrigeration system. The models includes both the temperature dependent and the property dependent models. The performance evaluation of the system is investigated by considering the temperature model. It is demonstrated that the irreversible losses due to the rate of heat transfer has negligible effect on the variation of COP_{total}, however the model shows a value of reduced temperature θ when the COP of the LP cycle is same as that of the HP cycle.

The property dependent model showed the existence of an optimum interstage

saturation temperature at which the system has maximum COP_{total}. In addition, the optimum distribution of total heat exchanger area between the condenser and the evaporator of the system is also investigated. It is found that the COP_{total} of the system is maximum when a large fraction of the total area is allocated to the condenser as compared to evaporator of the system. It is also demonstrated that this optimum distribution occurs when irreversibilities due to the finite rate of heat transfer in the heat exchangers of the system are minimum.

It is expected that inclusion of compressor efficiency as a function of suction-to-discharge pressure as well as comparison with experimental data of two-stage reciprocating refrigeration system would be useful to validate the modelling strategy presented in this thesis. In this regard, it is recommended to carry out experiments over a wide range of condensing and evaporating temperatures of two-stage system.

Bibliography

[1] J.L. Threlkeld. A thermodynamic study of vapor compression heat pump cycles. *Refrigeration Engineering*, 61(2):1202–1206, 1953.

[2] T. Wilson. Second law analysis of compression refrigeration system. *ASHRAE Journal*, 8(1):49–57, 1966.

[3] G. Alefeld. Efficiency of compressor heat pumps and refrigerators derived from the second law of thermodynamics. *International Journal of Refrigeration*, 10(6):331–341, 1987.

[4] A. Bejan. Theory of heat transfer-irreversible refirgeration plants. *International Journal Of Heat And Mass Transfer*, 32(9):1631–1638, 1989.

[5] R. Swers, Y.P. Patel, and R.B. Stewart. Thermodynamic analysis of vapor compression refrigeration system. *ASHRAE Transactions*, 78(1):143-152, 1972.

[6] ASHRAE HANDBOOK OF FUNDAMENTALS. *American Society of Heating, Refrigeration and Air-conditioning Engineers*, pages 1.1 1.20. USA, 1989.

[7] H. Auracher. The application of exergy to refrigeration process optimization. In *Proc. of XV. International Congress of Refrigeration*, volume 2, pages 239–256, Venice, 1979.

[8] H. Auracher, editor. *Saving of Energy in Refrigeration.* International Institute of Refrigeration, Paris, 1980.

[9] C.L.D. Huang, S.A. Fartaj, and D.L. Fenton. Analysis of the thermal systems using the entropy balance method. *International Journal of Energy Research*, 16, 1992.

[10] S.A. Klein. Design considerations for refrigeration cycles. *International Journal of Refrigeration*, 15(2):181–185, 1994.

[11] V. Radcenco, J.V.C. Vargas, A. Bejan, and J.S. Lim. Two design aspects of defrosting refrigerators. *International Journal of Refrigeration*, 18(2):76–86, 1995.

[12] A. Bejan. *Entropy Generation through Heat and Fluid Flow.* John Wiley and Sons, New York, 1982.

[13] A. Bejan. Power and refrigeration plants for minimum heat exchanger inventory. *Journal of Energy Resources Technology*, 115, 1993.

[14] A. Bejan. Power generation and refrigeration models with heat transfer irreversibilities. *Journal of Heat Transfer Society of Japan*, 33(128):68–75, 1994.

[15] J.M. Gordon, H.T. Chua, and K.C. NG. Experimental study of the fundamental properties of the reciprocating chillers and their relation to the thermodynamic modelling and chiller design. *International Journal Of Heat And Mass Transfer*. 39(11):2195-2204, 1996.

[16] J.M. Gordon and N.G. Choon. Predictive and diagonastic aspects of a universal thermodynamic model for chillers. *International Journal Of Heat And Mass Transfer*. 38(5):807-818, 1995.

[17] J.M. Gordon and N.K. Choon. Thermodynamic modelling of reciprocating chillers. *Journal Of Applied Physics*. 75(6):2679-2774, 1994.

[18] J.M. Gordon, K.C. Ng, and H.T. Chua. Centrifugal chillers: thermodynamic modelling and a diagonastic case study. *International Journal of Refrigeration*. 16(2):253–257, 1995.

[19] D.J. Leverenz and N.E. Bergan. Development and validation of a reciprocating chiller model for hourly energy analysis programs. *ASHRAE Transactions*. 89(1):156–174, 1983.

[20] J.M. Gordon, K.C. Ng, and H.T. Chua. Optimizing chiller operation based on finite-time thermodynamics: universal modelling and experimental confirmation. *International Journal of Refrigeration*. 20(3):191 200, 1997.

[21] T.Y. Bong, K.C. Ng, and K.O. Lau. Test facility for water-cooled chiller. *ASHRAE TRANSACTIONS*, 96(3):205–212, 1990.

[22] H.T. Chua, J.M. Gordon, K.C. Ng, and Q. Han. Entropy production analysis and experimental confirmation of absorption systems. *International Journal of Refrigeration*, 20(3):179–190, 1997.

[23] V. Bahel and S.M. Zubair. Mechanical subcooling improves supermarket refrigeration performance. *Heating Piping Air Conditioning*, 60(2):105–107, 1988.

[24] S.M. Zubair. Thermodynamics of a vapor compression refrigeration cycle with mechanical subcooling. *Energy*, 19(6):707–715, 1994.

[25] S.M. Zubair, M. Yaqub, and S.H. Khan. Second-law-based thermodynamic analysis of two-stage and mechanical-subcooling refrigeration cycles. *International Journal of Refrigeration*, 19(8):506–516, 1996.

[26] S.H. Khan. Second law based thermodynamic analysis of vapor-compression refrigeration cycles. Master's thesis, KFUPM KSA., 1992.

[27] S.M. Zubair and S.H. Khan. On optimum interstage pressure for two-stage and mechanical-subcooling vapor-compression refrigeration cycles. *Transactions of the ASME*, 117(1):64–66, 1995.

[28] J.W. Thornton, S.A Klein, and J.W. Mitchell. Dedicated mechanical subcooling design strategies for supermarket applications. *International Journal Of Refrigeration*, 17(8):508-515, 1994.

[29] R.J. Couvillion, M.W Larson, and M.H. Somerville. Analysis of a vapor-compression refrigeration system with mechanical subcooling. *ASHRAE Transactions*, 94(2):641-660, 1988.

[30] H.P. Soumerai. Simplified analysis of two-stage low temperature refrigeration system. *Refrigeration Engineering*, 61(7):746-750, 1965.

[31] M. Prasad. *Refrigeration and Air Conditioning*. Wiley Eastern Limited, New Delhi, 1983.

[32] R. Lal. *Selection of intermediate pressure in compound refrigeration system*. PhD thesis, University of Roorke INDIA., 1970.

[33] H.K. Verma and V. Charan. Intermediate pressure for 2-stage compression system with flash intercooling. In *Proc. of the Second National Symposium on Refrigeration and Air Conditioning*, pages 75–79, Roorkee, INDIA, March 1973.

[34] S. Katz. Best operating points for staged systems. *Industrial Engg. Chemistry Fundamentels*, 1(4):226-240, November 1962.

[35] C.P. Arora and P.L. Dhar. Optimization of multi-stage refrigerant compressors. In *Progress in Refrigeration Science and Technology*, volume 2, pages 693-700. IIR Paris, 1971.

[36] M.A. Ait-Ali. *Optimal mixed refrigerant liquefaction of natural gas.* PhD thesis. Stanford University, CA, U.S.A, 1979.

[37] M.A. Ait-Ali and D.J. Wilde. *Minimum work multi stage cascade refrigeration cycles.* ASME, 1980.

[38] S. Czaplinski. Uber den optimalin zwischendruck bei kalteprozessen. *Allgemeine Warmetechnick*, 91(2):3-6, 1959.

[39] M. Prasad. Optimum interstage pressure for 2-stage refrigeration system. *ASHRAE*; 23(1):58-60, 1981.

[40] W.B. Gosney. *Principles of Refrigeration.* Cambridge University Press, New York, 1982.

[41] W.F. Stoecker and J.W. Jones. *Refrigeration and Air Conditioning.* McGraw-Hill, New York, 1982.

[42] W.M. Kays and A.L. London. *Compact Heat Exchangers.* McGraw-Hill, New York, 1964.

[43] G.T. Kartsounes and R.A. Erth. Computer calculations of the thermodynamic properties of refrigerants 12, 22, and 502. *ASHRAE Transactions*, 77(2):88 103. 1971.

[44] S.K. Fisher and C.K Rice. *The Oak Ridge Heat Pump Models: 1. A Steady-state Computer Design Model for Air-to-Air Heat Pumps.* Oak Ridge, TN, 1983.

[45] D.P. Wilson and R.S. Basu. Thermodynamic properties of a new stratospherically safe working fluid - refrigerant 134a. *ASHRAE Transactions*, 94(2):2095 2115, 1988.

[46] S.M. Zubair and S.H. Khan. Thermodynamic analysis of the cfc-12 and hfc-134a refrigeration cycles. *Energy*, 18(7):717–726, 1993.

[47] M.O. McLinden. Measurement and formulation of the thermodynamic properties of refrigerant 134a and 123. *ASHRAE Transactions*, 95(2):263–283, 1989.

[48] H.T. Kuehn and H. Liang. Irreversibility analysis of a water to water mechanical-compression heat pump. *Energy*, 16(6):883–896, 1991.

[49] F.P. Incropera and D.P. DeWitt. *Introduction to Heat Transfer.* John Wiley and Sons, New York, 1985.

[50] G.J. Van Wylen and R.E. Sonntag. *Fundamentals of Classical Thermodynamics.* John Wiley and Sons, New York, 1986.

Vitae

- Jameel-Ur-Rehman Khan
- Born on July 11, 1972 in Hyderabad, India
- Received Bachelor of Science (**BS**) degree in Mechanical Engineering from **OUCE** Osmania University College of Engineering, Hyderabad, India in August 1994
- Joined the Department of Mechanical Engineering at King Fahd University of Petroleum and Minerals (**KFUPM**), Dhahran, Saudi Arabia as a Research Assistant in September 1995
- Received Master of Science (**MS**) degree in Mechanical Engineering from KFUPM, Saudi Arabia in November 1997